AD NUMBER
AD595823
CLASSIFICATION CHANGES
TO: **UNCLASSIFIED**
FROM: **CONFIDENTIAL**
LIMITATION CHANGES
TO: **Approved for public release; distribution is unlimited.**
FROM: **Distribution: Further dissemination only as directed by Defense Advanced Research Projects Agency, ATTN: TIO, 675 North Randolph Street, Arlington, VA 22203-2114, 10 OCT 1967, or higher DoD authority.**
AUTHORITY
31 Aug 1979, Group 4, DoDD 5200.10; ESD ltr dtd 10 Apr 1980

DISCLAIMER NOTICE

THIS DOCUMENT IS THE BEST QUALITY AVAILABLE.

COPY FURNISHED CONTAINED A SIGNIFICANT NUMBER OF PAGES WHICH DO NOT REPRODUCE LEGIBLY.

SECURITY MARKING

The classified or limited status of this report applies to each page, unless otherwise marked.
Separate page printouts MUST be marked accordingly.

Project Report

EPS-1
(Earth Propagation Studies)

Geodar
(Title UNCLASSIFIED)

R. W. Chick
R. G. Entricknap
R. A. Guillette
R. M. Lerner
O. G. Nackoney

1 August 1967
Reissued 10 October 1967

Prepared for the Advanced Research Projects Agency
under Electronic Systems Division Contract AF 19(628)-5167 by

Lincoln Laboratory
MASSACHUSETTS INSTITUTE OF TECHNOLOGY
Lexington, Massachusetts

The work reported in this document was performed at Lincoln Laboratory, a center for research operated by Massachusetts Institute of Technology. This research is a part of Project Vela Uniform, which is sponsored by the U. S. Advanced Research Projects Agency of the Department of Defense; it is supported by ARPA under Air Force Contract AF 19(628)-5167 (ARPA Order 512).

This document comprises 124 pages, No. 6 of 75 copies. Series A.

MASSACHUSETTS INSTITUTE OF TECHNOLOGY

LINCOLN LABORATORY

GEODAR

(Title UNCLASSIFIED)

R. M. LERNER

R. G. ENTICKNAP *R. A. GUILLETTE* *O. G. NACKONEY*

Group 65

R. W. CHICK

Group 63

PROJECT REPORT EPS-1 (Earth Propagation Studies)

1 AUGUST 1967

REISSUED 10 OCTOBER 1967

LEXINGTON MASSACHUSETTS

Paragraphs on each page of this document are of the same classification as the page unless indicated otherwise by specific markings.

ABSTRACT

The development of Geodar, a radar for detecting tunnels, is described. The characteristics of the system and its component parts are treated in detail. Soil properties and their effect on Geodar performance are described briefly. Performance data on the operation of experimental systems at several test sites are reported.

CONTENTS

	ABSTRACT	iii
1	BACKGROUND AND BASIC DESIGN CONSIDERATIONS	1
2	THE ANTENNA AND COUPLING SYSTEM	15
3	PULSER	37
4	RECEIVER	41
5	CONTROL CIRCUIT	59
6	SAMPLING UNIT	65
7	OSCILLOSCOPE DISPLAY	69
8	HELIX RECORDER	71
9	POWER	85
10	PULSE PROPAGATION MEASUREMENTS ON SELECTED SOILS	91
11	BACKSCATTERING FROM CYLINDERS IMMERSED IN AN UNBOUNDED DISSIPATIVE MEDIUM	97
12	TEST RESULTS	107

1. BACKGROUND AND BASIC DESIGN CONSIDERATIONS

Conception of the particular electromagnetic tunnel location device described herein, and the early experiments demonstrating its feasibility, were the contribution of Dr. R. M. Lerner.

Information on the nature of the operational problem came principally from newspaper articles and television (Huntley-Brinkley) newscasts. One noteworthy exception was a report by an Australian field officer, made available to Lincoln Laboratory through the Advanced Research Projects Agency, that described tunnel complexes and operations in considerable detail.

During the summer and fall of 1966, discussions were held with others working on this problem, to determine, in particular: (1) if other approaches were more promising, and (2) if electromagnetic systems had fundamental problems that would make pursuit of a development program unprofitable. The investigative discussions indicated work should begin on an experimental electromagnetic system.

The basic, distinguishing concept of the Lincoln approach was that the antenna radiates directly into the ground, rather than into the air, and then through the air/ground interface. Since it is operationally unattractive to consider a system with a buried antenna, the antenna system conceived is in the ground plane, close to the ground's surface. The dimensions selected made the antenna an efficient radiator in the ground for the chosen frequency band and, by definition, an inefficient radiator in air.

Optimum frequency for ground penetration is a function of the particular type of soil. Since soil characteristics vary, and would be unknown to the operator, a tunable device would be unsatisfactory. It was therefore decided to use a wide band of frequencies (50 to 150 MHz). The generator would produce a narrow (3- to 5-nsec) DC pulse, and the receiver would be a wide-band video amplifier. The antenna would control the useful frequency range of the system.

The basic system concept is shown in Fig. 1-1.

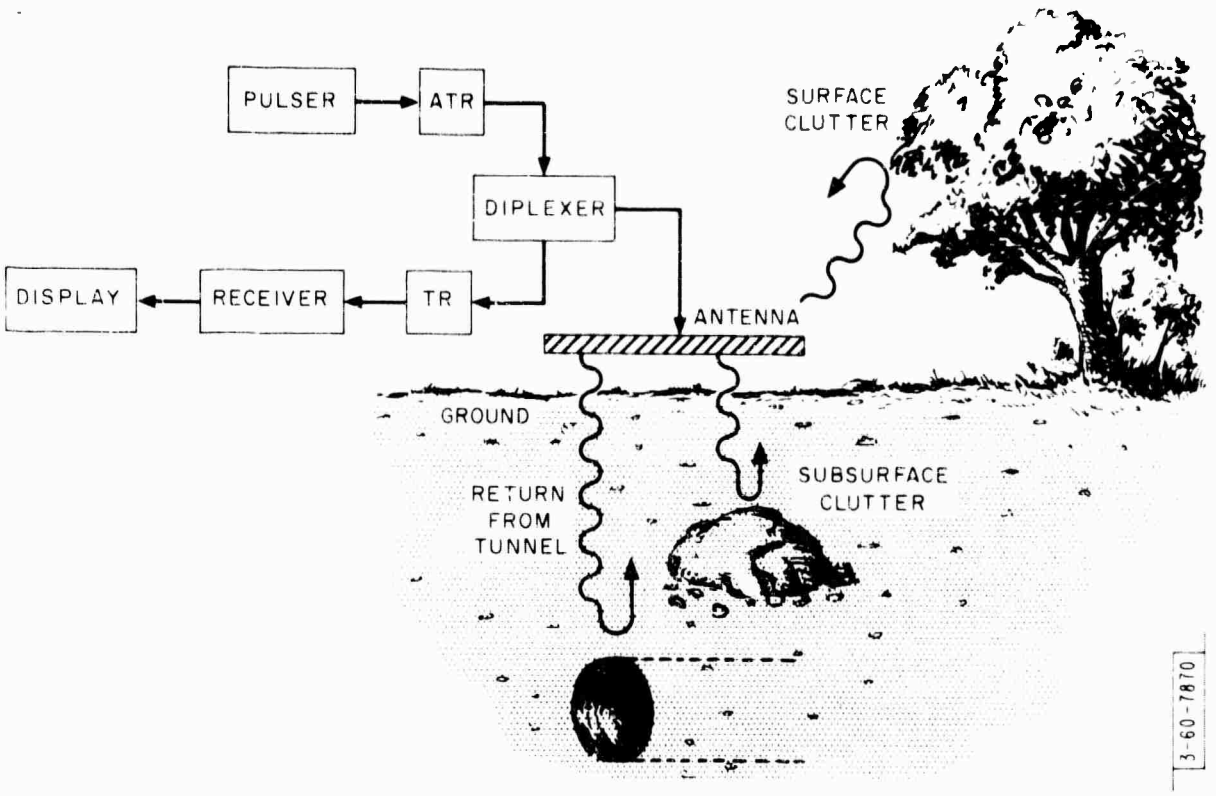

Fig. 1-1. Geodar system.

The first system assembled used commercial laboratory components except for the antenna and coupler. Attempts to

detect underground utility pipes at known locations outside Lincoln Laboratory buildings were only partially successful because scrap building materials in the soil distorted interpretation of the findings. As a consequence, a test range [Figs. 1-2 (a, b)] simulating field soil conditions was built at the Lexington Field Station during the early winter. A number of voids made with wood forms were buried at specified depths in a pile of screened loam. Tests made with the experimental equipment on this site proved voids could be detected.

A formal test program was established and a project team assembled to develop a demonstration system with field performance capability. Simultaneously, (1) the affect of soild properties on radar performance was examined, (2) suitable system components were developed, (3) a system for field testing was assembled, and (4) backscattering from voids in lossy dielectric media was examined theoretically.

Data on soils in Vietnam came from a number of sources. Richard Sherman, a consultant from Metcalf & Eddy, sought out

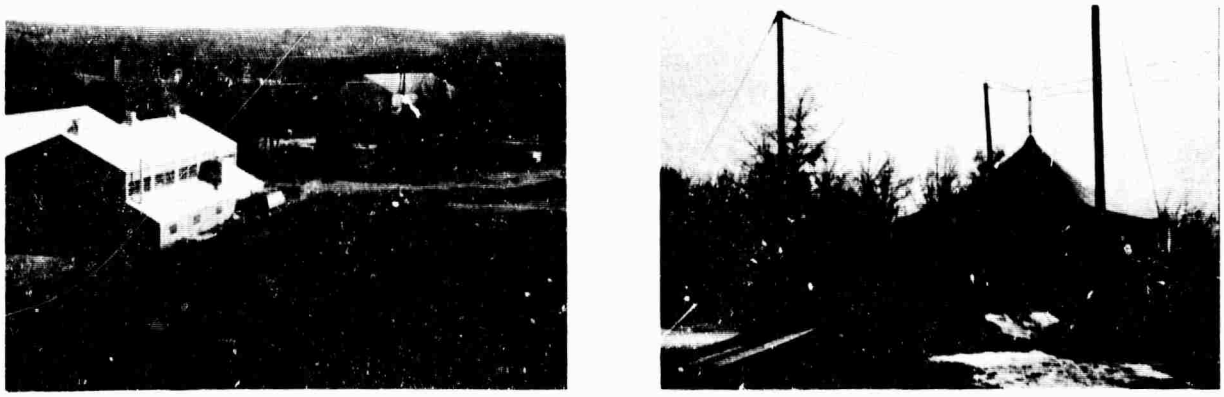

(a) (b)

Fig. 1-2. Lexington Field Station test site.

most of the information and obtained representative samples of a number of soil types of interest.

A. System Calculations

Calculations of potential performance margin for a radar system depend on the system's frequency range. For Geodar, the following considerations favor high frequency operation:

1. Sufficient bandwidth to resolve five to ten nanoseconds of delay, corresponding to one foot through the ground.

2. A small, therefore inefficient, antenna in the air.

3. Operation above the dielectric relaxation frequency so that initially compact wave packets will not become dispersed.

4. Small electrical wavelengths in terms of the objects to be observed, so the objects will reflect signals efficiently.

Two factors favor low frequency operation:

1. Larger antenna size means higher signal gathering power.

2. Attenuation tends to rise sharply above 50 to 100 MHz in soils containing clay.

The last consideration--radically affecting potential range--is the crucial one. Because of the wide range of soil propaga-

tion conditions, and because of the desire to have resolution in time of a few nanoseconds, no single narrowband frequency range was chosen for Geodar. Instead, an antenna with about 3/4 m^2 of effective area was chosen. This antenna is so constructed that the transient response between two of these antennas facing each other is approximately three half cycles of an 80-MHz sine wave, the outer half cycles having 1/3 to 1/2 the amplitude of the middle one. The speed of propagation in normal soils is about one fourth that of the speed in air. When the antenna is placed over such soils, most of the radiated power is within 50 to 150 MHz. For higher propagation speeds, the center of gravity of the radiated power spectrum shifts upward in frequency.

Of the three factors that enter into an estimate of radar system performance, viz., antenna radiation, soil propagation, and effective reflection from the target, only propagation of the far-field through homogenous soil is easily calculated To substitute for the difficult calculations, a 3- to 5-nsec pulse was applied to a known antenna, and the reflection from a 0.7-m wide tunnel one meter below the antenna in soil of known attenuation properties was observed. The peak-to-peak return signal was about 35 db below the peak of the pulse delivered by the transmitter to the antenna system. The magnitude of this return scaled linearly as the width of the underground reflector (a long box) varied from 18 to 30 inches.

Using 35 db as the total round-trip loss for the tunnel specified at 1 m depth in soil whose dielectric constant is 20, other system losses, gains and limitations can be introduced. What remains is the margin to "see" deeper objects (Table 1-1).

The margins for additional range (Table 1-1) must encompass

TABLE I-1

GEODAR MARGIN CHART

Contributors to System Gain or Loss	Mark I		Potential System	
Peak pulse power		13 dbw		13 dbw
ATR loses	4 db		3 db	
Hybrid coupling loss (Transmit)	3 db		3 db	
Estimated antenna efficiency		(−10 db)		(−10 db)
Estimated average power radiated		(−29 dbw)		(−28 dbw)
Hybrid loss, receive	3 db		3 db	
Standard loss to box (depth: 1 m)	35 db		35 db	
TR loss	4 db		2 db	
Time varying gain control	4 db			
Margin for reliable signal detection	13 db*		13 db*	
	66 db		59 db	
Preamp gain		26 db		not limited
Background noise in sampling scope	−83 dbw			
Additional reflection loss for dielectric constant k, 6 instead of 20	6 db		6 db	
KT in 10^8 Hz bandwidth			−124 dbw	
Receiver noise figure			3 db	
Gain from sampling rate-to-presentation rate ratio				20 db†
Totals	−11 db	41 dbw	−56 dbw	33 dbw
Margin available beyond 1 m		50 db		89 db

* Display integration improvement from sweep to sweep in A- and B-scope presentation not considered.

† The total sweep range of 1000 nsec at 1 MHz repetition rate divided into 300 resolution cells by the 3 nsec transmit pulse. At the 100 kHz sampling rate of the IS1 (30 sweeps per sec) there are 3000 samples per sweep, or 10 samples for integration per resolution cell. Since 300 MHz, rather than 3000 MHz, is the required bandwidth for Geodar; the sampling rate could be raised to 1000 kHz to provide 100 samples per resolution cell, or 20 db of integrable gain over a single pulse. This gain is included in the calculations for the potential system.

the normal free space radar losses and excess propagation losses due to soil conductivity. Conventionally, the free space radar loss varies as the inverse fourth pow of range. However, with the sizes and separations of antennas and tunnels considered, the Geodar "sees" more tunnel length the farther away it is moved from the tunnel, making the inverse cube of distance a more realistic estimate of this loss. Excess loss has been assumed to be directly proportional to range. The third- or fourth-degree equation resulting from this transaction can be solved by trial and error and interpolating the ranges that just use up the margins available. These calculations have been made for assumed excess losses of 8 and 12 db per meter (Table 1-2).

Thirty-five db of extra system performance extends the detection range by about two to three meters; about four meters in quite lossy soils seems guaranteed. The practical limitation to detecting objects near the ultimate range for these theoretical calculations is, principally, the degree to which the baseline transients from the earlier pulses have been suppressed successfully.

TABLE 1-2
RANGES DETERMINED BY THIRD- AND FOURTH-DEGREE EQUATIONS

System	α = 8 db/m		α = 12 db/m	
	$1/D^4$ Law (meters)	$1/D^3$ Law (meters)	$1/D^4$ Law (meters)	$1/D^3$ Law (meters)
Mark I	4.3	5.0	3.4	3.8
Potential	7.5	8.4	5.2	6.3

B. Mark I and II

The first radar for detecting tunnels, Geodar Mark I (Fig. 1-3), was completed in early March. Details of the device and its developmental form, together with test data, are contained in this report. Also included are measurements made on tunnels at Fort Belvoir, Virginia, and Raleigh, North Carolina, as well as data on voids at 5-1/2 and 9-1/2 foot depths constructed at Millstone Hill (a second formal Lincoln Laboratory test range).

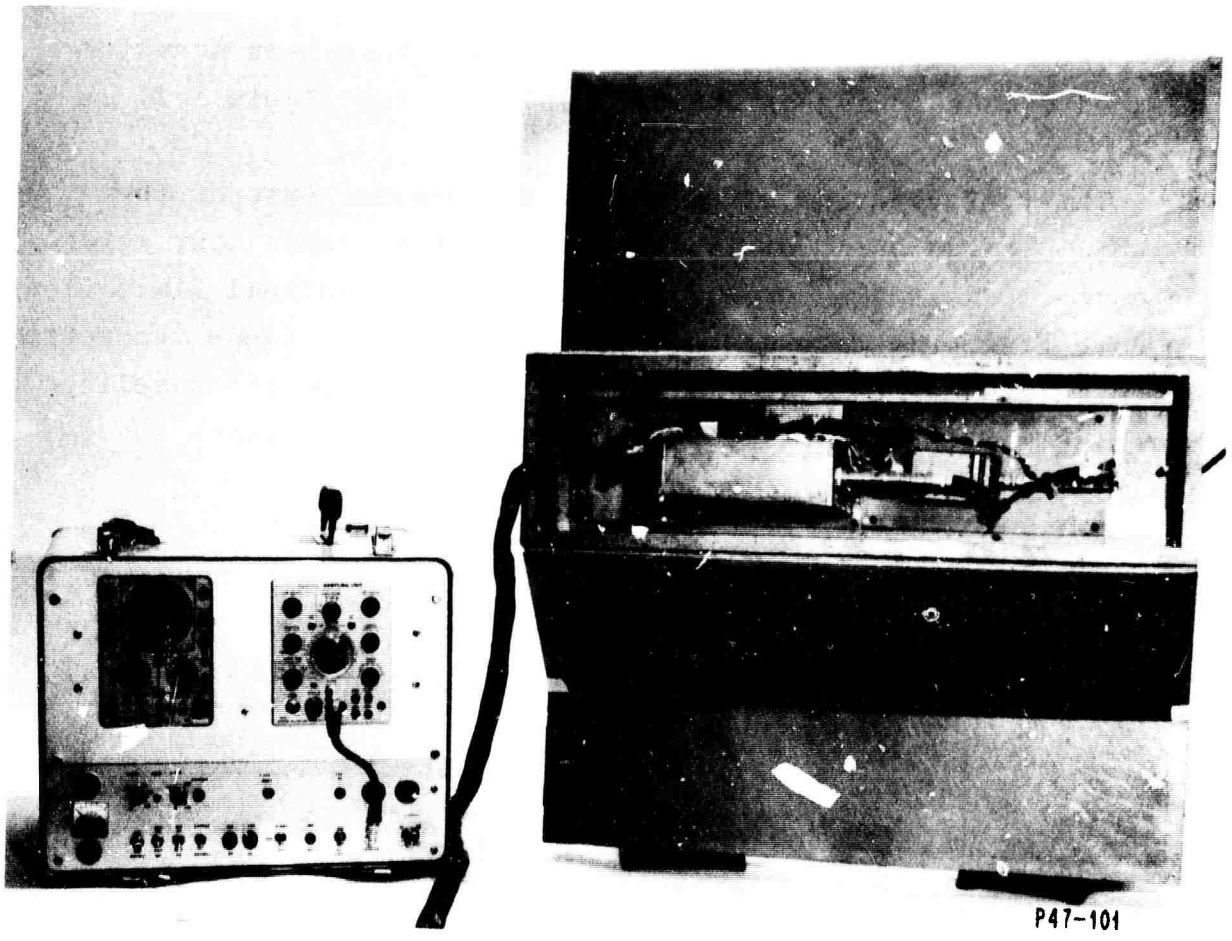

Fig. 1-3. Mark I antenna (right) and display unit.

Geodar Mark II (Fig. 1-4), completed in mid-June, has several improvements over Mark I, but time has not permitted as comprehensive testing as that made with the earlier field test model. Both Geodar units have detected voids at a maximum of 1-1/2 feet below the surface. Calculations indicated Mark II can detect 36-inch-in-diameter voids at depths of 15 to 18 feet in soil whose electrical characteristics are similar to those at Millstone Hill.

(U) Functionally, Mark I and II are similar. Their block diagrams are shown in Figs. 1-5 (a and b), and their electrical characteristics are given in Table 1-3.

(U) Each model consists of two basic parts--an antenna unit and a display unit. The flat, 30- x 34-inch antenna, plus RF components, are mounted on a Teflon skid structure that is

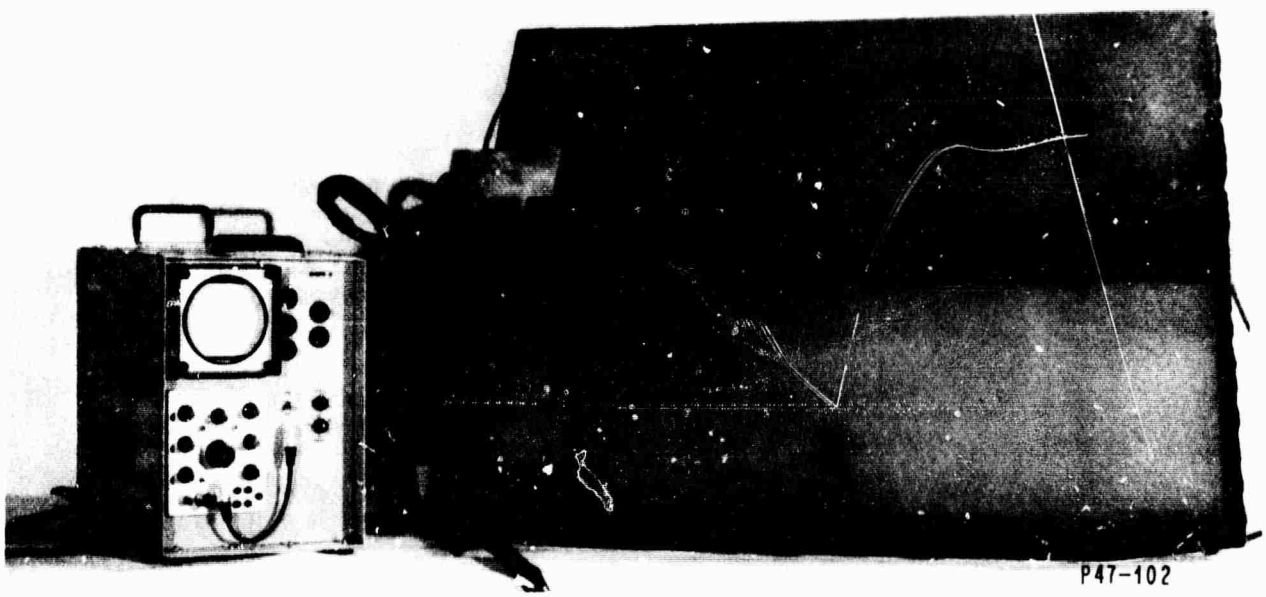

Fig. 1-4. Mark II antenna (right) and display unit

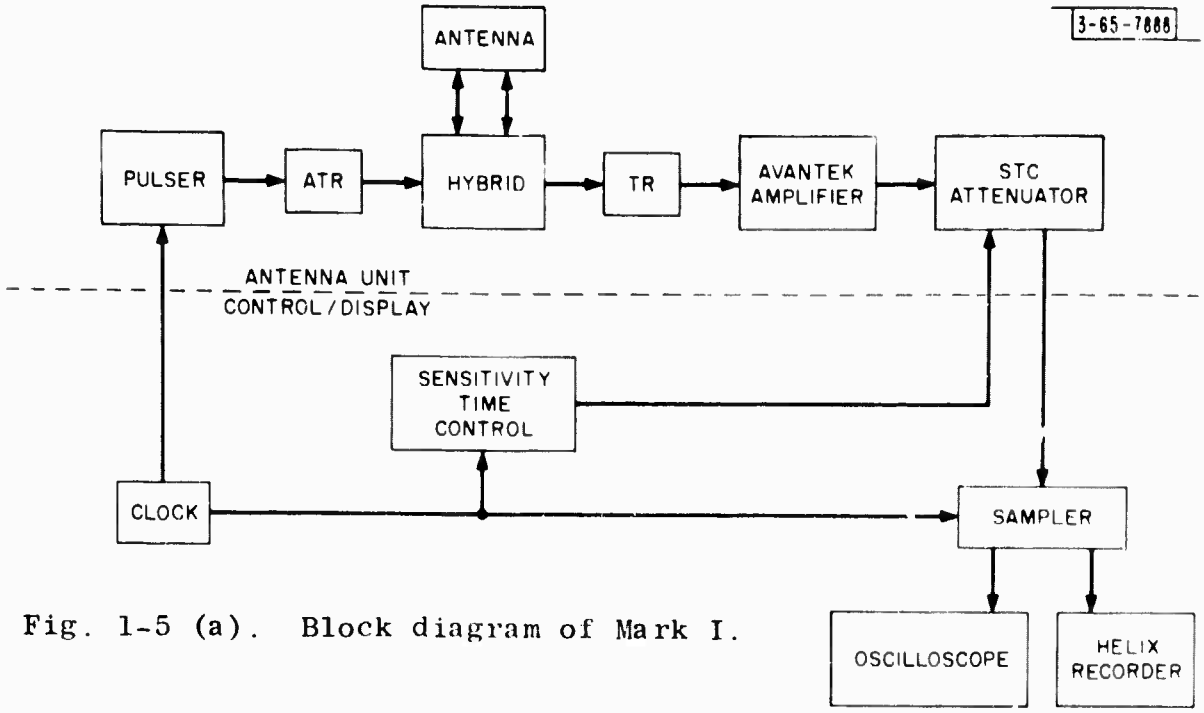

Fig. 1-5 (a). Block diagram of Mark I.

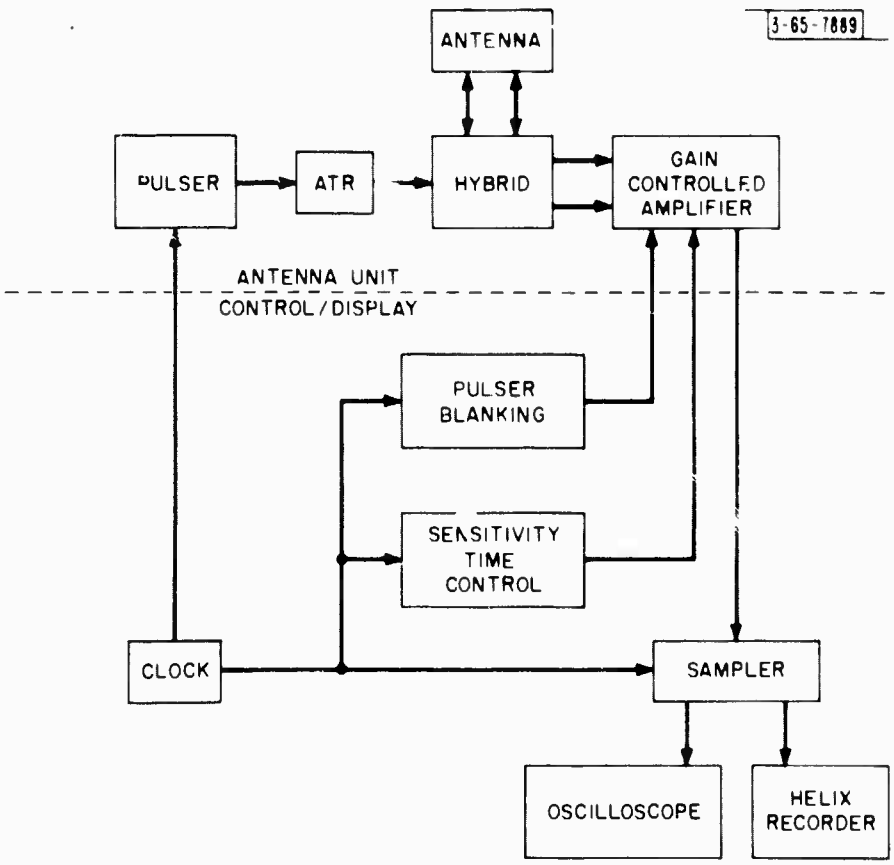

Fig. 1-5 (b). Block diagram of Mark II.

dragged across the ground. In Mark I, the pulser, hybrid, and receiver are mounted separately in one equipment compartment on the antenna structure; in Mark II, improved more compact versions of the pulser, hybrid, and receiver are combined in a single package mounted on the antenna structure.

Mark I and II display units contain the control unit, power

TABLE I-3
ELECTRICAL CHARACTERISTICS OF MARK I AND II

Characteristic	Mark I	Mark II
Pulser		
Pulse width	3 nsec	5 nsec
Pulse amplitude	30 v	35 v
Repetition rate	1 MHz	1 MHz
Antenna	Mark I (Fig. 2-8)	Mark I (Fig. 2-8)
Hybrid		
Isolation	40 db	45 db
Bandwidth	250 MHz	300 MHz
Transmit losses	3 db	1 db
Receive losses	3 db	1 db
Receiver		
Gain	28 db	30 db
Frequency response	1 – 300 MHz	1 – 325 MHz
STC – minimum attenuation	2 db	0 db
STC – maximum attenuation	32 db	50 db

distribution system, sampling unit, and oscilloscope. The 19- x 19- x 15-inch Mark I has a 3-inch oscilloscope display; the 22- x 12- x 16-inch Mark II has a 5-inch display.

The sonar-type display is in two separate units (Fig. 1-6): one contains the sweep circuits, amplifier, and power supplies; the other is the Alden recorder. The latter was not packaged with the rest of the system because of its late arrival.

A flexible, 50-foot umbilical cord connects the antenna and display assemblies.

Geodar system components (Fig. 1-7) are portable. During

P47-100

Fig. 1-6. Helix recorder (left) and interfacing unit.

field operations the display units and generator are carried in a vehicle, and the antenna unit is dragged across the ground by two men (Fig. 1-8).

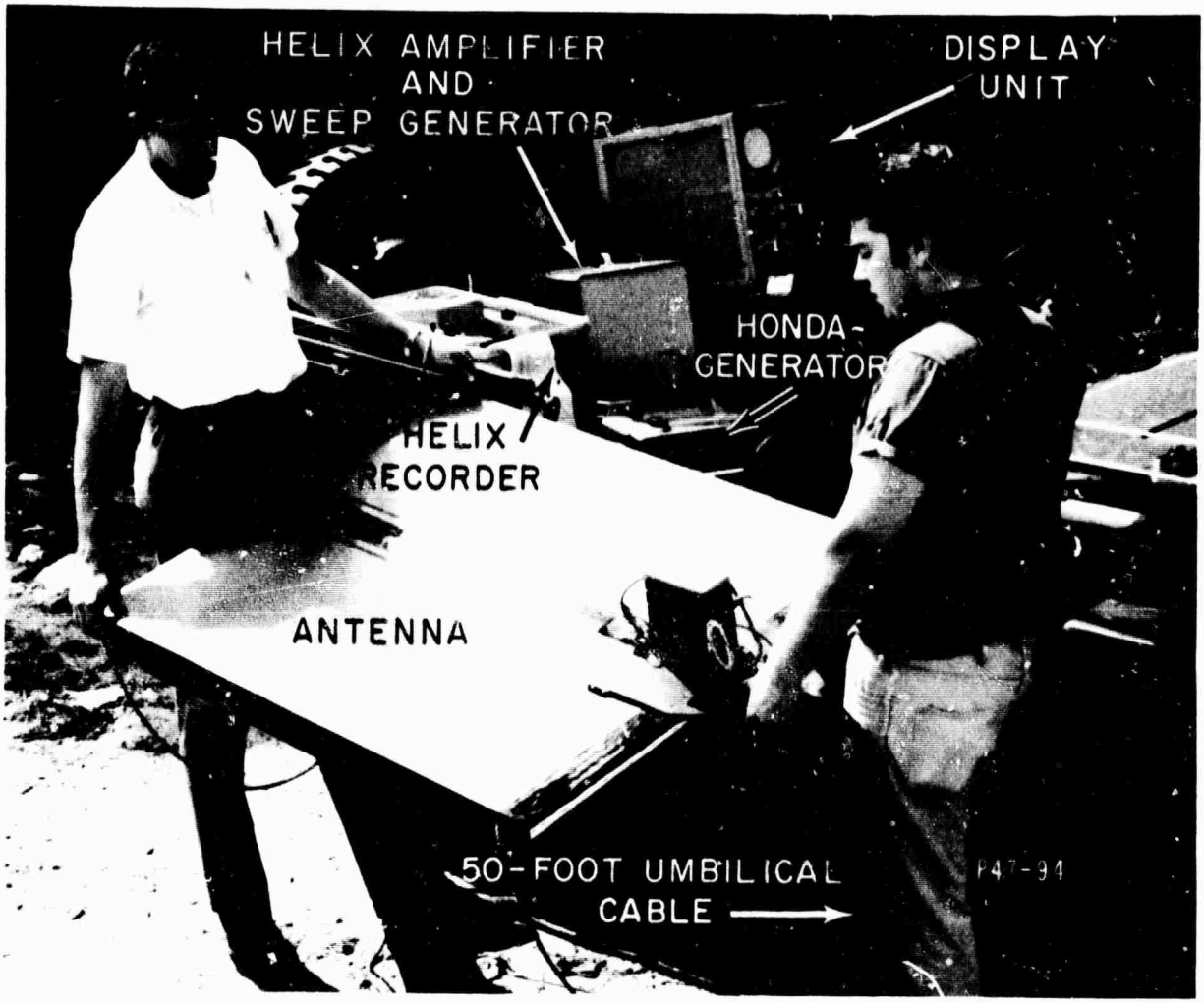

Fig. 1-7. Components of the Geodar system.

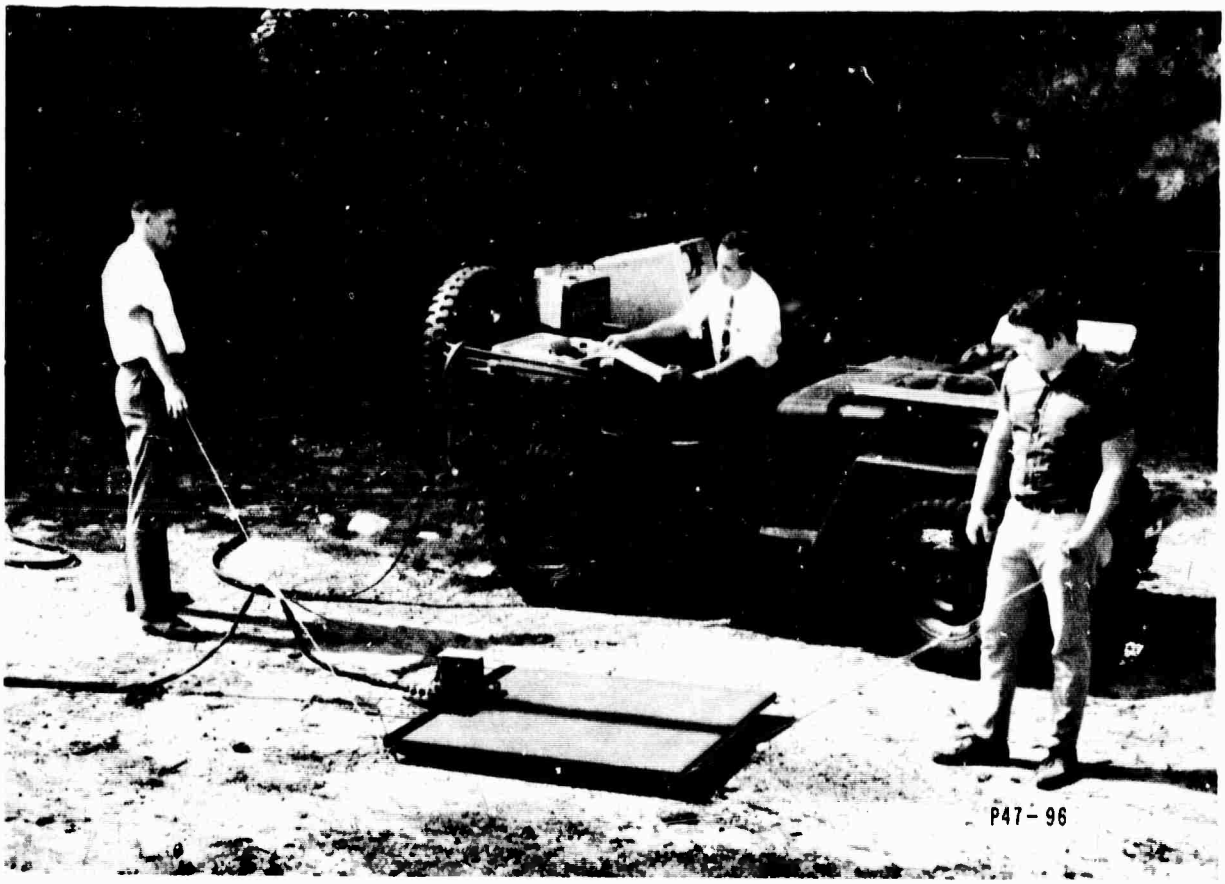

Fig. 1-8. Field operation of the Geodar system.

2. THE ANTENNA AND COUPLING SYSTEM

A crucial part of Geodar is its antenna and antenna-coupling system that must radiate effectively over a wide bandwidth (50 to 150 MHz), and must ring down quickly for target returns to be observed in tens of nanoseconds after transmission of each pulse. This chapter states the design problems for Geodar in terms of problems met in conventional short-pulse radar; and explains how the problems were handled for Mark I. (Changes in the design of Mark I and incorporated in Mark II are explained in Chapters 3 and 4.)

The Mark I antenna is a flat, rectangular-shaped, transmission-line structure, approximately 2-1/2 x 3 feet; driven and terminated at the middle of opposing long sides where the impedance is 360 ohms. The total pulse-travel-time from input to termination is about 7 nsec; longer than might be anticipated from the physical dimensions of the elements.

The antenna is coupled through a four-port hybrid coupler to the pulse generator and receiver. As soon as the transmitter pulse stops, the hybrid is terminated properly to present a matched termination to transients in the antenna. The hybrid is coupled to the pulse generator by a 50-ohm transmission line, approximately one-foot long, and a diode ATR to block possible source noise during the receive interval for reflected signals. A diode TR network protects the receiver from accidental unbalance of the hybrid resulting in overload.

A. Conventional Radar vs Geodar

The transmitter for a short-pulse radar (Fig. 2-1) usually generates a "short" burst (microseconds long) of RF energy, at carrier frequencies of 1 to 10 GHz. Some kind of hybrid or circulator (diplexer) directs this energy to the antenna instead of to the receiver. Despite isolation provided by the diplexer, a protective device called a TR is necessary to prevent the transmitted pulse from damaging the low-level stages of the receiver input. Similarly, an attenuating switch called an ATR prevents noise generated by the transmitter between pulses from reaching the receiver. Because diplexer isolation is 20 to 30 db, it can be omitted in a low-performance system. The transmitted pulse, though short, is long compared with a cycle at the carrier frequency. Thus, system bandwidth, though it may be large in an absolute sense, is usually small when reckoned as a percentage of the carrier frequency. The antenna is typically many wavelengths in extent, and this fact is used to form beams that can be pointed in a desired direction. The RF feed system length is short compared with the distance (time delay) at which it is desired--or indeed, possible--to see echoes from interesting targets. Generally, it is difficult to observe anything within the first few hundred yards of a short-pulse radar because the pulse is too long, and the object is obscured by clutter returns from the surrounding terrain.

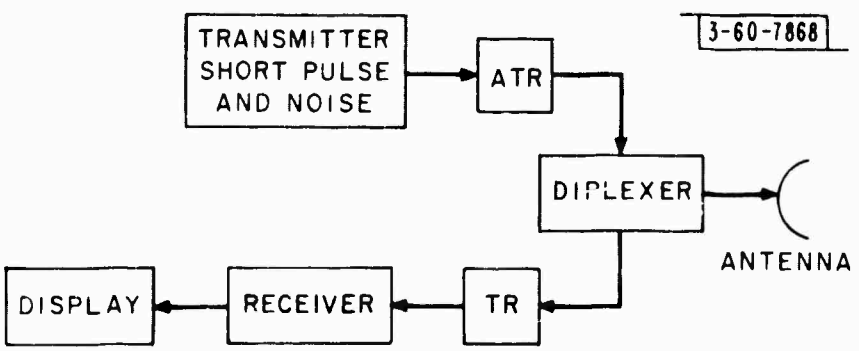

Fig. 2-1. Typical radar system.

Geodar (Fig. 2-2) contrasts with classical radar in the five following important ways:

(U) (1) The frequencies that the ground will transmit and the wavelengths required to observe a void of a given size are not fixed a priori, but are determined by soil conditions. Therefore, no carrier frequency is used on the transmitted pulse. A short (3-nsec) video pulse (exact length is not critical) is applied directly to the antenna. The antenna's bandpass characteristics, soil attenuation, and effective cross section of an object determine which one of the broad band of frequencies in the original video pulse is observed at the display.

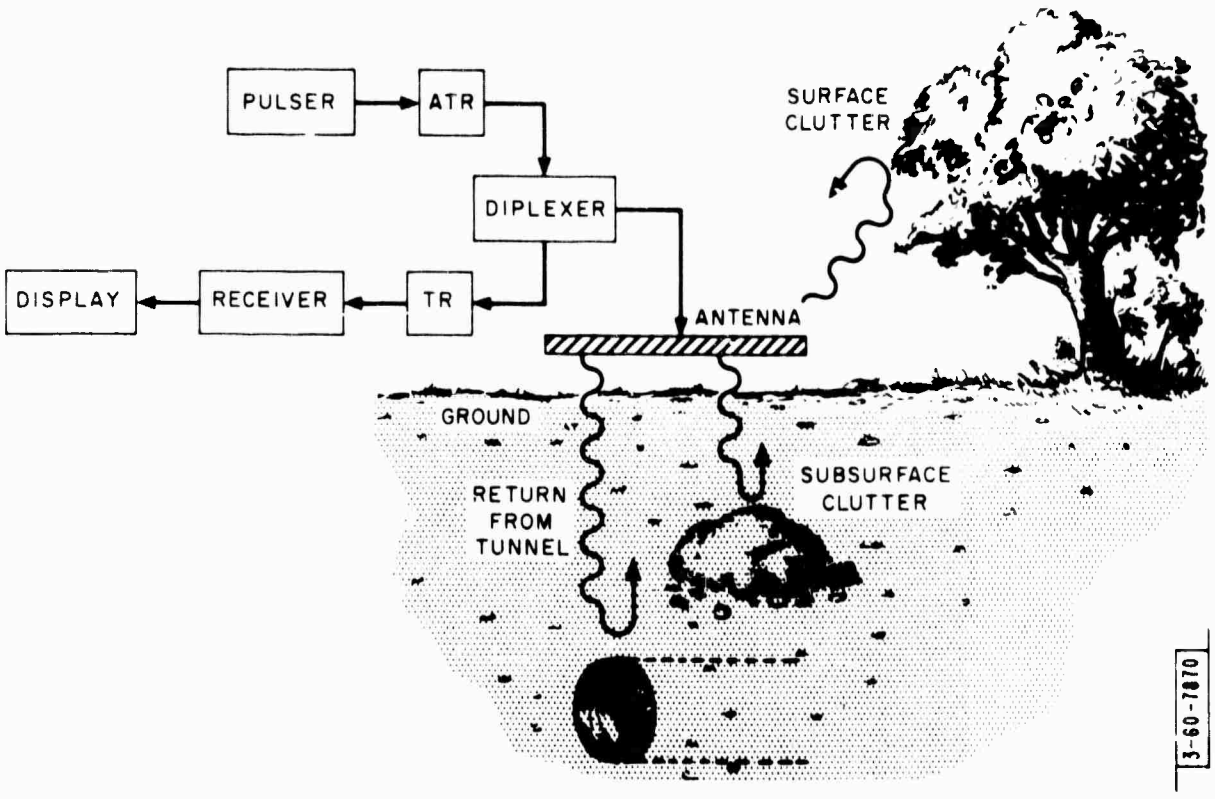

Fig. 2-2. Geodar system.

(U) (3) The antenna is small in terms of electrical transmission line wavelengths. Indeed, it is the smallest antenna-consistent with radiation in the necessary frequency range for reasonable losses in clay soil--having an electrical length of one-half wavelength in air at about 70 MHz.

(3) Internal reflections in the antenna and antenna feed system, are sources of signal-obscuring clutter. The electrical travel times in the Geodar antenna and antenna feed systems, are comparable with the range at which it is desired to see reflected returns. For example, the minimum time required for a Mark I pulse to reach the end of the antenna and for its reflection to return to the antenna input terminals is about 15 nsec; from an object or void three feet deep in the ground, 20 nsec; with total round-trip losses of 40 db. For the pulse to be visible amid clutter from internal reflections, the clutter must be 10 to 15 db below the signal return. Attenuation of internal reflection, or ring down of the antenna system, is thus an important design problem. Required ring down in the example cited is 50 to 60 db in 30 to 40 nsec.

(4) Substantial excess attenuation exists beyond the usual free-space radar path losses. The excess attenuation is of the order of 5- to 15-db-per-meter of radar range into the ground, and range in the ground is limited to a few tens of feet. For extended objects or voids, this means the antenna and the object are usually within the near-field diffraction zones of each other. Thus, the classical $(\text{distance})^{-4}$ law for free-space

path losses tends not to hold, being generally less than that given by the fourth power rule.

(5) All sources of external clutter are not equally attenuated as a function of range. Some energy escapes from the antenna into the air, and is reflected from trees, vehicles, people, etc., into the receiving system (Fig. 2-2). This clutter does not suffer the additional 5- to 15-db attenuation per meter of range as do signals from within the ground. This situation would be serious, except for two compensating factors. First, the antenna is an inefficient radiator into the air in the frequency range used. This inefficiency is due partly to modest size and internal termination, and partly to the shielding effect from operation close to the ground. Second, the velocity of propagation is normally three to five times slower in the ground than it is in air. Consequently, clutter arriving through the air at a given time comes three to five times further away than the corresponding signal from the ground, and is further attenuated.

B. Geodar Antenna Design Objectives

(U) Primary design objectives for the Geodar antenna system were to:

(U) (1) Let the antenna radiate a useful range of frequencies in terms of propagation and effective reflection within the ground.

(U) (2) Make the antenna a relatively ineffective radiator into the air above the ground.

(3) Cause clutter in the antenna system to be attenuated more rapidly with time than the potential return signal.

C. Mark I Antenna System

The Mark I antenna system (Fig. 2-3) has four parts: ATR, hybrid, TR, and antenna. The first three units were designed to keep the reflection coefficient presented to the antenna by the hybrid under 0.1 for a 3-nsec pulse.

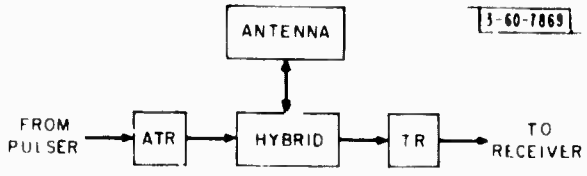

Fig. 2-3. Mark I antenna system.

The ATR network (Fig. 2-4) is a hot carrier diode, reverse-biased by about 3- to 4-v when 30-v pulses are delivered from the source with a 0.3-percent duty cycle. This diode isolates the antenna from pulser noise, and ensures that the coax line to the hybrid will be terminated properly in 50 ohms during the receive interval. Two ATRs are used at opposite ends of the pulser box output cable. Whether both are actually necessary, or whether the one just described would suffice, is an open question.

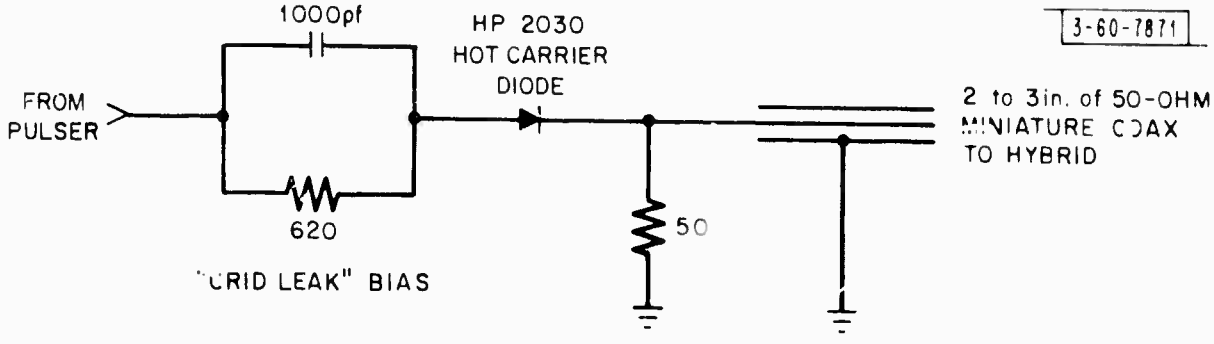

Fig. 2-4. ATR network.

The hybrid (Fig. 2-5) was constructed on a one-inch square of laminated fiberglass attached to a brass clamp that physically supports the hybrid and input and output coax lines to the pulser ATR and receiver TR, respectively. The hybrid is wired point-to-point and uses a conventional transformer circuit. The essential component of this hybrid is a VHF/UHF transformer (Fig. 2-6) developed by R. M. Lerner and R. W. Chick. This transformer is wound on two or three ferrite beads of Indiana General's Ferramic H material. Using reasonable care, it was proved possible to wind both isolation and autotransformers with 1.5 to 2.0 GHz of ratio-bandwidth product (e.g., 3-db bandwidth of 800 MHz at 2:1 impedance ratio; 250-MHz bandwidth at 7:1 impedance ratio), with impedances in the 15- to 450-ohm range. The lower 3-db point of this transformer is between 0.5 and 1.0 MHz. The midband insertion loss is between 0.5 and 1.0 db.

Cores in the autotransformers that feed the antenna and its dummy equivalent were matched to within 1/2 percent at 100 kHz. This low-frequency balance is important in order to remove the

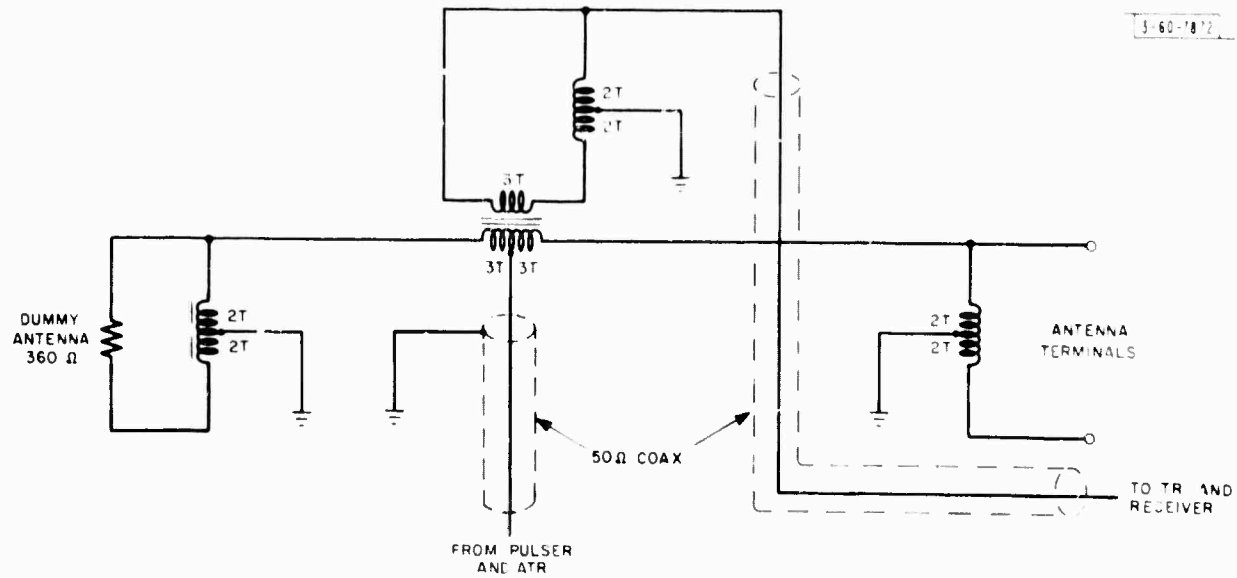

Fig. 2-5. Mark I hybrid.

low-frequency backswing transient formed by the autotransformer cores as they get rid of their magnetically stored energy following the main pulse. If left uncompensated, this backswing transient causes a serious base line tilt problem in the receiver output display. After some slight trimming of capacitive stray coupling, the hybrid exhibited generally 25 to 30 db of isolation at frequencies in the 50- to 100-MHz range, falling to 20 db at 250 MHz. The insertion loss midband is about 1.5 db, and the 3-db cutoff is over 300 MHz. Better hybrids were developed for Mark II.

The turns ratios in the hybrid were chosen for a 400-ohm antenna. The antenna used has 360 ohms. To be consistent with

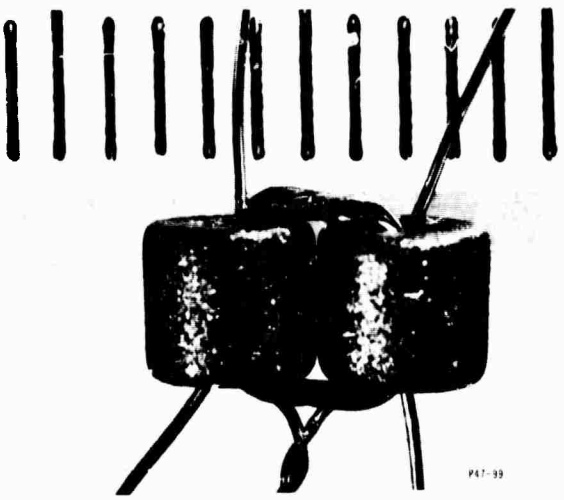

Fig. 2-6. (Left) Winding a ferrite-bead transformer. Scale: 1/16-in. between marks.

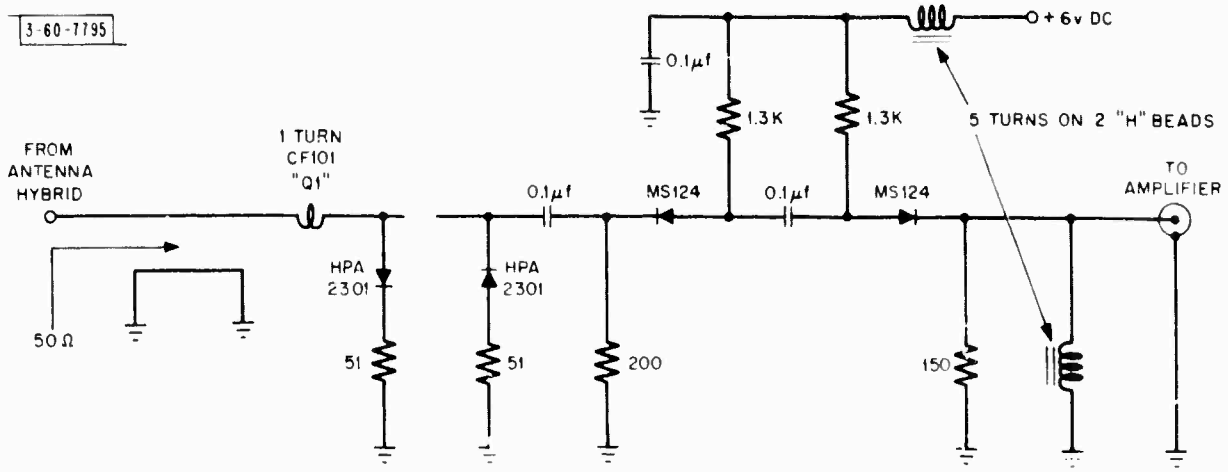

Fig. 2-7. Mark I TR circuit.

this impedance level, 300-ohm resistors were shunted across the ends of the coax leads to the ATR and TR.

The purpose of the TR is to protect the receiver against the high-power transmitter pulse (Fig. 2-7). Most of this isolation is provided by the hybrid, but it is necessary to protect the receiver against high pulse levels when the hybrid is accidently or deliberately unbalanced. All diodes are hot carrier types for speed of operation. CR3 and CR4 are low forward impedance types, selected for reverse breakdown near 20 volts. They are normally biased "on," at about 3.5 ma of current. Large signals due to internal antenna reflections or hybrid unbalance cause these diodes to turn off, disconnecting the receiver, while CR3 or CR4 turn on, maintaining the impedance match presented to the hybrid. Over a range of amplitudes up to 5 v, this circuit has a reflection coefficient for a 3-nsec pulse that is less than 0.1.

Matched sections of transmission line were put together to make the antenna (Fig. 2-8). The input and termination sections I and III, respectively, are sections of conical-type transmission lines. They are actually flat fans. If the angular width of a single gore of such a fan is 2α, then the free-space Z_0 of such a fan (with equal and opposite gores) is given by

$$Z_0 = \frac{377}{2} \frac{K(\cos \alpha)}{K(\sin \alpha)},$$

where the function K is the complete elliptic integral of the first kind. Note that when α is 45°, Z_0 is one-half that of free space, as required by Babinet's principle.

In the actual antenna, the gores of the fan narrow to 7/16 in. rather than to sharp points. This amounts to the use of a tapered transmission line, tapering to lower impedances as one

approaches the drive and termination points. The tapering also introduces a shunt capacitive component to the Z_0 as observed from these point. The theoretical Z_0 of transmission lines I and III is 450 ohms, each line having an overall length of about 36 in. As a matter of actual measurement with 1- to 10-nsec pulses, the

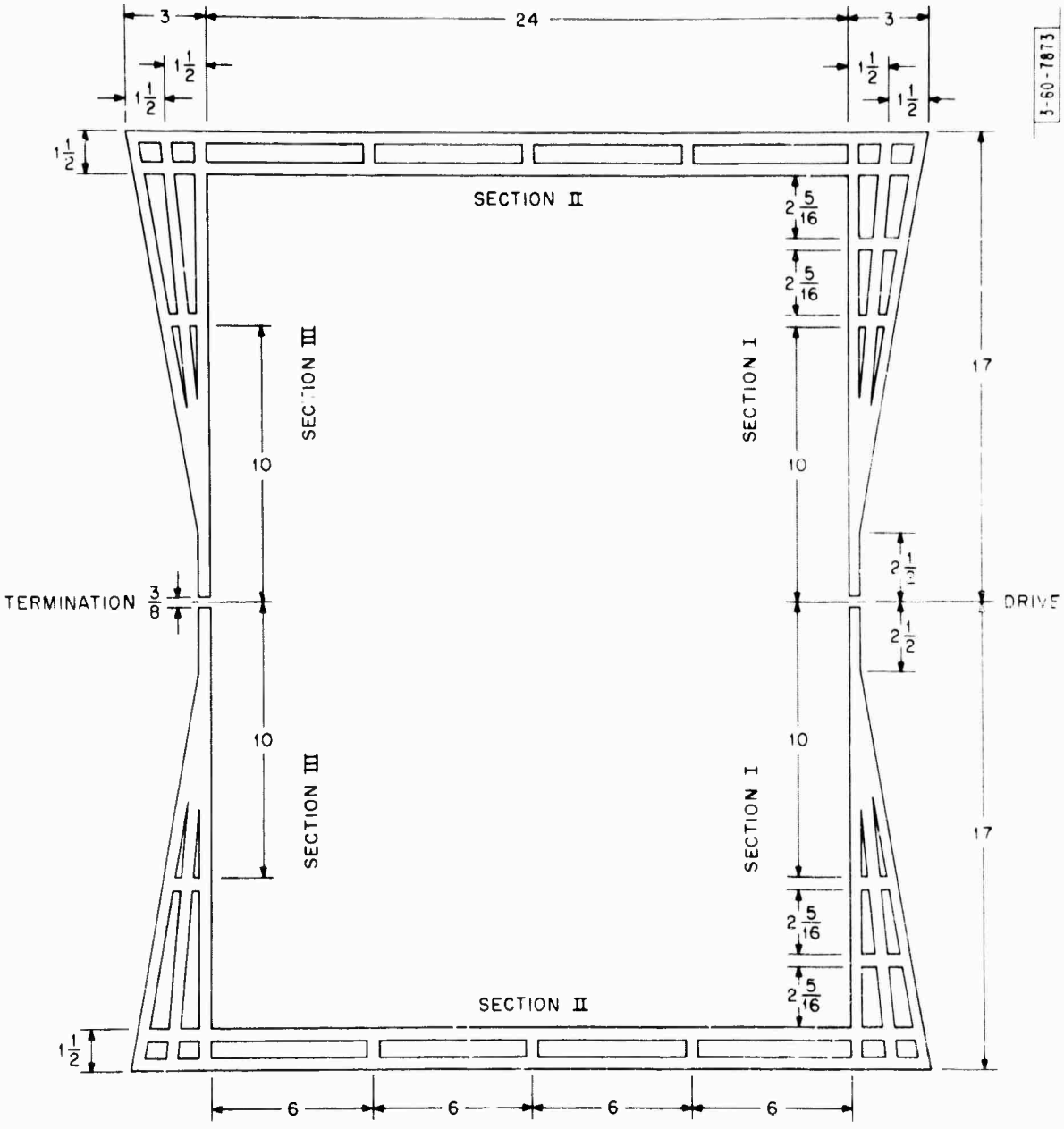

Fig. 2-8. Mark I antenna made of 7/16-in.-wide copper tape.

real part of the Z_0 as transformed by tapering is matched by a 1/8-watt, 360-ohm metal film resistor, and the capacitive part by three turns of wire (No. 30 was used, but adjacent sizes are possible), wound on an Indiana General CF101-style toroid of Q2 ferrite material. The resulting termination match is in the 25- to 30-db reflection loss class, the best match having been set up with the antenna six inches above damp, compacted, loamy soil.

The parallel strip transmission line II is built by photo-etching or by laying down adhesive-backed copper tapes on a flat sheet of laminated fiber glass, in the plane of the input and output fans. The moveable tapes facilitated experimental adjustment of antenna configurations. In particular, the width of strip-forming transmission line II was determined by reducing the reflections from the corners where II meets I and III to a minimum by using 1-nsec pulses.

When using 3- to 10-nsec test pulses, the residual sources of reflection within the antenna appear to be located near the points at which the tapered sections of I and III meet the untapered sections.

D. Antenna Construction Requirements

The amplifiers, gain control circuits, and pulse generator are mounted in separate boxes on the Mark I antenna, but are collected in one box near one edge of the Mark II antenna. These circuits and the umbilical that connects the antenna to the display unit form a system of conductors near the antenna, and in the near-field of the antenna, that can create resonant loops and other reflections, which if unrestricted, will obscure the desired signal. To avoid these problems, all the following measures proved necessary:

(U) (1) Antenna is driven balanced to ground.

(U) (2) Component boxes and connections to the umbilical have been placed in, or close to, vertical neutral plane of the balanced antenna.

(U) (3) Leads between boxes have been kept short.

(U) (4) Ferrite "shielding beads" (many are actually toroids) have been used liberally to break up potential reflections and resonant loops in connections between boxes on the antenna, and, in particular, to negate ground loops formed by outer conductor on coaxial cables.

(U) (5) Umbilical is "choked" with toroidal "beads" at one-foot intervals for the 10 feet closest to the antenna.

(U) (6) Pulser is packaged in a ventilated, RF-tight box.

With these precautions, plus the antenna layout and termination described previously, the Mark I antenna system rings down with internal clutter falling in steps of about 20 to 25 db every 10 nsec after the main pulse, when the antenna is 2 to 12 in. above well-compacted loam.

(U) Three considerations lie behind the choice of a flat antenna operating close to the ground:

(U) (1) If radiation takes place first into air and then via far field into ground, it will be difficult to prevent most of the radiated power from going into the air to produce clutter returns from people, trees, etc.

(U) (2) By maintaining proximity to the ground, it is possible to radiate low frequencies that would not be radiated if the near-field of the antenna is away from the ground. This radiation of low frequencies from the near-field of the antenna takes place at angles away from the vertical because the antenna is large compared with a wavelength in the ground at, e.g., 50 MHz, although it is much too small to radiate in terms of wavelengths in the air. (This antenna is not being operated for high efficiency, so this low-frequency radiation does not result in major changes in transmission line behavior of antenna elements.)

(3) There is a critical angle phenomenon associated with the reflection of a travelling wave across a dielectric interface, such as that between air and ground. The effect of this phenomenon is to restrict the angle of the cone of visibility underneath antenna to a half-angle of from 12 to 20 degrees (depending on the dielectric constant of the ground) unless the ground intercepts a substantial part of the near-field zone of the antenna structure. (A wide angle of subsurface visibility is essential to success of the sonar display scheme to separate interesting objects from clutter induced by layering in the ground.)

Lifting the radiating center of the antenna off the ground degrades the three foregoing conditions, but for lack of sufficient extensive experimental facilities, it is not possible to support these facts with meaningful quantitative measurements. Qualitatively, there is little difference in the Mark I return when the antenna is 2 to 8 in. above ground, but precipitous degradation in reflection occurs at the two-foot level. Measurements of

returns as a function of height above the ground are included in Chapter 12. Time and lack of appropriate test facilities prevented obtaining corresponding data on the increase of clutter and external interferences as the antenna is raised.

E. Antenna Development History

(U) Geodar was conceived as an airborne system analogous to vertical-sounding sonar systems that "see" below the ocean bottom. A few rough calculations showed that the potential signal-to-clutter ratio for such a system was disasterously defective. Clutter rejection with non-real-time artificial apertures also seemed unequal to the task. In addition, there were awkward problems concerning the size antenna required. The calculations were then repeated with the antenna a few meters above ground. The clutter problem improved, but the antenna was still uncomfortably high for a simple reflectometer system, and antenna awkwardness remained. The situation became tractable when the antenna was placed electrically close to the ground.

Given that operation close to the ground was contemplated, detection by acoustic means was considered, and found to suffer from the following difficulties:

(1) Problems in the design and construction of portable transducers that make good contact with the ground.

(2) The fact that acoustic propagation is inherently more complicated than electromagnetic propagation (being governed by a fourth-order partial differential equation, instead of a second-order one) acoustic propagation would be prone to see more discontinuities (clutter) within the ground.

(3) Owing to soil compaction with depth, there tends to be strong positive gradient of acoustic velocity with increasing depth into the ground that tends to prevent penetration of wavelength range of interest in precisely the same manner as does the ionosphere for electric waves, the deep ocean inversion layer for sonar waves, and the interface refraction for someone trying to look out of water into air. In contrast, electromagnetic propagation tends to be, if anything, slower as one goes down into the ground--owing to increasing moisture content; like looking from the air into water.

In any event, a number of organizations were at work investigating the possibilities of acoustic techniques, whereas the electromagnetic technique appeared to have had limited exploration. The electromagnetic method had been tried at Ft. Belvoir, but without success. The failure appeared to have been a matter of detail in concept and execution, and not of using a short-pulse reflectometer.

From the beginning, then, the concept was one of an electromagnetic antenna with broad bandwidth and fast ring down operating electrically close to the ground. In keeping with this concept, the antennas tried, with few exceptions, have been flat structures. The major exception was a qualitative experiment with probes or rods stuck into the ground. The impedance of such probes was probably both high and not well defined. Regardless, signal returns were too small to encourage further efforts with the probes.

(U) In consideration of the desired broad bandwidth, the first antenna structure tried at Lincoln Laboratory was log-periodic (Fig. 2-9). It was two feet in diameter and calculated to have

a driving point impedance of 188 ohms. The two outer arms were brought together with a pair of 360-ohm terminations to eliminate unwanted low-frequency components. Admittedly, this was crude termination, but it uncovered the next layer of difficulty, namely, the inherent phase distortion in log-periodic structures. This phase distortion results in a system transient response that is not compact in time, but smeared out in an oscillatory manner. It is inherent in log-periodic systems because the delay, as well as other properties of the antenna, must vary logarithmically with frequency. It is particularly severe in multiple resonance structures like that in Fig. 2-9. In effect, each of the resonant arms and slots of the structure is excited by the transient and ring down as a medium to high Q structure.

Just as it is possible, in principle, to compensate for delay distortion in a lumped element structure, so too, it would be possible, in principle, to do the same for a dispersive antenna structure. Given the ring down requirement, this would be an unattractive practical prospect even with lumped circuits. It was considered as unattractive for the log-period antenna.

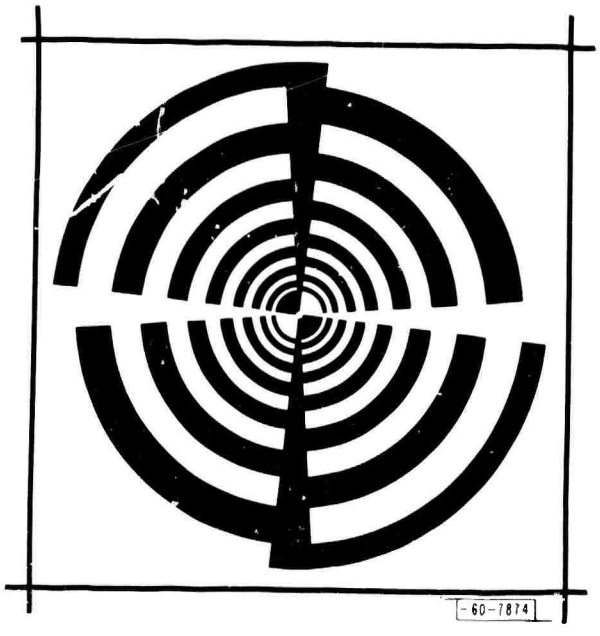

Fig. 2-9. Original antenna.

The arms were cut off the structure outside the 45° lines, and strapping was used to convert the shape into a pair of flat, triangular fans or gores, each coupling opposite quadrants of the

(U) former circle. These steps retained the 188-ohm impedance. The long outer arms were also kept for the purpose of supporting the terminating resistors. With this crude antenna, plus a commercial hybrid, pulse generator, and sampling oscilloscope, it was possible to "see" steam pipes five feet below the Laboratory's front lawn and a wooden box three feet beneath the surface of compacted loam.

With this antenna, measurements were made to determine how close the antenna should be operated above the ground. Figure 2-10 is the return with the antenna on the surface of the loam pile, and Fig. 2-11 is the same return with the antenna lifted 4 inches above the surface. A radical change occurred within the first inch as the air, in effect, insulates the transmission line antenna from the high dielectric constant of the ground. On the basis of this change, it was decided to design all future antennas for operation at least two inches above the surface of the ground.

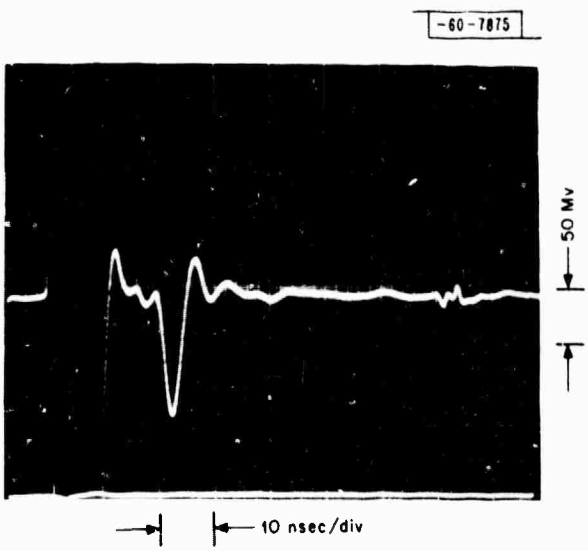

Fig. 2-10. Oscilloscope display of signal return from tunnel 3 ft below the surface of a loam pile with antenna on the surface.

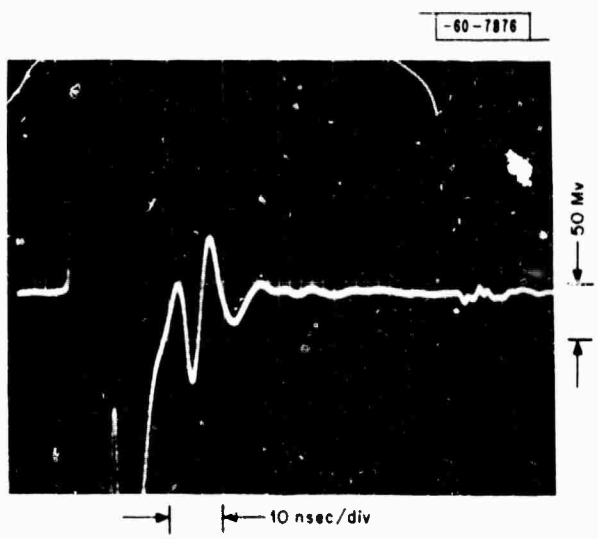

Fig. 2-11. Oscilloscope display of signal return from tunnel 3 ft below the surface of a loam pile with antenna 4 in. above the surface.

(U) The next step was to try to decrease the internal reflections in the antenna by designing the return arms--containing the terminations--with twice the characteristic impedance of the central fan. The central fans were narrowed to subtend angles of approximately 60°, which Z_0 computed to be 240 ohms. The return legs were computed to be 480 ohms, and were so terminated (Fig. 2-12). The central fan was still only two feet long, but the addition of return transmission lines raised the width to about 34 inches. A pronounced internal reflection (15 percent) then appeared where the fans touched, but was reduced by inserting a series resistor between the fans.

With antennas at least two inches above the ground, the transient return from an object directly under the antenna seemed to be too short to be consistent with the frequency range necessary for satisfactory propagation through lossy soils. An electrically larger antenna seemed to be needed. There was reluctance to increase the physical size of the antenna because of increased awkwardness in portability and possible performance degradation of the antenna was made larger than the dimension of observed objects. As an alternative, an attempt was made to slow down the velocity of propagation on the transmission lines by inductive loading, and the center of the middle gore (largely inactive) was cut out to eliminate discontinuity where the central gore touched the two outer termination returns. It was possible to slow down the propagation to about 0.7 of the former velocity by inductive loading without substantially degrading the size of the return. Further loading lowered antenna efficiency and weakened signal returns. This antenna [Mark IA (Fig. 2-12)] was the first antenna used with the Mark I system.

(U) Meanwhile, A. R. Dion of the M.I.T. Lincoln Laboratory had

showed that it was possible to obtain the same transmission line delay, the same transient response between antennas in air, and lower internal reflections without the use of loading coils by running 3/8-in. tubing around the periphery of the area occupied by the Mark IA antenna. This antenna was driven in the middle of one of the long sides and terminated in the middle of the 300-ohm opposite side (Fig. 2-13). The revised version replaced the Mark IA antenna, and was called the Mark IB antenna.

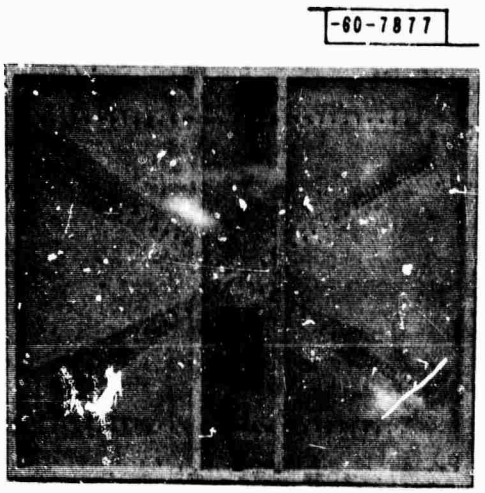

Fig.2-12. Mark IA antenna.

Two major difficulties became evident with continued operating experience with Mark I:

(1) The transient response of a transformer caused a base line slope problem. This problem was eliminated when Mark I was retrofitted with the hybrid, balanced at low frequencies.

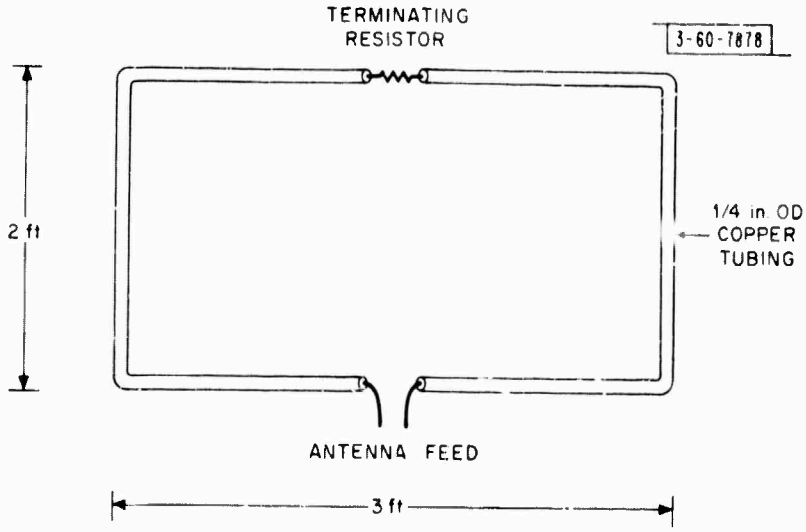

Fig. 2-13. The Mark IB antenna.

(U) (2) Ring down time was not good enough. The remedy was to make the antenna transmission line structure well-terminated at the source end, as well as at the termination end This termination involved replacing a simple diode TR device with a more complex circuit, and carefully attempting to obtain low reflection coefficients at the ends of the Mark IB antenna. The latter attempt showed that IB antenna did not have a well-defined broadband driving point or terminating impedance. The legs of the IB antenna were then replaced by the transmission line structures (Fig. 2-8). The redesigned antenna [Mark IC (Fig. 2-14)] is the antenna used for Mark I and II Geodar.

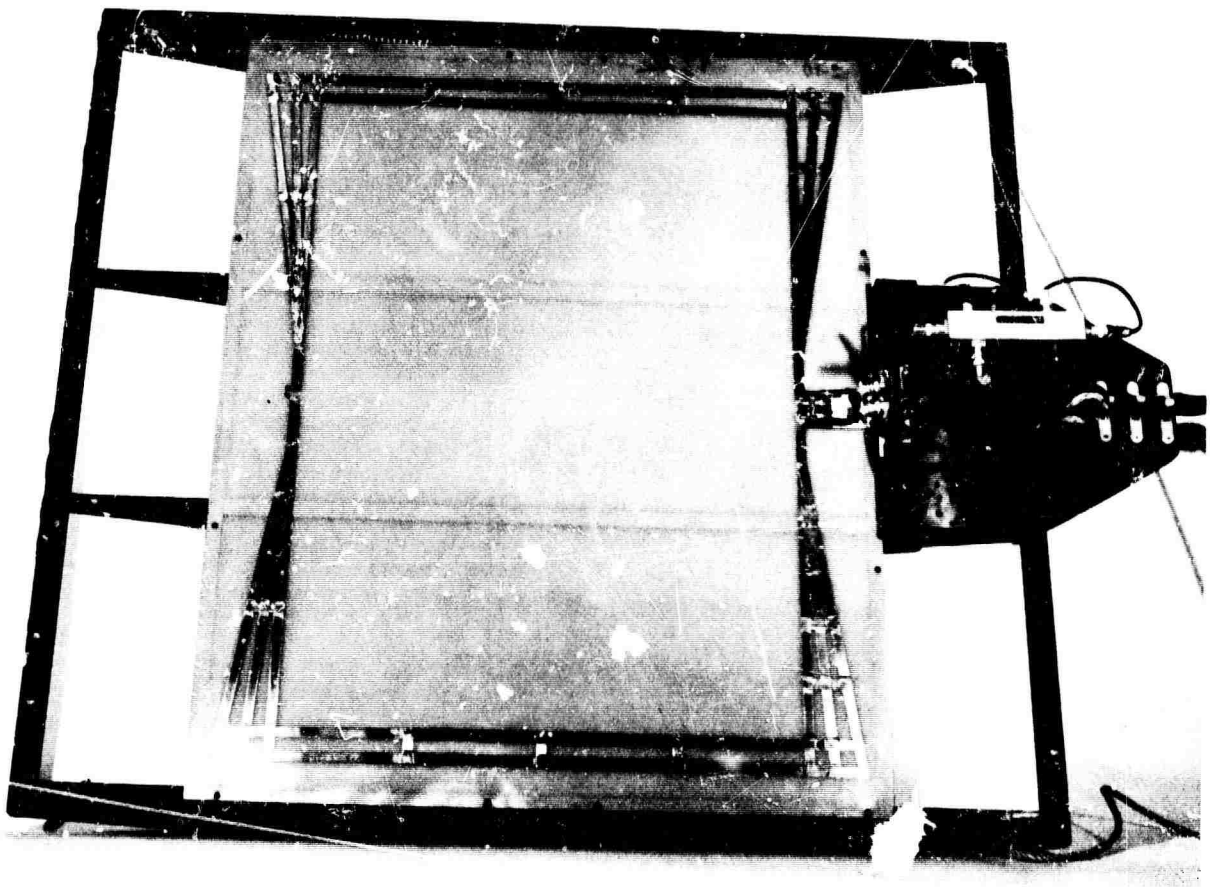

Fig. 2-14. Mark IC antenna.

A final experiment was made to adjust the dimensions of the IC antenna. The long dimension [legs I and II (Fig. 2-11)] was shortened to three-quarters, and, then, to one-half its original length. The return from a standard two-foot-wide object buried 5-1/2 feet below the surface of a pile of dirt dropped by a factor of two in the first shortening, and another factor of two in the second. The return from similar objects, 9-1/2 feet below the surface, dropped somewhat more in the first shortening, and completely disappeared in the second. On the basis of these tests, it was decided not to shorten antenna IC.

3. PULSER

A. Mark I

The Mark I pulse circuit is a repackaged version of the Texas Instruments (TI) 6701 pulse generator, and includes the pulse generator card and avalanche circuit protective circuitry from the TI pulse generator. The avalanche protection circuitry was remounted on the pulse generator card.

The frequency range adjustments on the pulse generator card were eliminated, and the circuit was wired for use in only the external trigger mode. A charge line was cut for an output pulse width of 3 nsec, and placed on the circuit board.

To allow the avalanche transistor to feed the 50-ohm output line directly, the output balun and amplitude adjustment control were removed from the output circuit.

The entire circuit was shielded in a square brass box and mounted in the antenna unit.

B. Mark II

The pulse circuit for Mark II (Fig. 3-1) uses the same transistor as the TI pulse generator in the voltage biased mode. The voltage on the avalanche transistor is set at about 160 v. The transistor is base triggered.

Transistors Q1 and Q5 in the trigger circuit for the avalanche circuit amplify and shape a 2- to 3-v input pulse to produce a 10-v 20-nsec trigger pulse at the input to the base of the avalanche transistor Q6.

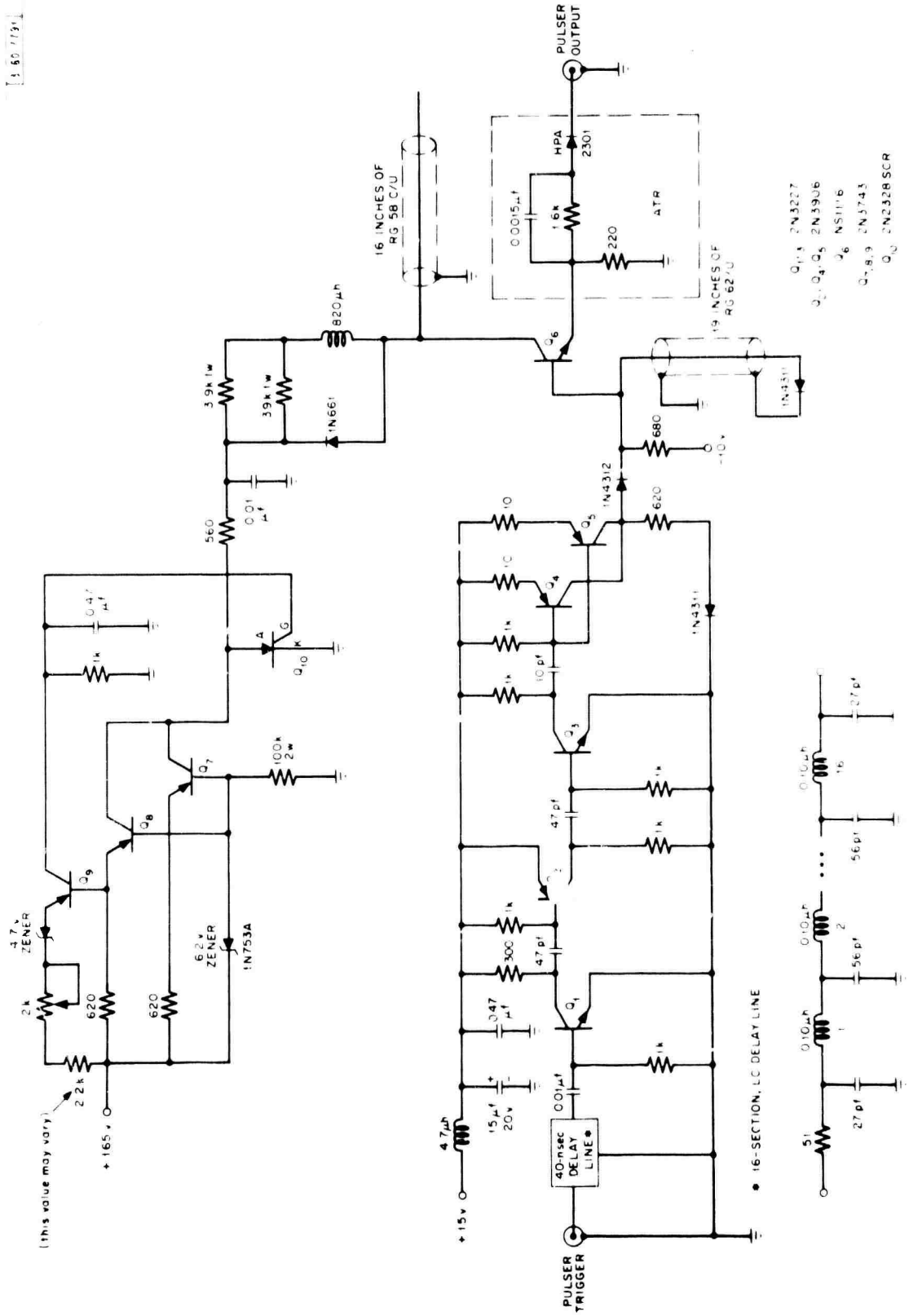

Fig. 3-1. Pulser, Mark II.

The output pulse width is determined by the charge line, which consists of about 16 inches of RG-58 cable connected to the collector of avalanche transistor Q6 (Fig. 3-1), and gives a 5-nsec pulse width. The falling edge of the output pulse is speeded up and shaped by the 19 inches of RG-62 cable connected to the base of Q6. The charge on the collector charge line is replaced rapidly by the coil-resistor-diode circuit in the collector circuit of Q6. This replacement is faster than using a simple RC charge circuit, and allows the avalanche circuit to be operated at repetition rates as high as the 1-MHz rate used in Mark I and II equipment.

The ATR switch consists of a RC network and diode connected to the emitter lead of Q6 and is designed to disconnect the pulse circuit from the output line after the pulse has passed through. This technique prevents the pulse circuit from introducing spurious signals into the system. This circuit is designed to feed the network with a resistive load or a transformer coupled load.

The transistors and SCR (Q7 through Q10) protect the avalanche transistor from being destroyed if an overload condition occu . Transistors Q7 and Q8 provide a constant current source of approximately 22 ma. Transistor Q9 is used to sense the current through the 620-ohm resistor and triggers the SCR (Q10) to conduct when about 18 ma is flowing to the avalanche transistor. This trigger point (18 ma) may be varied slightly by adjusting the 2-K ohm potentiometer in the emitter circuit of Q9. Once the SCR (Q10) has fired, the collector terminal of the avalanche transistor is clamped to zero volts, and the constant current circuit (Q7 and Q8) limits the current to 22 ma.

During the normal operation of the avalanche circuit, the current drawn by the avalanche transistor is about 14 ma. This current causes Q8 and Q9 to operate at saturation and biases the avalanche transistor at a constant voltage. When the overload circuit trips, constant current operation occurs. The circuit is reset by interrupting the supply line or by dropping the supply voltage momentarily to zero.

To ease timing requirements in the trigger source, the 40-nsec delay line in the input circuit is a 16-sec LC lumped delay line used to delay the trigger pulse.

4. RECEIVER

The receiver section of the system separates returns from the transmitted pulse and amplifies them to a level suitable for display. Block diagrams of the Mark I and II receiver arms, together with the pulse generator and antenna, are shown in Figs. 4-1 (a, b).

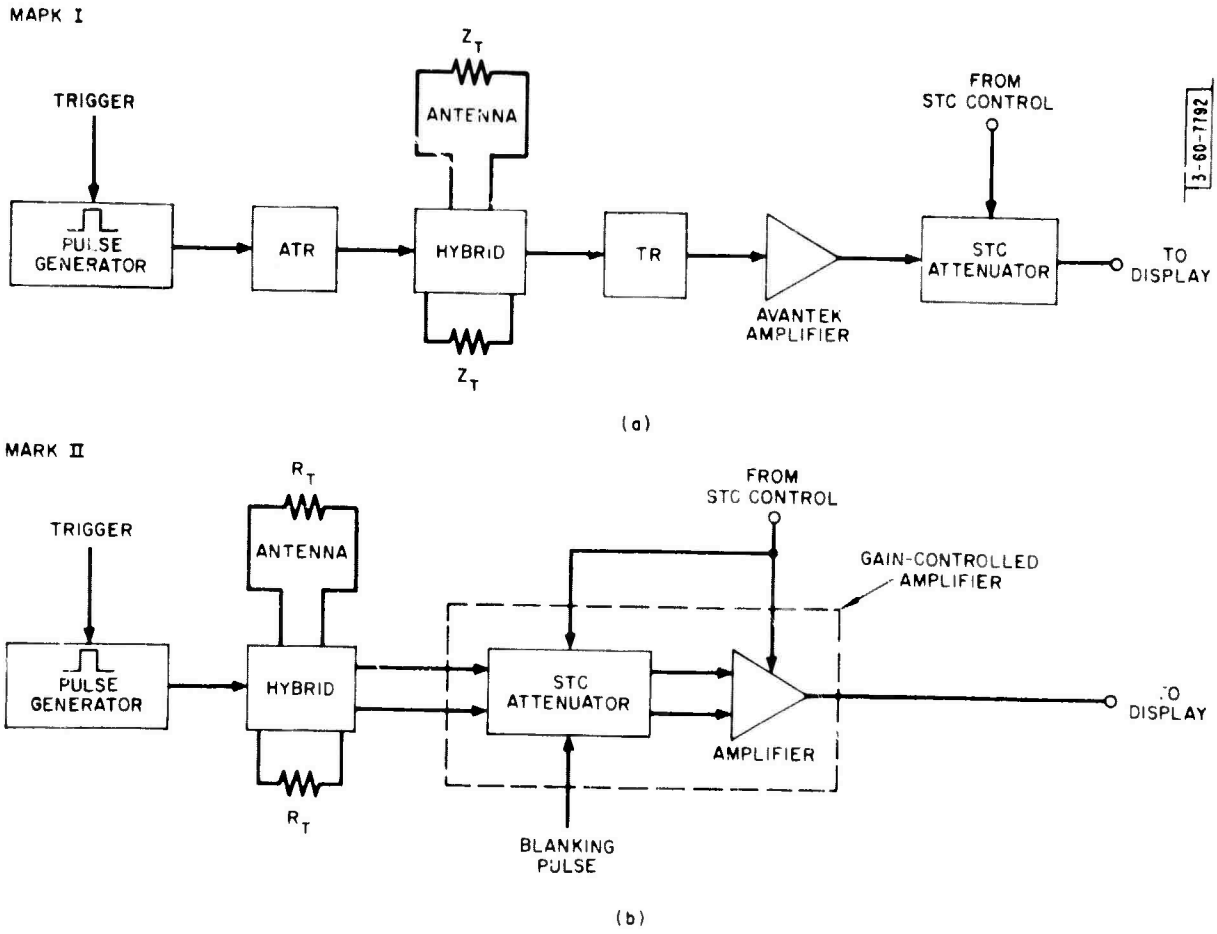

Fig. 4-1. RF block diagram for Mark I (a) and II (b).

A. Mark I and II Hybrids

In the Mark I hybrid (Fig. 4-2), transformer T1 prevents the common-mode, pulse generator current from coupling to the receiver amplifier balun (T4) when the loads provided by T2 and T3 are identical. T2 and T3 balance the drive to the antenna and dummy load. The remaining components serve as reactive compensation to broaden the bandwidth. Note that the load on T1 is

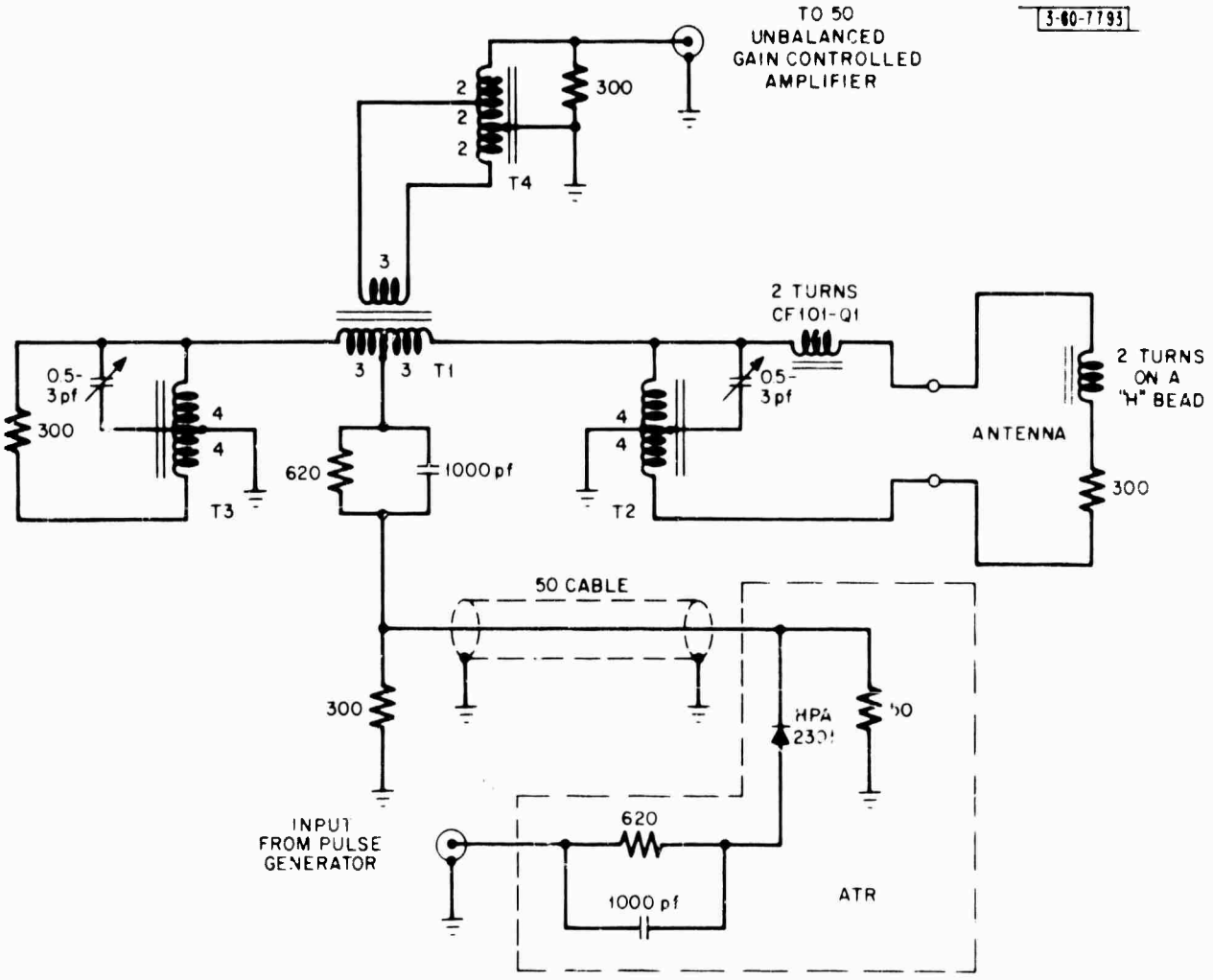

Fig. 4-2. Antenna hybrid circuit diagram, Mark I.

balanced even beyond the system passband to ensure good receiver decoupling, even at frequencies to which the antenna does not respond. About 40 db of receiver isolation was obtained with this hybrid, with about a 1-nsec degradation in transmitting pulse rise time to the antenna.

The ATR is located at the input to the hybrid in Mark I (Fig. 4-2), but is relocated within the pulse generator in Mark II. The ATR circuit eliminates noise voltages riding on the base line of the pulse generator output.

In principle, the Mark II hybrid (Fig. 4-3) is similar to the Mark I unit. Both T1 and T4 suppress common-mode currents

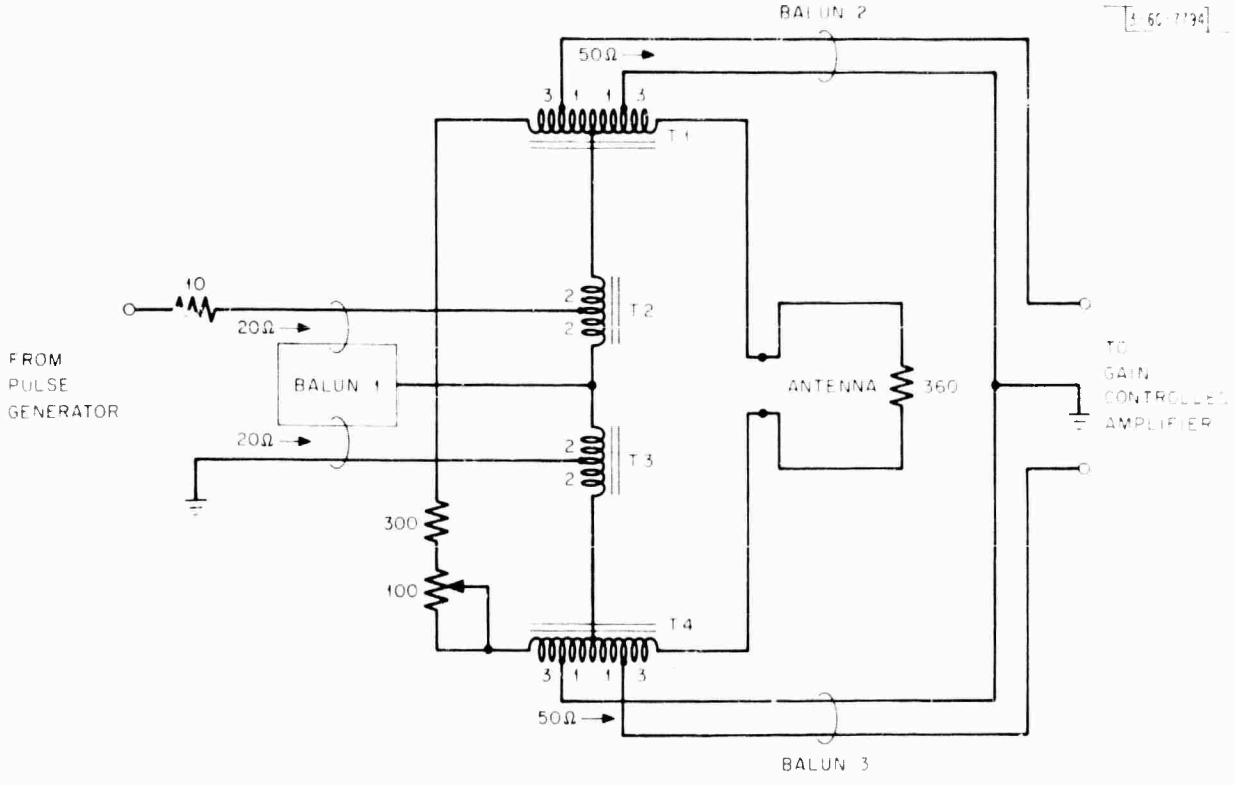

Fig. 4-3. Antenna hybrid circuit diagram, Mark II. Chokes for baluns consist of 17 H beads and two turns on 3E pot core. Cores for transformers consist of two H beads. One-turn windings on transformers T1 and T4 are 1/16-in., gold-plated strap separated by 1 mil mylar tape positioned to electrostatically decouple the three-turn segments.

to the receive amplifier, while T2 and T3 are simply impedance matching transformers. Baluns 1, 2, and 3 are transmission lines encased in ferrite. The lines of balun 1 are made of two straps of gold-plated copper (0.004 in. x 0.045 in.) separated by mylar tape (0.001 in.). In baluns 2 and 3 (Uniform Tubes UT-37), 50-ohm coaxial lines are used. Sixteen Indiana General Corporation (IGC) ferrite beads (FI650-1-H) were strung on each of these lines, and this structure was, in turn, wound in a ferrite pot core of higher permeability (two turns wound in Ferroxcube 2213-P-3E). The remaining transformers were wound on a ferrite core consisting of four of the above IGC H beads.

The winding configuration of transformers T1 and T4 is somewhat unique: the two one-turn windings consist of the two conductors in a 20-ohm strap transmission line; the two three-turn windings are then wound on opposite sides of the straps. These arrangements maintain a good capacitance balance in the transformer.

There are three principal advantages to the Mark II hybrid, which uses only autotransformers with simple windings: (1) much broader bandwidth, (2) slightly better isolation, and (3) improved impedance matching. As a result, there appears to be no requirement for reactive compensation.

The Mark I and II hybrids are wired on glass epoxy circuit boards. The printed circuit lands are arranged symmetrically, and node capacitances are reduced as much as possible.

B. Mark I TR, Amplifier, and STC

For signals greater than 0.3 v in the Mark I TR circuit (Fig. 4-4), the HPA 2301 hot carrier diodes in series with 51-ohm

resistors provide line termination, while the MS 124 diodes block the signal path to the amplifier input. At low signal levels, however, the HPA 2301s become open circuits, and the MS 124s couple the signal to the amplifier input. The reverse breakdown of MS 124 diodes restrict the maximum peak voltage to 5 v, but diodes with 30-v breakdown are available.

An Avantek AV-1, unbalanced, video amplifier is used in Mark I, and its specifications are detailed in Table 4-1.

The sensitivity time control for Mark I is achieved by using the STC attenuator (Fig. 4-5). Its electrical characteristics are listed in Table 4-2; and a curve for attenuator controlling voltage (with the 500-ohm STC potentiometer adjusted for maximum sensitivity vs attenuation) is given in Fig. 4-6. Because of the broad bandwidth required, isolating baluns T1 and T2 (Fig. 4-5) could not be electrostatically shielded. Instead, it was necessary to wind the transformers for optimal magnetic coupling to minimize the effect of capacitance unbalance and retain a broad bandwidth.

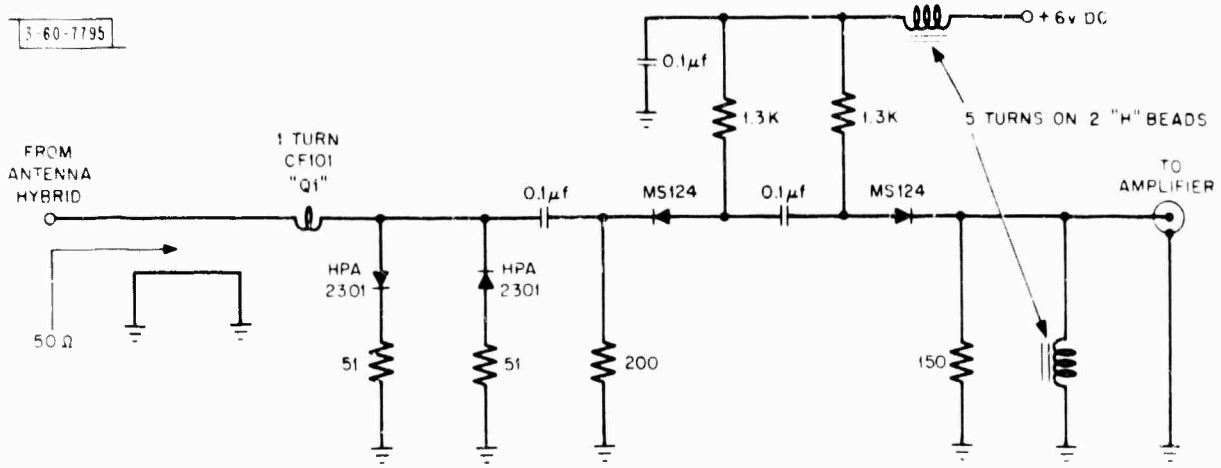

Fig. 4-4. TR circuit, Mark I.

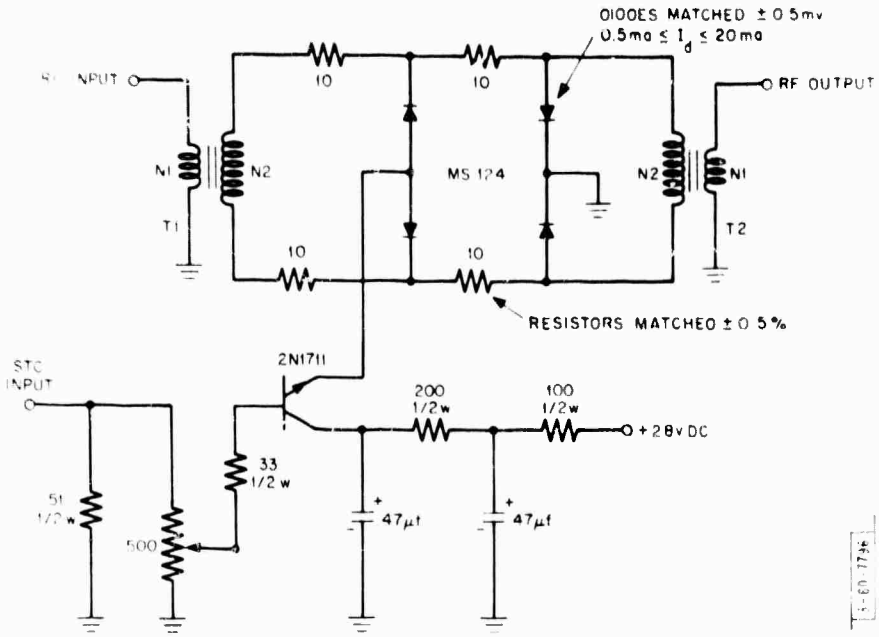

Fig. 4-5. STC attenuator, Mark I. Transformers T1 and T2 were constructed on a pair of Indiana General Corp. H ferrite beads. N1: 3 turns of No. 32 QF wire; N2: 6 turns of No. 36 AF wire.

TABLE 4-1

SPECIFICATIONS: AVANTEK AMPLIFIER AV-1 (10 kHz - 400 MHz)

Frequency range	10 kHz to 300 MHz min.
Gain	29 db min.
Impedance level	50 ohms in and out.
VSWR	2 to 1 max. 1.5 to 1 typical.
Rise time	1 nsec.
Saturated power output at 1 db gain comp point	+19 dbm min., typically +20 to +21 dbm, generally +17 dbm at 400 MHz.
Gain flatness	±1 db from 10 kHz to 300 MHz; typically down 3 db at 400 MHz.
Noise figure	8 db max. 6 to 7 db typical
Equivalent input noise level	30 μv max., 20 μv typical.

Pulse droop	20 percent max. for an 8 μs pulse.
Power input	+28 v DC at 200 ma.
Size	4-3/4 in. x 2-3/8 in. x 1-3/8 in.
Weight	12 oz.

TABLE 4-2

MARK I STC ATTENUATOR ELECTRICAL CHARACTERISTICS

Frequency response

-1 db, 2.1 - 320 MHz.

-3 db, 1.0 - 367 MHz.

Min attenuation (50 MHz), 2.0 db.

Response to a unit step (100 ps rise to 1/4-v amplitude)

Rise time, 1 nsec.

Overshoot, approximately 5 percent.

Pulse attenuation characteristics (input pulse 0.58-v peak with 1 nsec rise and fall times and 2 nsec width at peak)

Dynamic range--linear attenuation approximately 20 db.

Maximum signal compression--approximately 32 db.

Control signal isolation greater than 45 db for entire dynamic range using 1 MHz square wave as controlling signal.

Control speed, the attenuation may be varied at a rate greater than 2 db/nsec.

Impedance

Signal arm reflection coefficient for small signals in a 50-ohm system, about 0.4

Control arm input impedance 50 ohms.

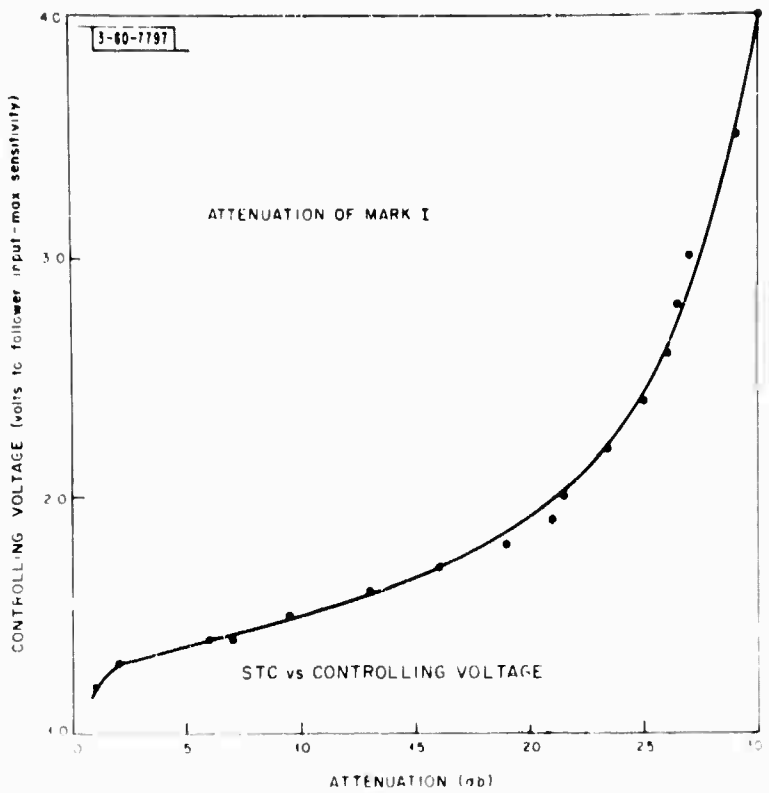

Fig. 4-6. Attenuation of Mark I STC vs controlling voltage.

C. Mark II Gain Controlled Amplifier

The functions of TR switching, amplification, and sensitivity time control are combined in Mark II (Fig. 4-7). The composite unit is called the gain controlled amplifier, or STC amplifier. The electrical characteristics for the amplifier are given in Table 4-3, and additional performance information is given in Figs. 4-8 to 4-11. Figures 4-9 and 4-10 show the pulse rise characteristics of the amplifier. The droop in these waveforms is attributable to the Anzac H81 hybrid, which has a 2-MHz, low frequency cutoff at the 1-db point. Typical amplifier gain variation (Figs. 4-8, -11) is a function of the STC controlling voltage. A change in the STC sensitivity settings changes the shape of the curve in Fig. 4-8.

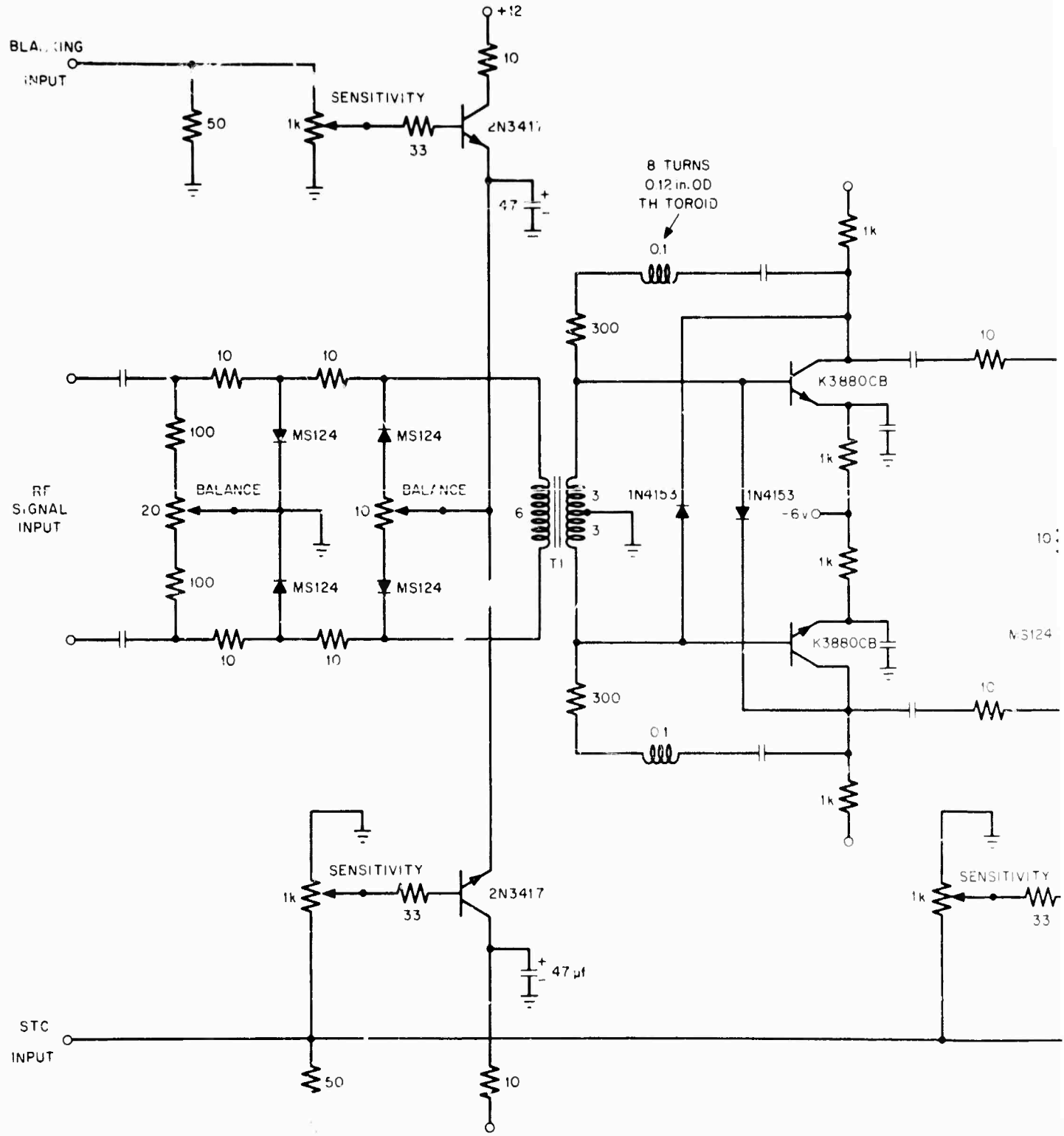
+12
10
BLA..ING
INPUT
50
SENSITIVITY
1k
33
2N3417
47
8 TURNS
0.12 in. OD
TH TOROID
0.1
1k
300
10
K3880CB
10
10
100
MS124
MS124
1k
RF
SIGNAL
INPUT
BALANCE
20
BALANCE
10
6
3
3
T1
1N4153
1N4153
-6v
100
MS124
MS124
1k
K3880CB
MS124
10
10
300
10
0.1
1k
SENSITIVITY
1k
2N3417
33
SENSITIVITY
1k
33
47 µf
STC
INPUT
50
10

2

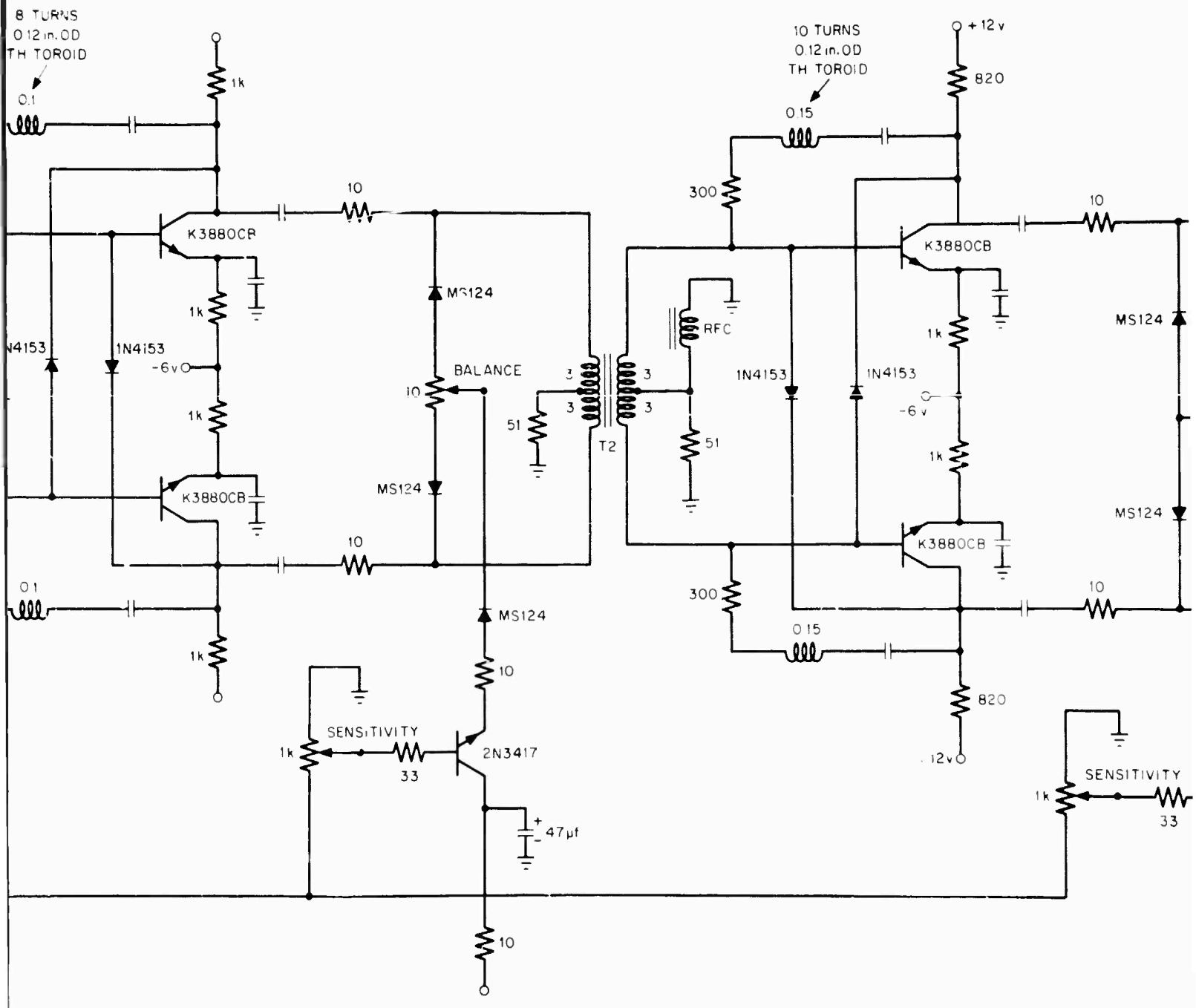
8 TURNS
0.12 in. OD
TH TOROID
0.1
1k
10
K3880CB
1k
1N4153
-6v
1k
K3880CB
MS124
BALANCE
10
MS124
10
0.1
1k
MS124
10
SENSITIVITY
1k
33
2N3417
47µf
10
T2
3
3
3
3
51
RFC
51
1N4153
1N4153
10 TURNS
0.12 in. OD
TH TOROID
0.15
300
+12v
820
10
K3880CB
1k
-6v
1k
K3880CB
MS124
MS124
300
0.15
10
820
12v
SENSITIVITY
1k
33

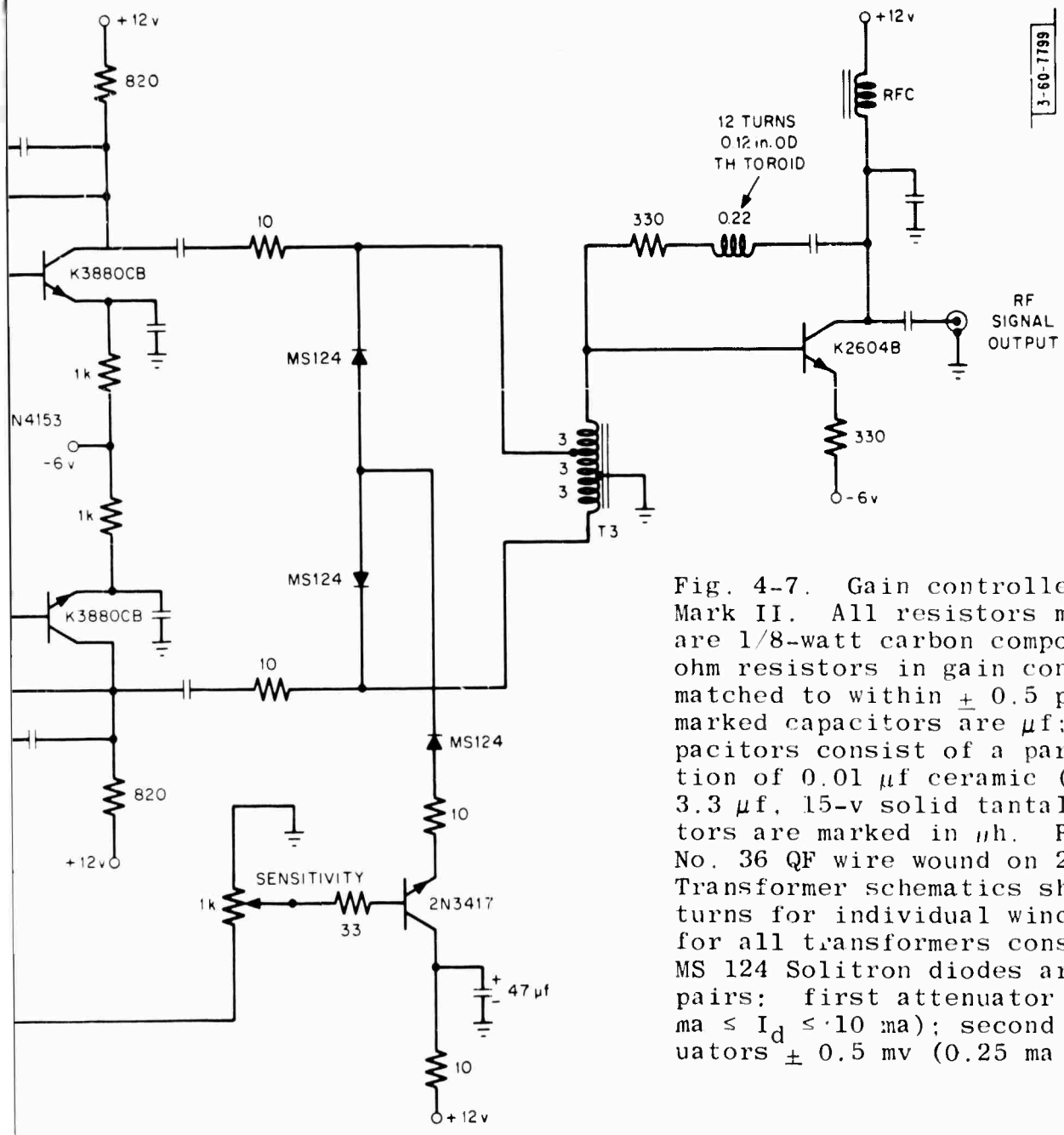

Fig. 4-7. Gain controlled amplifier, Mark II. All resistors marked in ohms are 1/8-watt carbon composition. Ten-ohm resistors in gain control circuits matched to within ± 0.5 percent. All marked capacitors are µf; unmarked capacitors consist of a parallel combination of 0.01 µf ceramic (0.022 µf) and 3.3 µf, 15-v solid tantalum. All inductors are marked in µh. RFC = 5 turns of No. 36 QF wire wound on 2 H ferrite beads. Transformer schematics show number of turns for individual windings. Cores for all transformers consist of 4 H beads. MS 124 Solitron diodes are matched in pairs: first attenuator ± 300 µv (0.25 ma ≤ I_d ≤ 10 ma); second and third attenuators ± 0.5 mv (0.25 ma ≤ I_d ≤ 10 ma).

TABLE 4-3

MARK II STC AMPLIFIER ELECTRICAL CHARACTERISTICS

Frequency response (no STC)

Gain = 30 db $^{+0.5}_{-1.0}$ from below 1 MHz to 325 MHz

Time domain response

Rise time < 1.5 nsec (Fig. 4-10)

Droop, overshoot (Fig. 4-9)

NOTE: Accurate droop measurements were not made--Anzac limits low frequency response of plots shown.

Impedance

Amplifier input impedance--100 ohms balanced

Input reflection coefficient $\leq$ 0.25 v (balanced)

Amplifier is assumed to be loaded with 50-ohm termination

Amplifier is unconditionally stable for all possible input and output terminations

Noise figure--10 db $\pm$ 1 db 30-350 MHz

NOTE: Noise losses in Anzac H-81 included

STC characteristics

Suppression of a 3-v peak STC pulse by input attenuator $\simeq$ 66 db

Usable amplifier dynamic range $\geq$ 50 db (-20 db to +30 db)

Maximum blanking of input attenuator $\simeq$ 50 db

DC characteristics (no STC)

+12 v DC 35 ma

- 6 v DC 35 ma

Mechanical dimensions

Mod I Box dimensions

2 in. x 3 in. x 6 in.

Mod I Amp dimensions

2 in. x 1 in. x 6 in.

Mod II Box dimensions

2 in. x 2 1/4 in. x 6 in.

Mod II Amp dimensions

2 in. x 1 in. x 4 in.

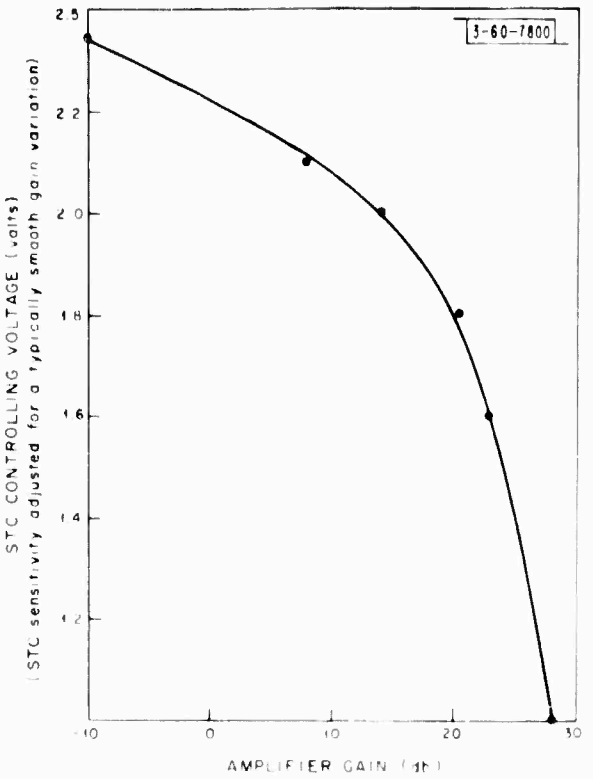

Fig. 4-8. Gain of STC amplifier vs control voltage for a typical sensitivity setting (Mark II, amplifier 2).

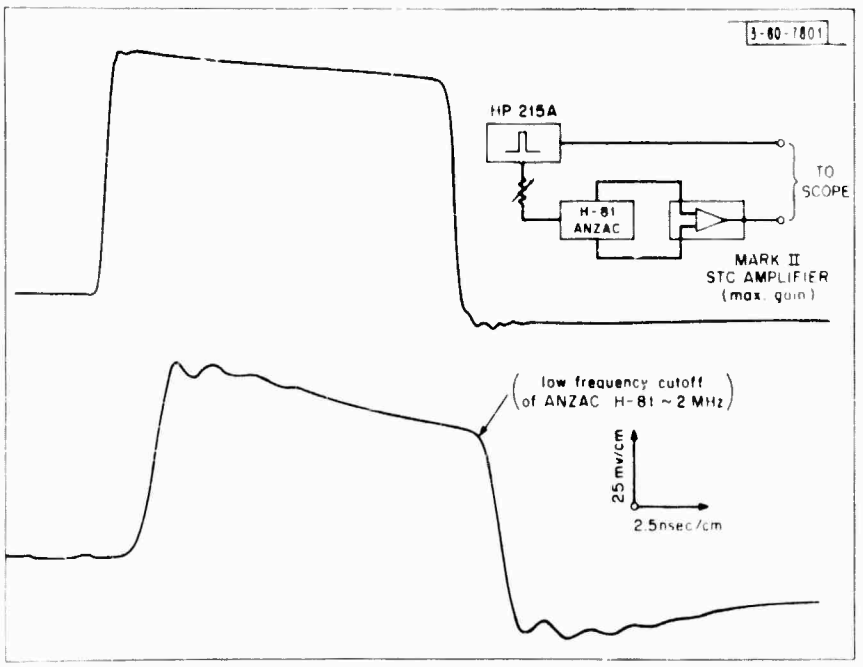

Fig. 4-9. STC amplifier pulse response.

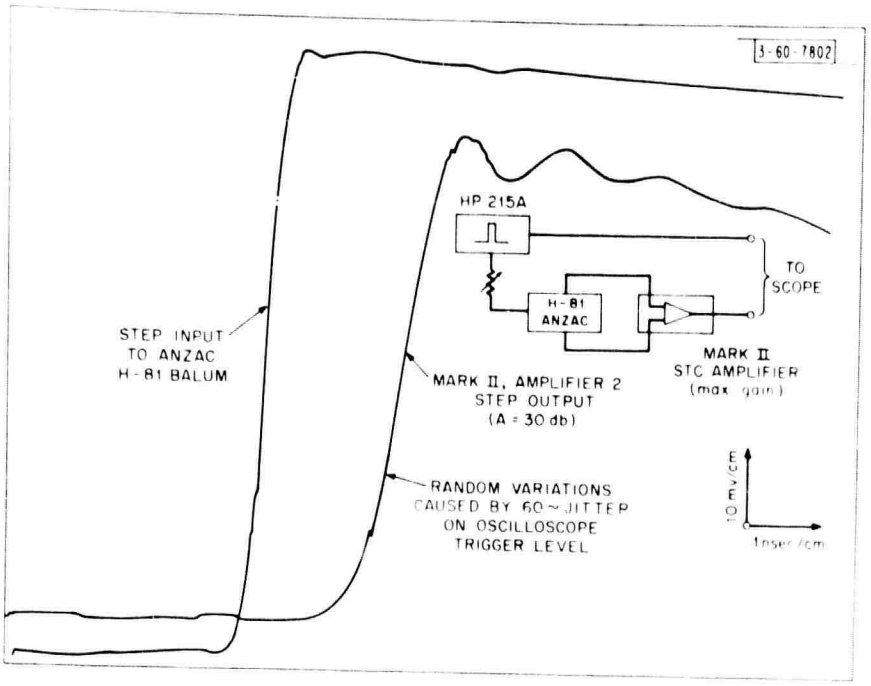

Fig. 4-10. Mark II STC amplifier step response.

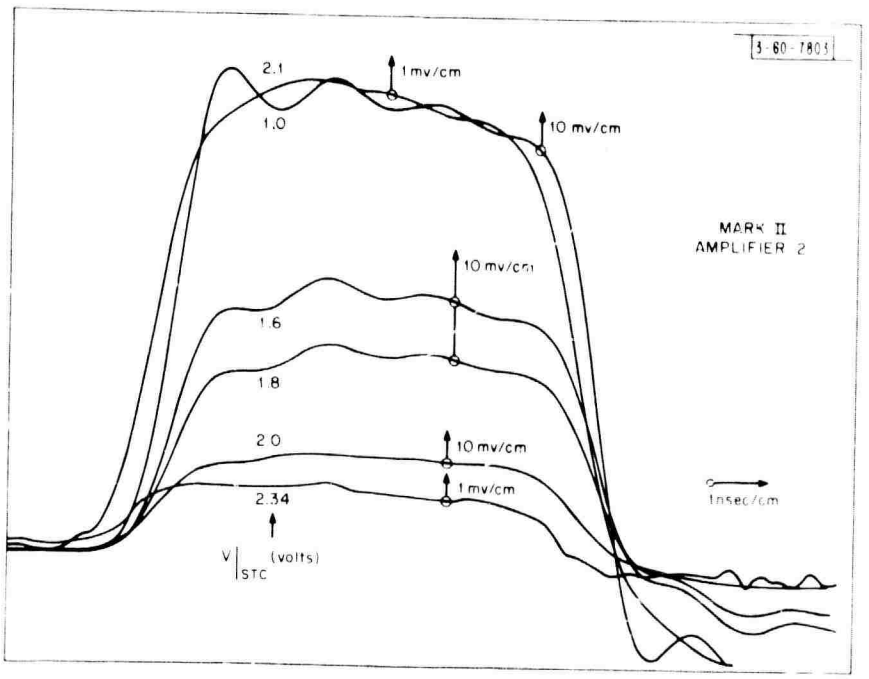

Fig. 4-11. Pulse response of STC amplifier vs STC voltage for a typical STC sensitivity setting.

In addition to the obvious consolidation of components, the following improvements are included in the Mark II amplifier:

(1) The STC circuit is relocated and divided into three sections. A four-diode attenuator is located at the amplifier input, and a two-diode attenuator appears at each interstage. This arrangement permits the Mark II amplifier to accept at least a 20-db increase in input signal level without clipping, even though the output stage is more efficiently biased and will saturate at output levels nearly 10 db below the Avantek. It is also important because the gain of the amplifier must be only a function of time. If the amplifier limits, a degradation in the displayed signal to clutter level results.

A disadvantage of the Mark II STC arrangement is that the display base line is more difficult to flatten. This difficulty occurs because signals cross coupled from the STC control line to the signal line are now amplified. The four-diode attenuator at the input is of particular importance since its STC isolation is degraded 30 db by the amplifier. It is difficult to achieve much suppression greater than 30 db of STC referred to the amplifier output, even with attenuator diodes and resistors matched to within $\pm$ 250 μv over the expected operating current range. Capacitive unbalance in the coupling transformers becomes a limiting factor, and is not easily dealt with. Superposed curves of a possible STC controlling voltage and the amplifier response with a termination at its input are given in Fig. 4-12. Fortunately, the base line can be compensated for within the relatively

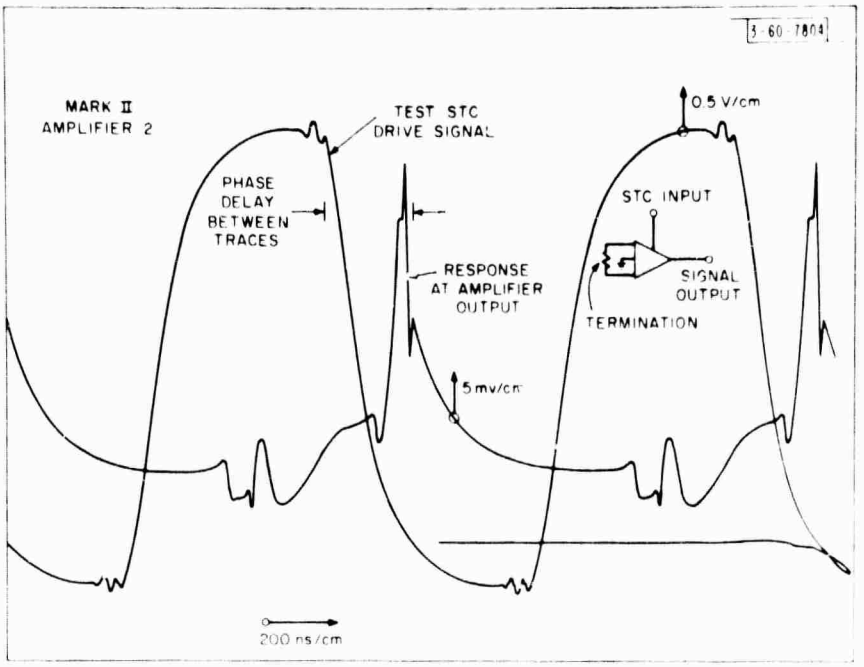

Fig. 4-12. STC control voltage cross coupling to amplifier output. STC suppression at first attenuator $\approx$ -30 db + 20 $\log_{10}$ $\frac{9 \times 10^{-2}}{6}$ =-66db.

short time period of interest by an alternate adjustment of the balance potentiometers performed while looking at the intended display time periods only.

(2) The TR switch has been eliminated. Instead, a blanking pulse is applied to the input attenuator during transmit time. This blanking arrangement provides up to 50 db additional suppression to the transmit pulse at any power level available from the antenna hybrid. Since the TR switch in Mark I passes all signals below about 300-mv peak with very little attenuation, the blanking technique offers a substantial advantage in transmit pulse compression.

No attempt was made to terminate properly the input attenuator for signal levels appreciably greater than 300-mv peak, because the antenna hybrid balances the

transmitted pulse to just about this level at the receiver.

(3) The first two stages of the amplifier are constructed in balanced form, while the output stage is unbalanced. Balanced amplifiers improve the isolation characteristics of the STC attenuators by eliminating many of the baluns. The balanced stages also offer improved reliability and amplifier linearity while minimizing power consumption.

D. Mark II Amplifier Design and Construction

The STC amplifier stages (Fig. 4-7) are coupled by broadband ferrite transformers. The common-emitter transistor configuration is used throughout the amplifier, and the gain is held constant over the band of interest by means of shunt feedback from the collector to the base of each transistor. In the balanced stages, additional high-frequency gain is obtained by using matched 1N4153 diodes to feed back a neutralizing voltage from the opposite collector.

The transistors used in this amplifier are silicon devices manufactured by the KMC Semiconductor Corporation, and have a minimum f_T of 1700 MHz. Type K388CCB retains a high-current gain over the range of emitter currents from 1 to 15 ma, while the K2604B is useful over the range from 5 to 30 ma. The chips were supplied on a 1/16-in. square ceramic substrate with an epoxy protective covering and flat, gold-plated ribbon leads. This package is particularly useful in a balanced high-frequency amplifier where it is desirable to retain circuit layout symmetry and reduce stray package reactances to an absolute minimum.

T2 is really a dual hybrid. If either of the preceding transistors should develop a collector-to-emitter short or open, the amplifier gain will be suppressed by about 6 db and the frequency response slightly degraded. This feature was sacrificed between stages 2 and 3 to obtain maximum coupling through auto-transforming balun T3. Each of the transformers is wound on a core of four IGC H beads. Wire sizes are chosen to fill the core windows.

MS124 hot carrier diodes were selected for the STC circuits because of their exceptionally low-series resistance and inductance (approximately 5 ohms and 1 nh). The low-series impedance is necessary to obtain a high dynamic attenuation range in these low-impedance circuits. The latest version of the amplifier (Fig. 4-7) contains an extra MS124 for the last two attenuators to make their STC drive characteristics match the first attenuator. The three attenuators are not identical because the dynamic range requirement is somewhat relaxed for the last two; and the design simplicity obtained by eliminating the diodes, improves the high-frequency response.

The amplifier is constructed on a 1/16-inch gold-plated, glass epoxy circuit board. The RF components are symmetrically arranged and located on one side of the board. The other side is reserved for a full ground plane and low frequency circuits. All printed circuit lands are made as small as possible to reduce lead inductance and node capacitances to ground.

5. CONTROL CIRCUIT

The control circuit: (1) determines the system's pulse repetition rate, (2) generates the synchronizing trigger pulses for the pulser and sampling unit, and (3) controls the shape of the sensitivity time control waveform. In Mark II, an additional control circuit generates a blanking pulse for the receiver.

In the Mark I and II basic control circuits [Fig. 5-1(a, b)], the multivibrators, consisting of transistors Q1 and Q2, generate positive pulses at the collector of Q2 at a repetition rate of 1 MHz. A frequency adjustment (R1) permits a ±10 percent change in frequency. Transistor Q3 inverts the multivibrator output and sharpens the trailing edge to 4 nsec. This transition is differentiated to drive emitter followers Q10, Q11, Q12, and Q13 for the trigger outputs to the pulser and sampler. The same transition is used to initiate the generation of the ramp output for the sensitivity time control.

Diode CR7 couples the multivibrator signal to the sensitivity time control circuit. Before transistor Q3 turns on, Q5 is conducting, and Q4 is cut off. When Q3 saturates, CR7 stops conducting, and the base voltage of Q4 rises as capacitor C10 charges to the voltage set by the ramp delay control (R30). Transistor Q4 turns on when its base voltage exceeds that of Q5. The collector current of Q4 is set by the ramp slope control (R31). Capacitor C11 is then linearly discharged to -0.6 volts by the difference between the collector current of Q4 and the constant current source, transistor Q6. Transistor Q4 turns off when the multi-

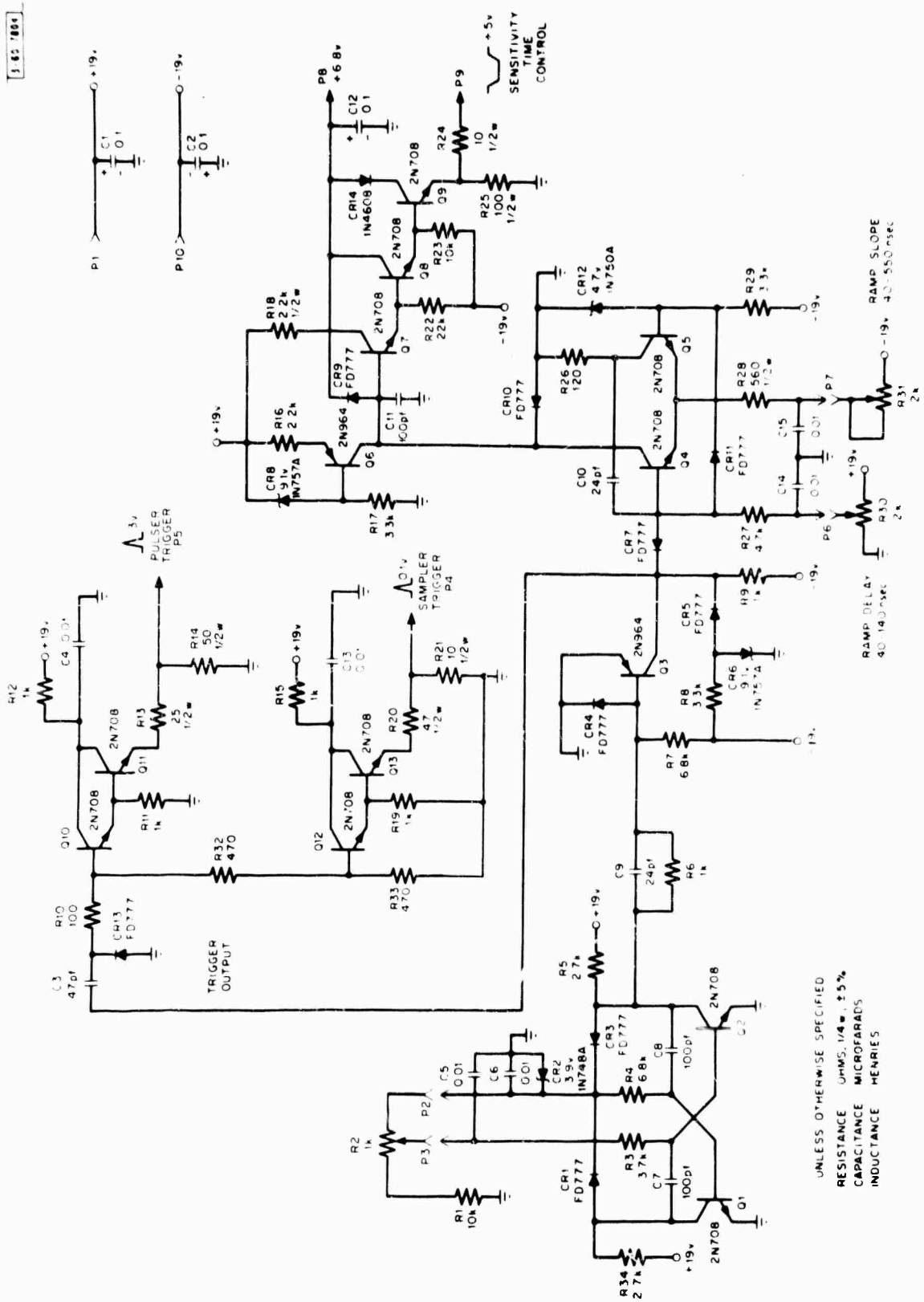

Fig. 5-1(a). Mark I control circuit.

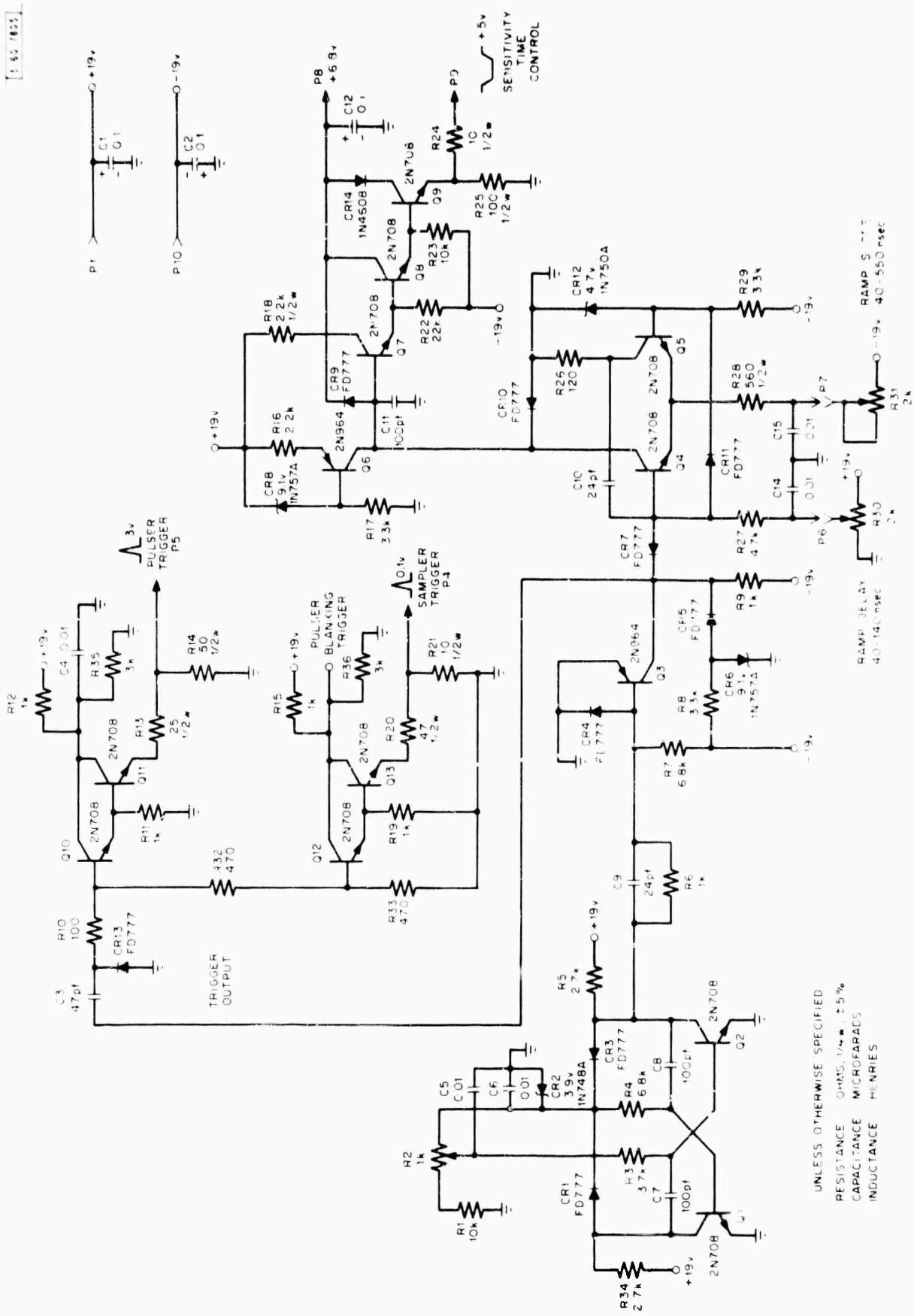

Fig. 5-1(b). Mark II control circuit.

vibrator switches to its opposite state, and capacitor C11 is charged by Q6 until it is clamped by CR9 to approximately 7.4 volts. This voltage waveform on capacitor C11 (Fig. 5-2) is transferred to the sensitivity time control output through emitter followers Q7, Q8, and Q9.

Figure 5-3 is the schematic for the pulse blanking circuit. A signal from the sampler trigger circuit (Fig. 5-1) triggers the common emitter monostable multivibrator, consisting of transistors Q1 and Q2. Clamping diodes D4 and D5 limit the collector swing of Q2 from -0.6 to 6.8 volts. The pulse width adjustment (R9) varies the duration of the positive pulse at the collector of Q2 from 35 to 100 nsec. This signal drives the emitter followers Q3 and Q4, and generates a 4.5-volt pulse driving a 50-ohm load. The fall time of this pulse is 7 nsec.

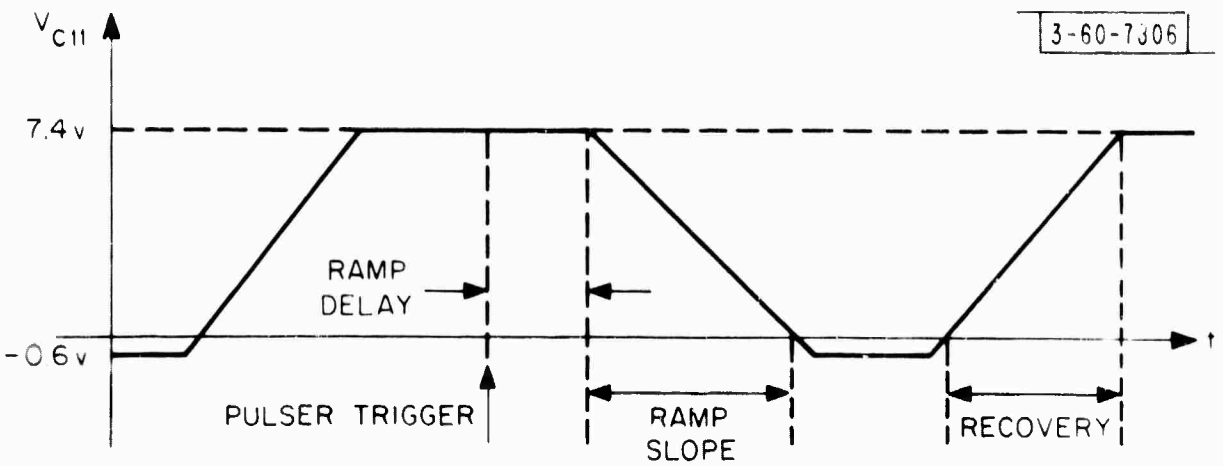

Fig. 5-2. Voltage on capacitor C11 as a function of time.

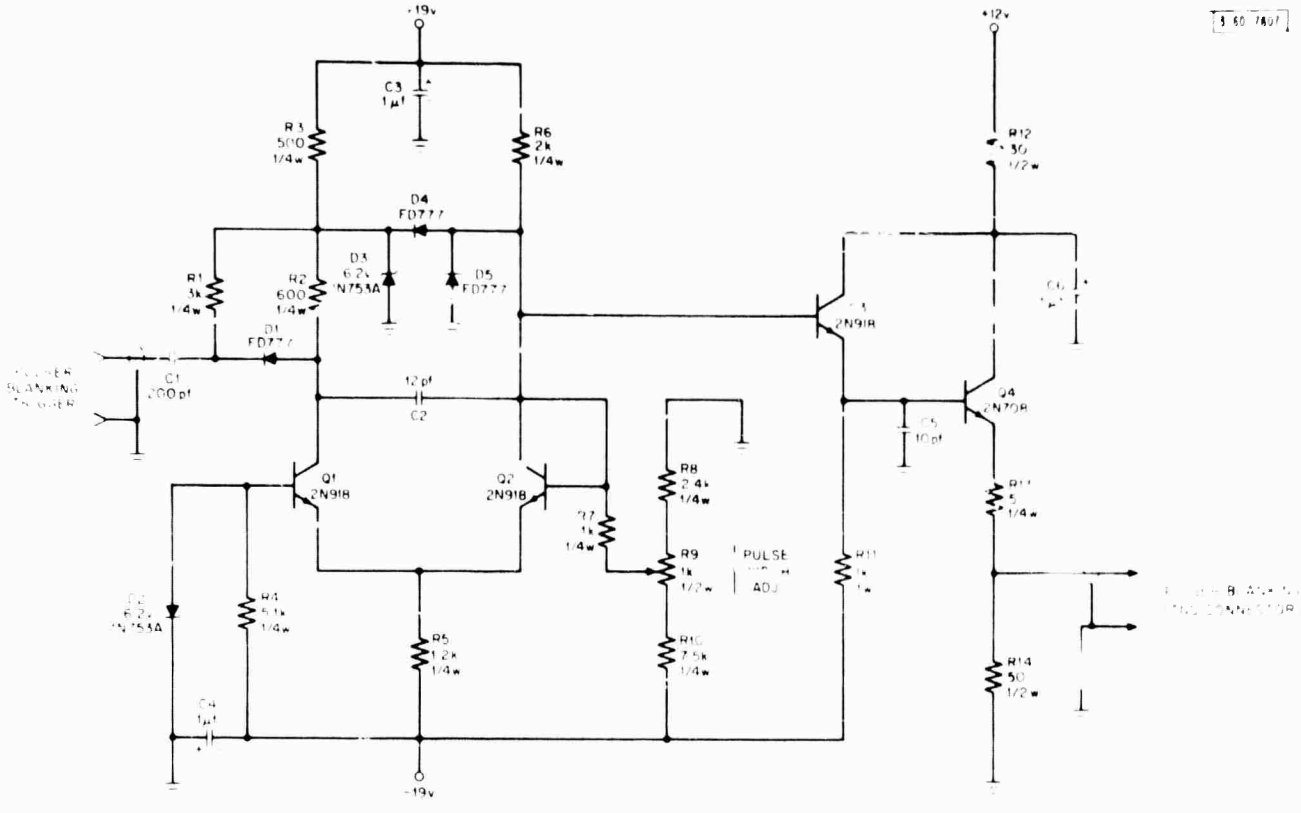

Fig. 5-3. Pulser blanking control circuit.

6. SAMPLING UNIT

The sampling unit is a Tektronix 1S1 Sampling Plug-in, which is modified: (1) for adaption to the oscilloscope display, (2) to reduce power dissipation, and (3) to simplify power supply requirements. Basic 1S1 specifications were not changed. The only nonoperable front panel controls are the variable vertical gain control (Mark I), and the vertical position control (Mark I and II).

Front-panel vertical and horizontal signals from the 1S1 drive the oscilloscope display. An interdot and retrace blanking circuit was added to the 1S1 for blanking the cathode-ray tube. To reduce power dissipation, the vacuum tube circuit for vertical gain and positioning was deleted and the remaining twin triode and nuvistor were replaced by three field effect transistors. The power supply requirements were consolidated and reduced to four voltages: +225, +19, -19, and -145. Total power drain on these supplies is 16 watts, compared with 30 watts required by an unmodified 1S1.

Figures 6-1, 6-2, and 6-3 show modifications made in the sampling preamplifier, memory operational amplifier, and staircase generator to convert tube circuits to field effect transistor circuits. The 2N3823 field effect transistor was selected for those circuit modifications because of its high transconductance and low gate capacitance. Mark I and II modifications are the same, except for the sampling preamplifier [Fig. 6-1(a, b)].

Figure 6-4 shows the retrace blanking signal from the collector of Q235 combined with the interdot blanking signal

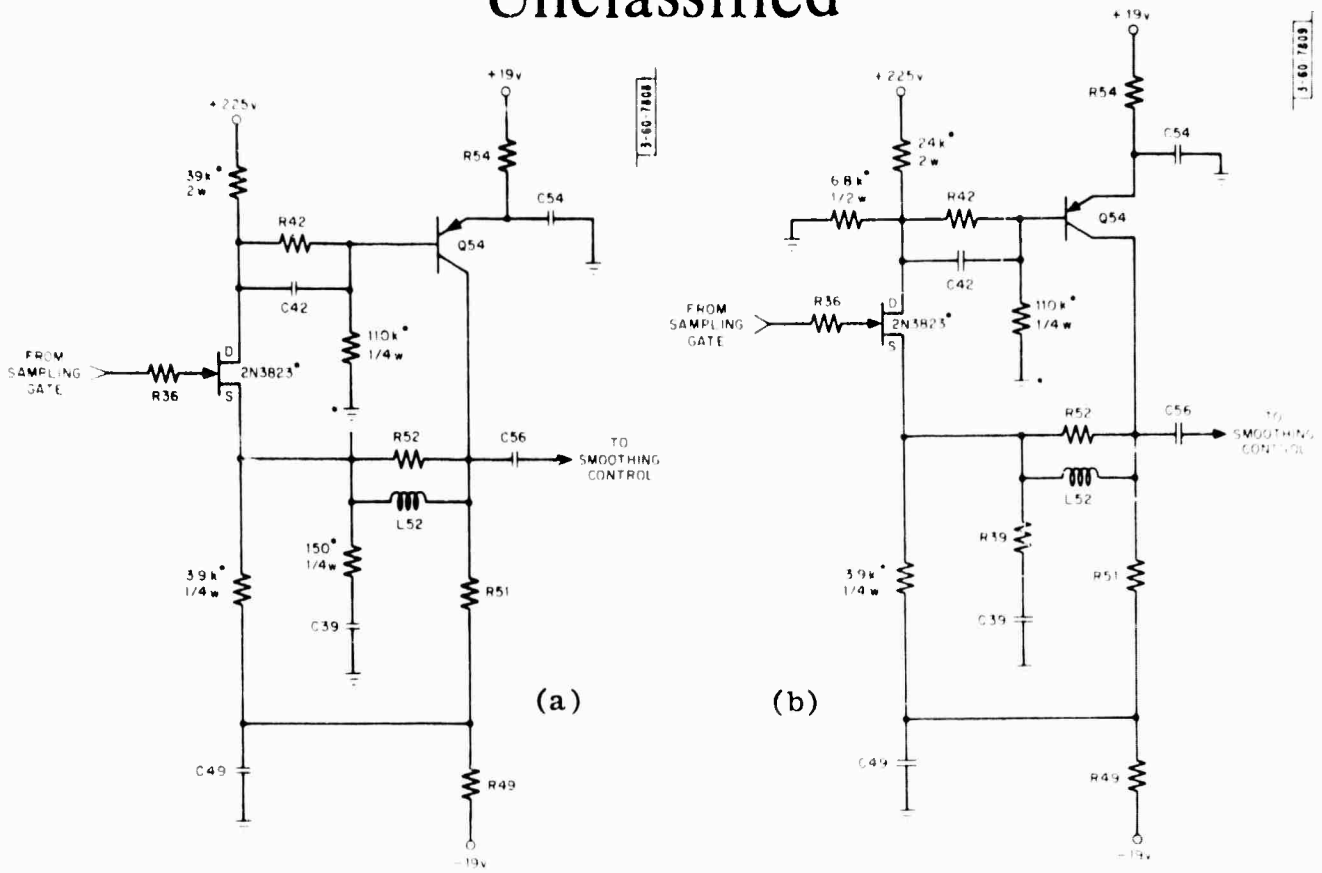

Fig. 6-1. Modifications (*) made to the (a) Mark I and (b) Mark II sampling amplifiers.

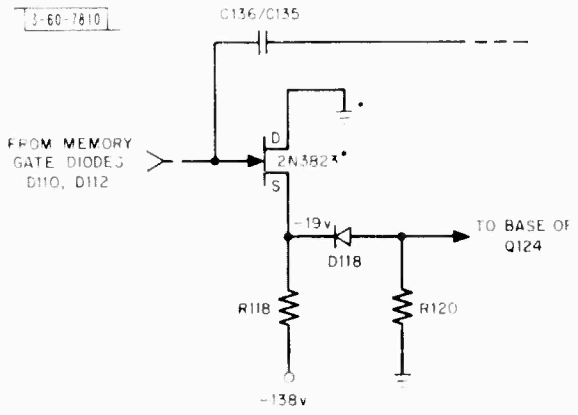

Fig. 6-2. Modifications (*) made to the memory operational amplifier.

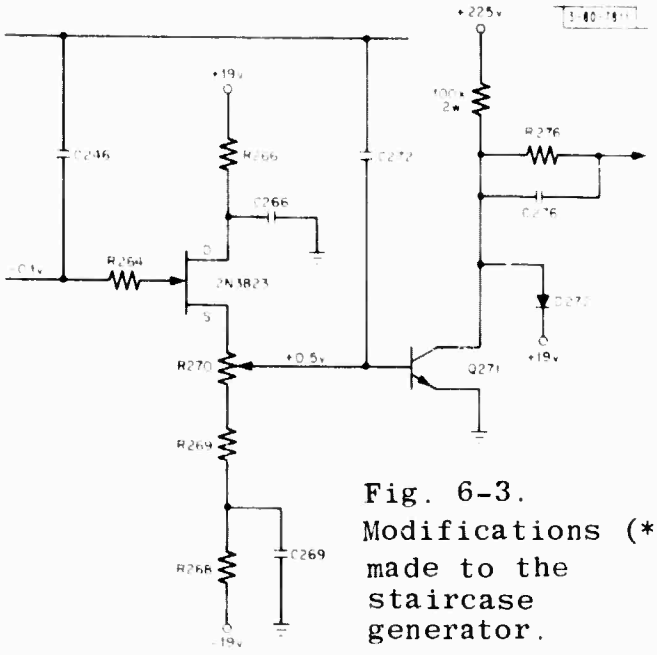

Fig. 6-3. Modifications (*) made to the staircase generator.

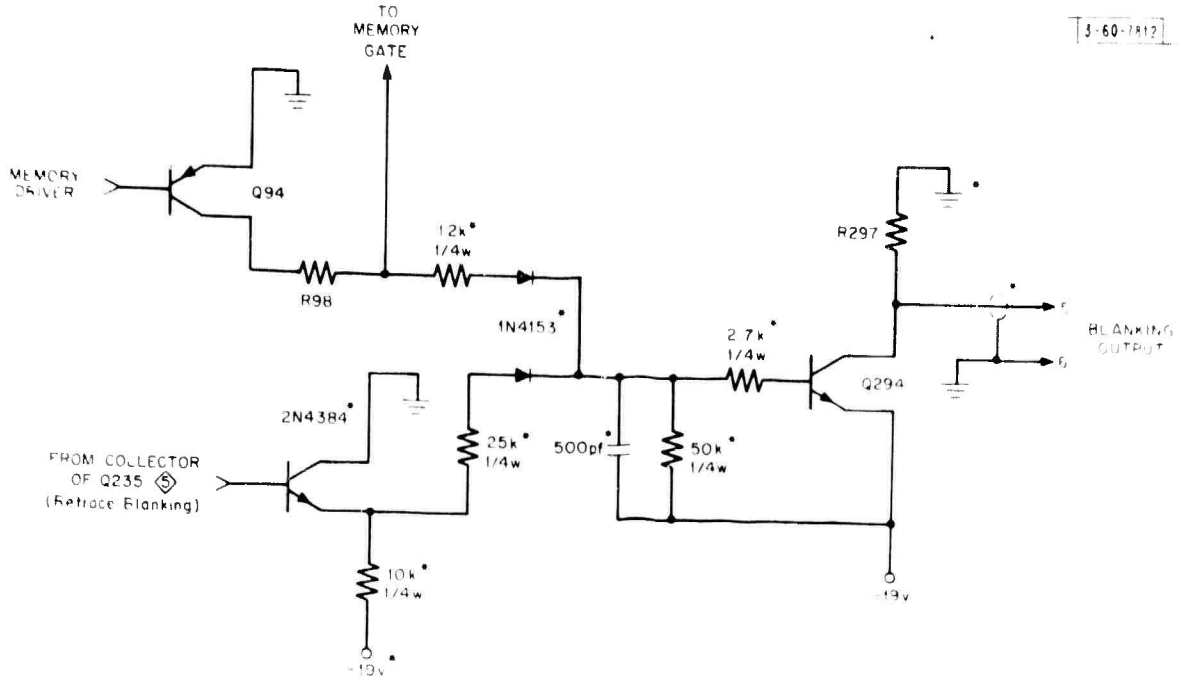

Fig. 6-4. Modifications (*) made to the interdot and retrace blanking circuit.

through the 1N4153 diodes. The combined signal is amplified by Q294 and fed to the blanking output of the 1S1.

The modification of the Mark II variable gain-control circuit is shown in Fig. 6-5.

Modifications made to the power distribution and the rear connector of the 1S1 are shown in Fig. 6-6.

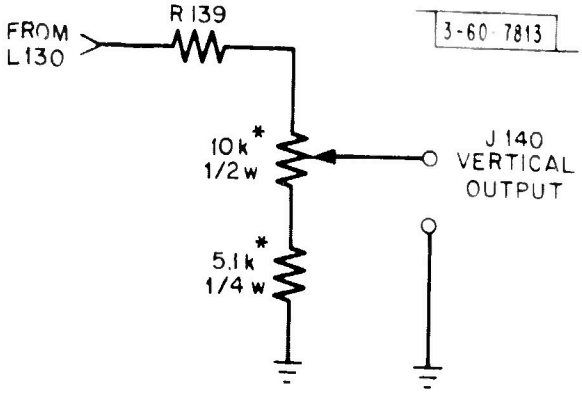

Fig. 6-5. Modifications (*) made to the Mark II variable vertical gain control.

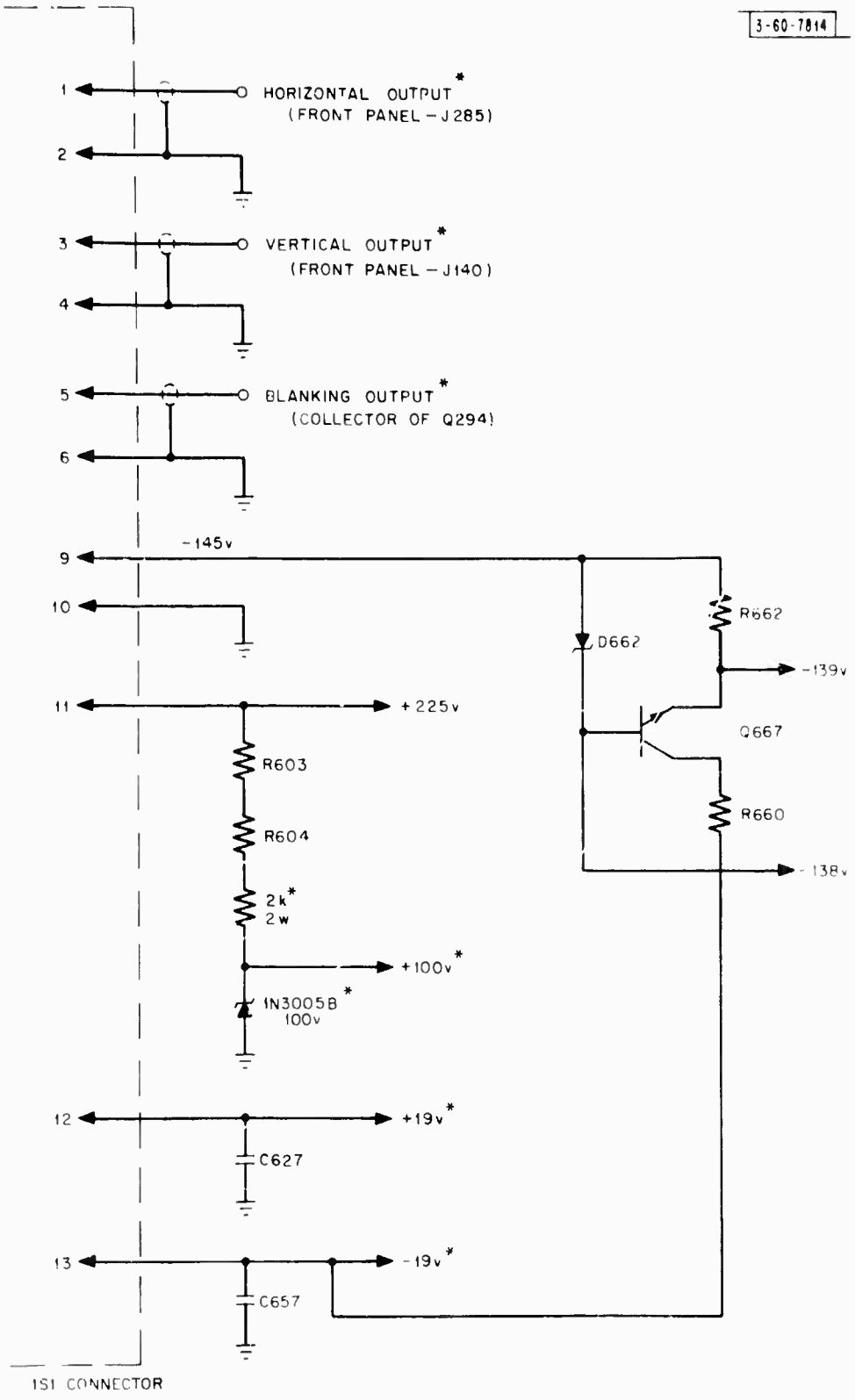

Fig. 6-6. Modifications (*) made to the power and signal outputs.

7. OSCILLOSCOPE DISPLAY

In Mark I, a Tektronix 321 oscilloscope displays the vertical and horizontal signals from the sampling unit. The vertical sampling signal is coupled directly into the front panel vertical input of the 321 oscilloscope, and calibration is attained by setting the vertical sensitivity control to 0.2 volts per division. An inverting and level shifting circuit (Fig. 7-1) was added to couple the horizontal sampling signal into the horizontal driver of the 321 oscilloscope. When operating the display, the time base control must be set to external horizontal input. The blanking signal from the 1S1 is coupled directly to the cathode-ray tube (CRT) grid input of the 321 oscilloscope.

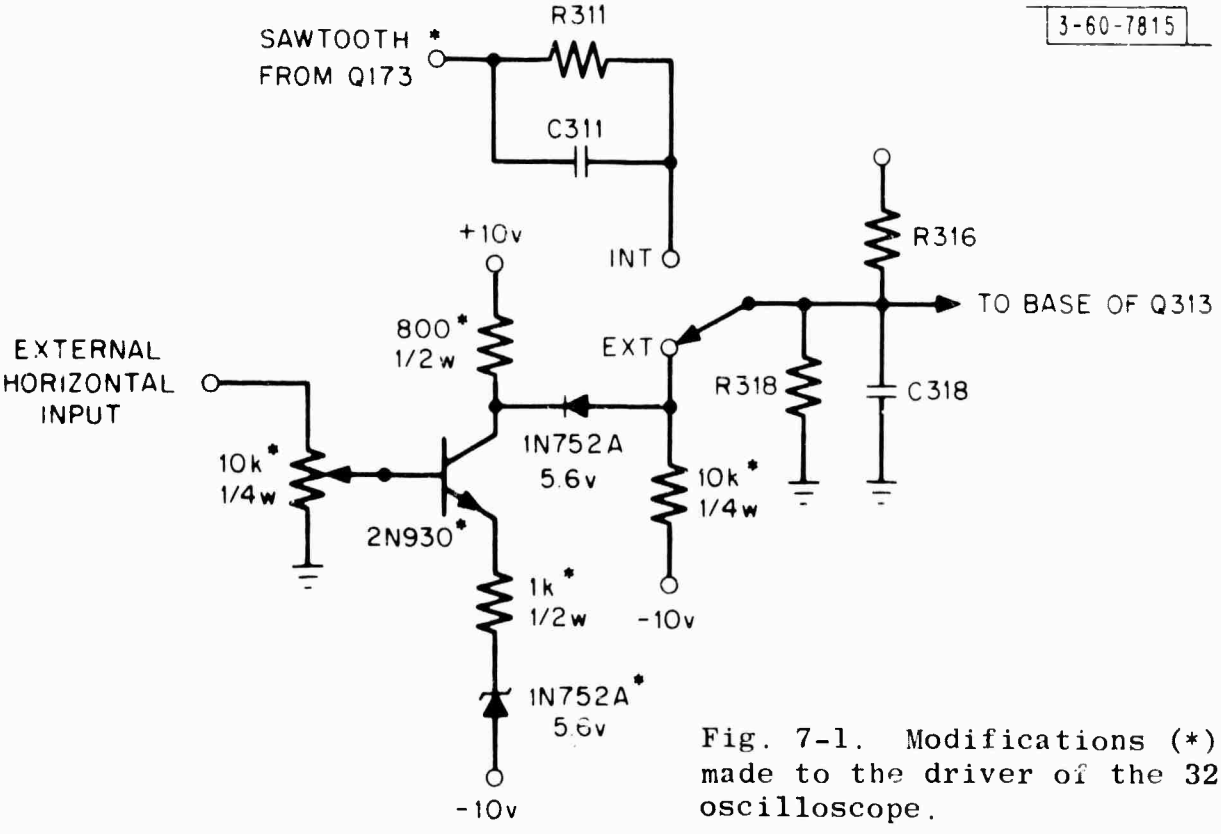

Fig. 7-1. Modifications (*) made to the driver of the 321 oscilloscope.

The Mark II oscilloscope display is a modified Benrus RA-850 oscilloscope with Benrus VA226 and HA325 plug-in amplifiers. The 1S1 vertical signal is connected directly to the vertical input of the oscilloscope, and the 1S1 horizontal signal is connected to the horizontal input through a 300-K ohm resistor.

To simplify the Mark II front panel control on the oscilloscope, the vertical and horizontal gain controls were relocated to the left side of the chassis, and adjusted for proper calibration of the display. Circuit modifications (Fig. 7-2) were made to the oscilloscope to provide adequate blanking of the CRT. Additional filtering has been added to the CRT high-voltage supply, and the 1S1 blanking signal is AC coupled directly into the blanking grid.

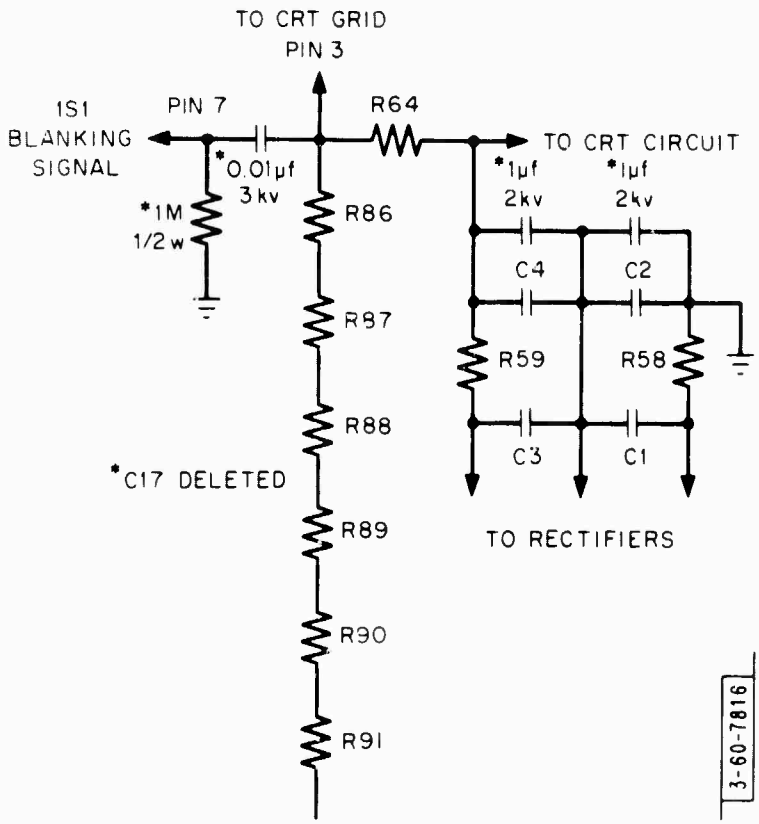

Fig. 7-2. Modifications (*) made to the blanking circuit for Benrus oscilloscope RA-850.

8. HELIX RECORDER

(U) A B-scope display improves the capabilities of the Geodar system by integrating the output from the receiver and providing a permanent record of the integrated signal as the antenna is scanned over the ground. An Alden helix recorder was added to Mark I and Mark II to provide such a display.

Field experience indicates that signal integration enhances the identification of tunnel returns. Signal integration is needed because surface clutter, changes in the coupling of the antenna, and unwanted reflections from discontinuities in the ground create signal perturbations at the output of the receiver. These signals tend to fluctuate rapidly, unlike a reflection from a tunnel. An operator observing the A-scope display can be distracted by these signal fluctuations, and would experience some difficulty in identifying a tunnel reflection under high clutter conditions.

A recording of the signals received is important when searching an area for tunnels. Tunnel reflections from sweeps across the area can be correlated to aid the operator in mapping a tunnel or tunnel complex. The helix recorder has the added advantage of conveying a profile of the ground structure. A similar application of this recorder is recording and displaying sonar signals.

A. Description

(U) The helix recorder (Fig. 8-1) consists of four basic parts: (1) rotating drum, (2) helix wire, (3) blade, and (4) recording paper. The recording paper is electrosensitive and feeds between the blade and one-turn helix wire mounted on the drum. When the

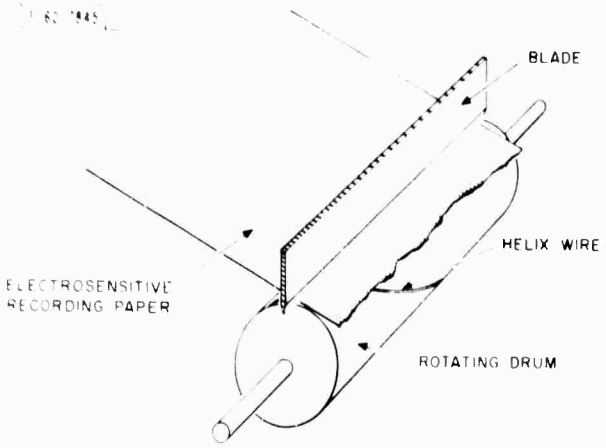

Fig. 8-1. Basic parts of helix recorder.

drum is rotating and voltage is applied between the helix wire and blade, consecutive line traces are recorded. The intensity of the trace is controlled by the magnitude of the voltage.

(U) Signal output from the sampling unit is amplified and recorded by the helix recorder. Intensity of the line trace is controlled by the sampling unit, which is synchronized with the rotation of the drum to provide a direct relationship between the arrival time of the signal and position of the recorded signal on the paper.

(U) The Alden 305DA helix recorder used for Geodar is the smallest recorder available from Alden, and has a 5-inch printing width. The following items were ordered as part of the recorder: continuous blade drive, helix drive motor, paper feed motor, magnetic reed switch.

B. Typical Tunnel Signal Pattern

Consider the case where the antenna is moved perpendicularly over a tunnel. When the antenna is directly over the tunnel, the strongest signal return is received and the shortest travel time

for the reflection occurs. As the antenna is moved away from the tunnel, the magnitude of the signal return decreases while the travel time for the reflection increases.

Figure 8-2 shows a typical signal pattern on the helix

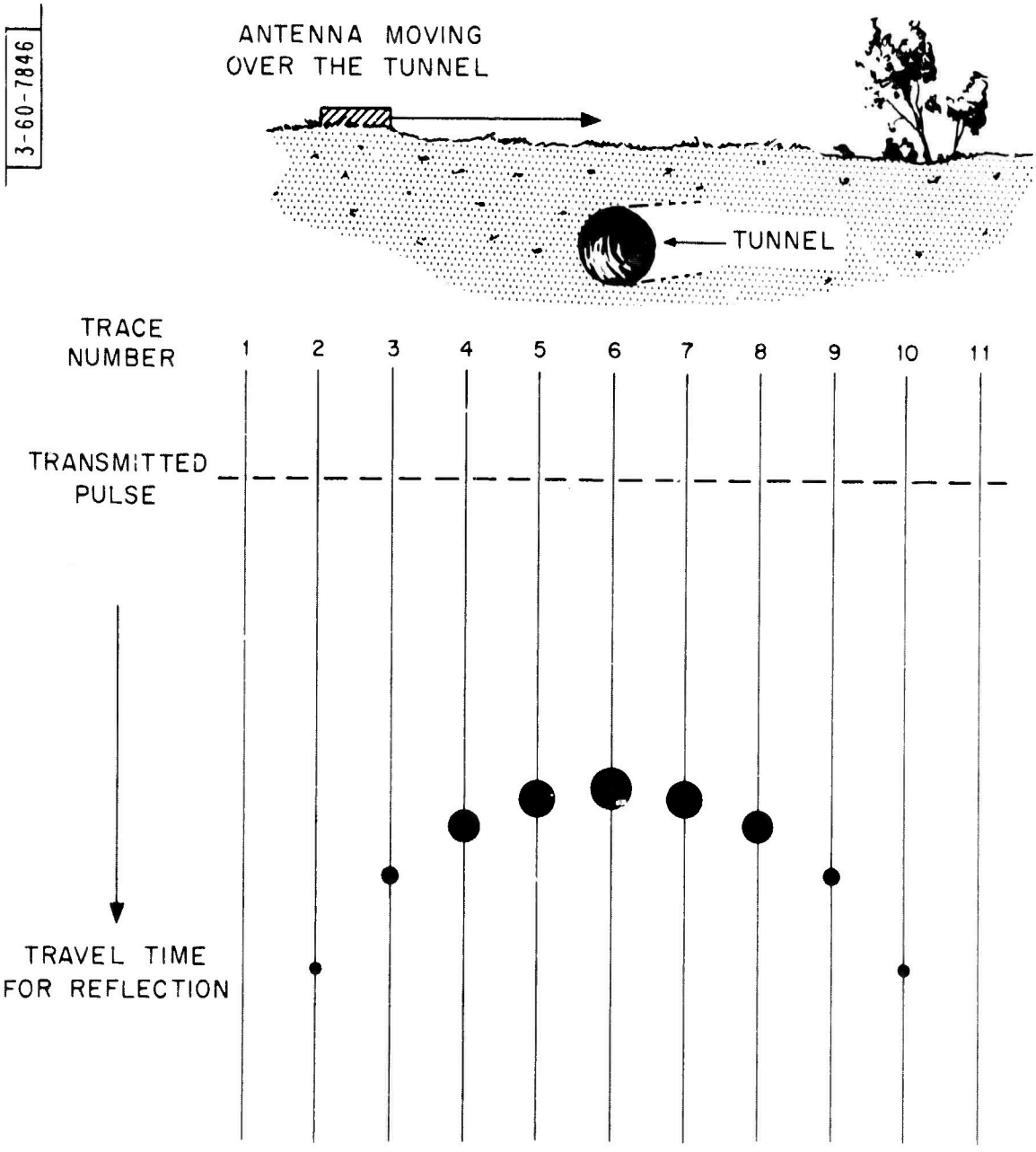

Fig. 8-2. Typical helix recording as antenna is moved over tunnel.

recorder of a tunnel reflection as the antenna is moved over the tunnel. The size of the dots indicates the intensity of the signal.

C. Interfacing Unit

(U) A DC power amplifier (Fig. 8-3) is needed to boost the below-1-volt signal from the sampling unit to the recording level of the helix recorder. A typical signal requirement to record a middle tone on the recording paper is a 50-volt signal at an impedance level of 500 ohms. The field effect transistor (FET) input stage, transistor Q1 drives the differential amplifier consisting of transistors Q2 and Q3. The signal is then amplified

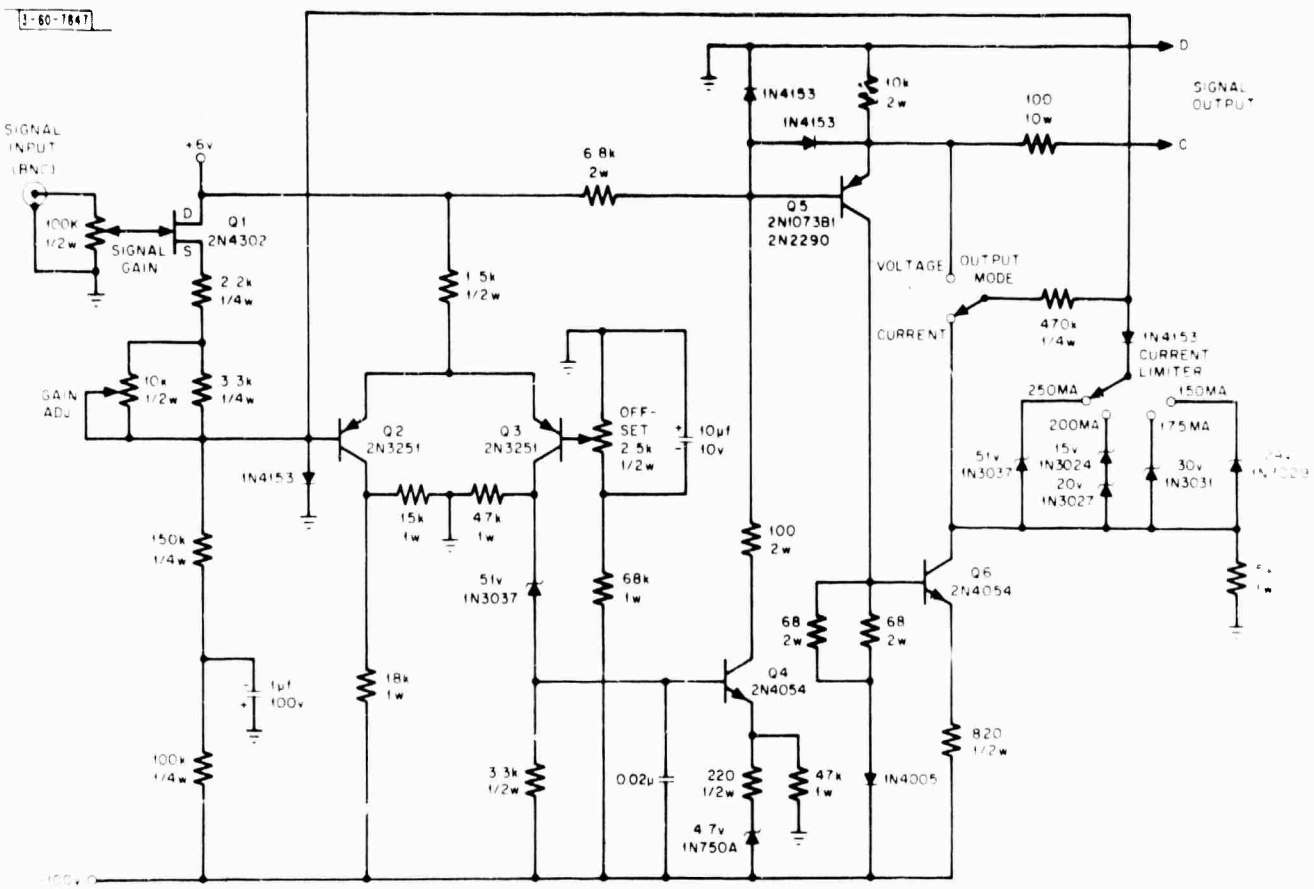

Fig. 8-3. Circuit diagram for DC power amplifier.

by transistor Q4 and fed to the output emitter follower (Q5). Transistor Q6 monitors the output current of the amplifier. The collector voltage of Q6 is proportional to the output current.

Feedback in the amplifier is selected by the output mode switch. When the output mode switch is in the voltage position, the input signal controls the amplifier output voltage; in the current position, the input signal controls the output current. The current limiting switch selects the maximum output current of the amplifier. When the current reaches the selected level, the output is limited by direct feedback through the zener diodes connected to the collector of Q6. The signal gain and offset controls determine the signal levels for the amplifier.

The rotating drum on the helix recorder is driven by a synchronous 60-Hz, 115-v AC motor. Mounted on the shaft of the drum is a magnetic reed switch to mark the start of the trace. Closure of this switch initiates the sweep signal for the sampling unit.

Figure 8-4 is the circuit for the sweep generator. To prevent multiple triggering due to contact bounce, the magnetic reed switch activates a Schmitt trigger consisting of transistors Q1 and Q2. The positive signal transition at the collector of Q1 is differentiated and amplified by transistor Q3. The resulting signal at the collector of Q3 is a 0.2 msec pulse to reset the sweep circuit.

The sweep circuit consists of the current source transistor (Q5) charging capacitor C4. Each time the magnetic reed switch closes, transistor Q4 saturates and discharges the capacitor. The capacitor is then charged linearly until it is again reset

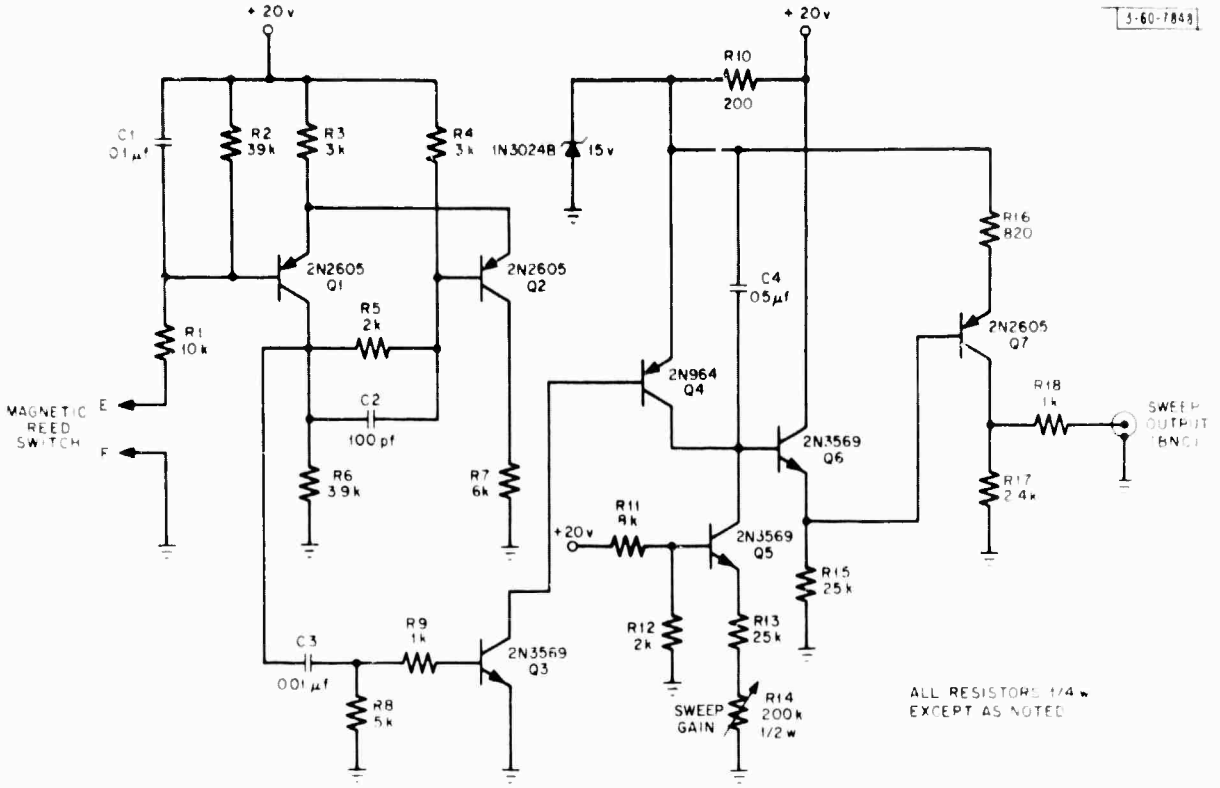

Fig. 8-4. Circuit diagram for sweep generator.

by another pulse generated by the closure of the magnetic reed switch. Emitter follower Q6 has a high input impedance to isolate the charging signal from the output amplifier stage (Q7). The slope of the output sweep is controlled by the sweep gain control (R14).

Figure 8-5 shows the interconnection of the power supply modules, sweep generator, and DC amplifier. The external connections to the helix recorder and sampler are also noted.

D. Operation of Recorder

To operate the helix recorder from the sampling unit, two front panel connections are made to the sampling unit. The

vertical output of the sampler is connected to the signal input of the DC amplifier and the sweep generator output is connected to the external horizontal input of the sampler. In conjunction with externally driving the sweep of the sampler, the display mode switch must be changed from normal to external horizontal, and the external horizontal attenuator control is set to minimum attenuation (clockwise).

The sweep gain control is adjusted so that the base line on the oscilloscope display extends completely across the graticule, but does not saturate on the right side.

The current output mode was used in all our recordings, because the recorded tone is more nearly proportional to current than to voltage.

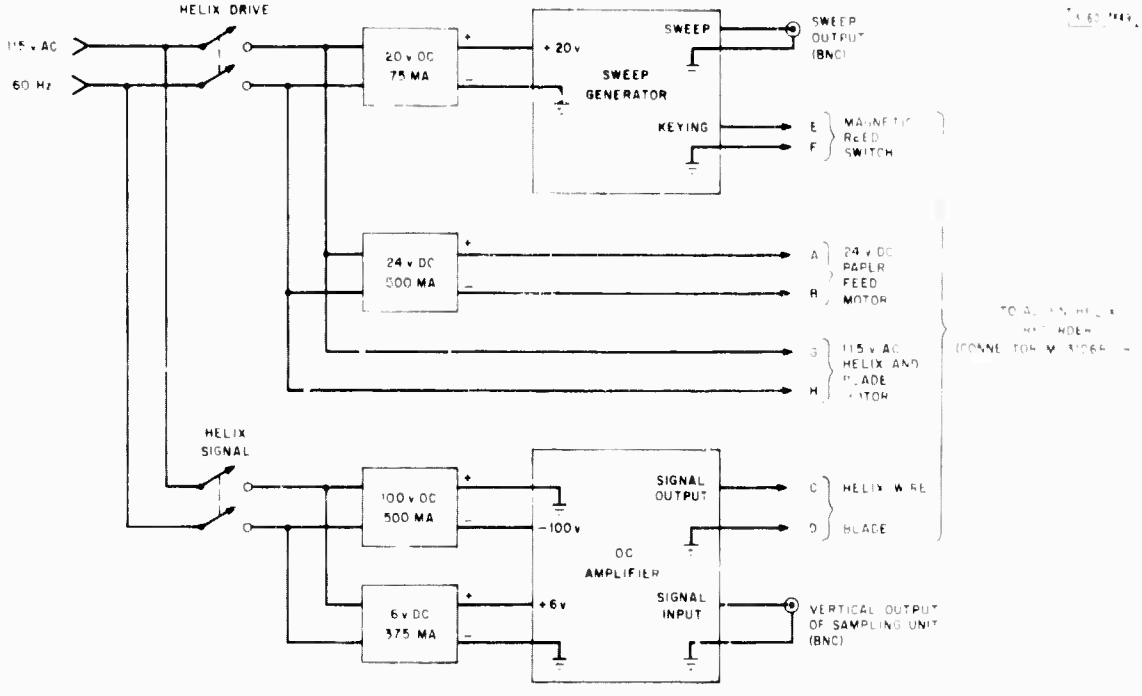

Fig. 8-5. Interconnecting diagram of power supplies, sweep generator, and DC power amplifier.

(U) By using different combinations of gears to drive the helix drum, the sweep rate of the recorder can be operated at 7.5, 15, and 30 Hz. The 15-Hz sweep rate with a 12-inch-per-minute paper rate was used for our recordings. These rates were adequate for a normal walking speed.

(U) The output current of the DC amplifier must be limited to prevent the recording paper from electrically breaking down, and damaging the helix wire, support and blade. The current-limiting control was set to 250 ma at the 15-Hz sweep rate.

(U) One roll of recording paper lasts about two hours at the 12-inch-per-minute feed rate. The helix wire, wire support, and blade must be replaced after 10, 25, and 50 rolls of operation, respectively. These parts are subject to wear, but are easily removed and installed.

E. Helix Recordings

Figures 8-6 and -7 are helix recordings of the tunnels 5-1/2 feet and 9-1/2 feet below the surface at the Millstone Hill test site. The helix recordings start at the left of the record and end at the right. At the top of the recordings, the alternate dark and light bands are the transient signals in the receiver caused by the transmitted pulse. Below these bands is a 200-nsec region for displaying signal returns. Two distinct signal returns are in this region. The upper signal is a return from the tunnel, and the lower one is a return from a layer of gravel placed below the tunnel for water drainage. Both returns have a light curved band followed by a dark curved band. The light portion represents a negative signal excursion from the base line, and the dark portion, a positive excursion. The signal return from the tunnel is not a symmetrical crescent shape as shown in Fig. 8-2, because of different lobe patterns at the front and back of the antenna.

Fig. 8-6. Helix recording (actual size) of tunnel 5-1/2 ft below surface at Millstone Hill test site.

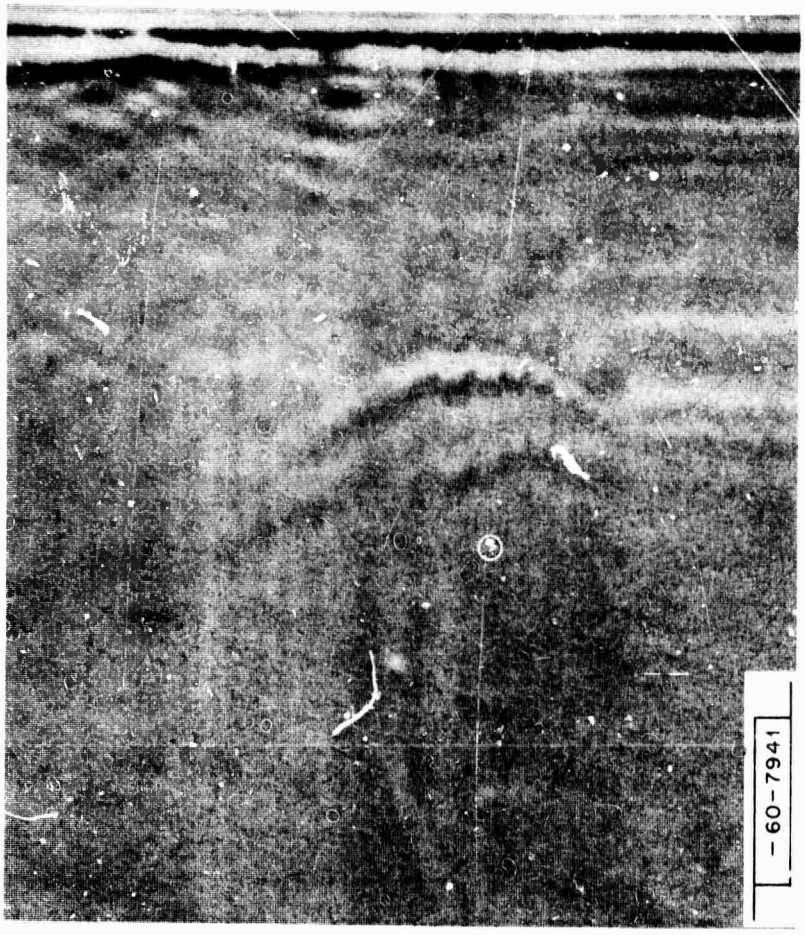

Fig. 8-7. Helix recording (actual size) of tunnel 9-1/2 ft below surface at Millstone Hill test site.

At the Raleigh, North Carolina test site an area 75-foot square was marked off, and eight passes were made across the area (Fig. 8-8). Passes one, two, and three were made over a hand-dug tunnel 6 to 9 feet below the surface. The sequence of helix recordings shown in Fig. 8-9 correspond to the passes made across the area. Signal returns from the tunnel are clearly recorded only on passes one, two, and three. The time scale used in these recordings was 100 nsec across the paper.

A helix recording (Fig. 8-10) was made over a tunnel 6 feet below the surface in a wooded area at the Ft. Belvoir test site. Just above the broad light-then-dark curved recording of the

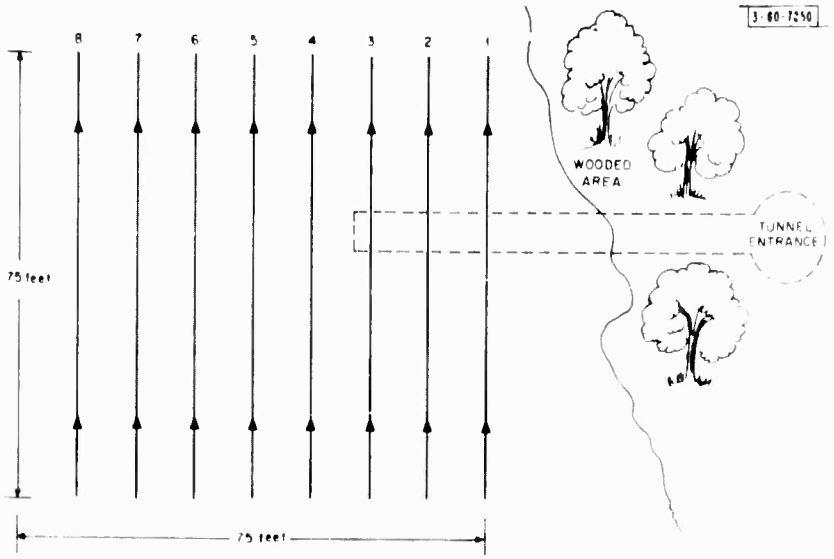

Fig. 8-8. Diagram of passes made over marked-off area at Raleigh, N. C., test site.

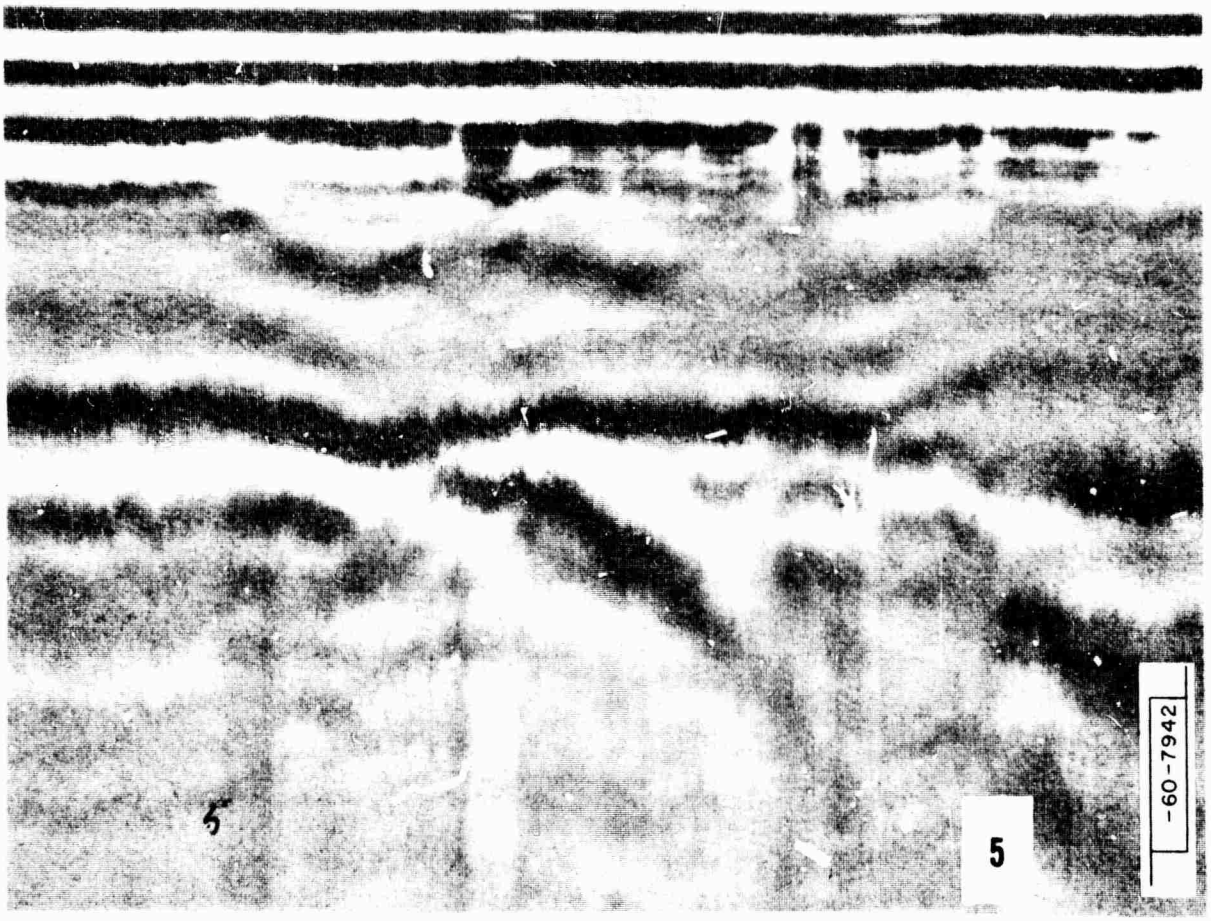

Fig. 8-10. Helix recording (actual size) of tunnel 6 ft below surface at Ft. Belvoir test site.

tunnel is a dark band. This signal reflection is caused by a layer of clay in the ground. The other dark bands in the recording indicate further stratification in the soil. Because of this clay stratification, detection of this tunnel by using only the A-scope display was very difficult. Figure 8-11 is a typical oscilloscope waveform directly over the tunnel. It shows the multiple signal reflections caused by the soil stratification.

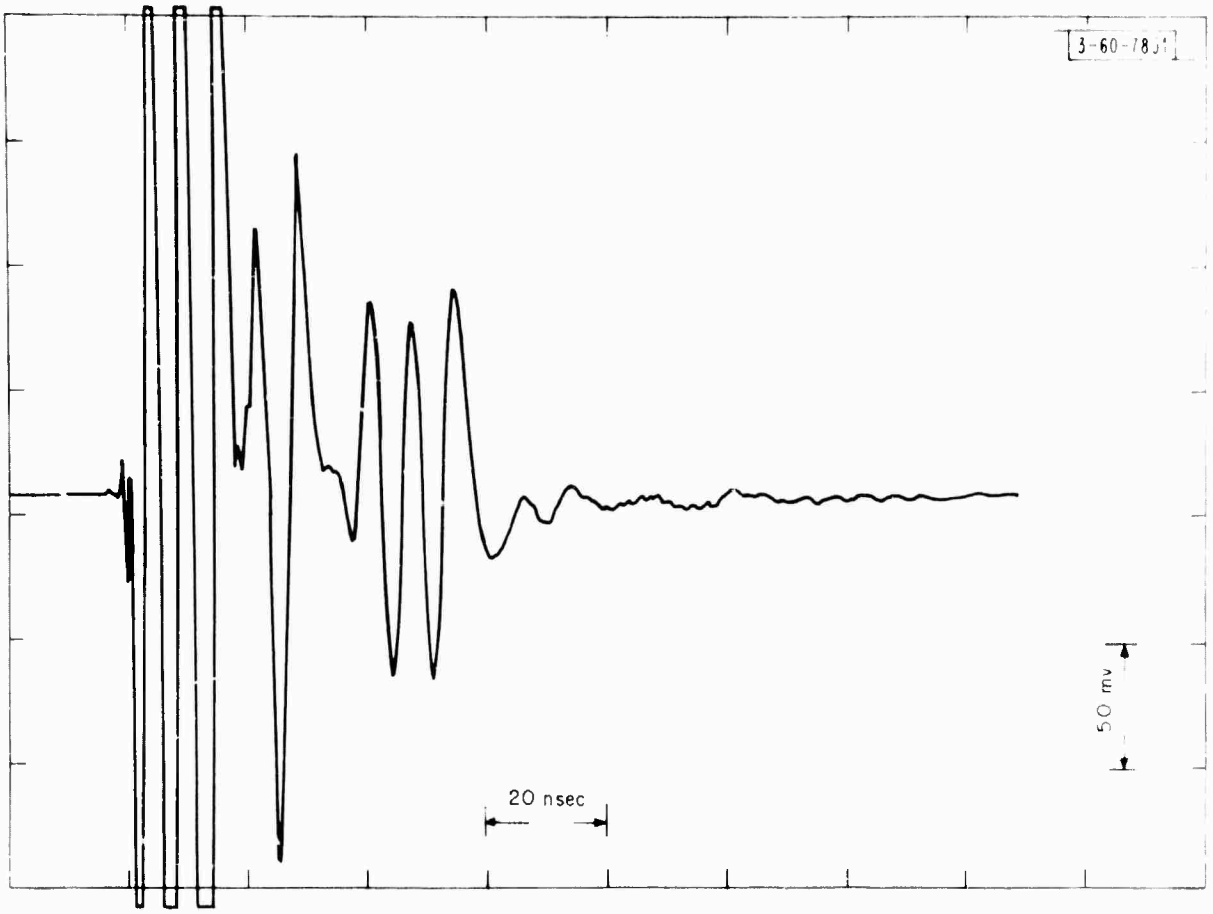

Fig. 8-11. Oscilloscope display directly over tunnel at Ft. Belvoir test site.


8
8


4

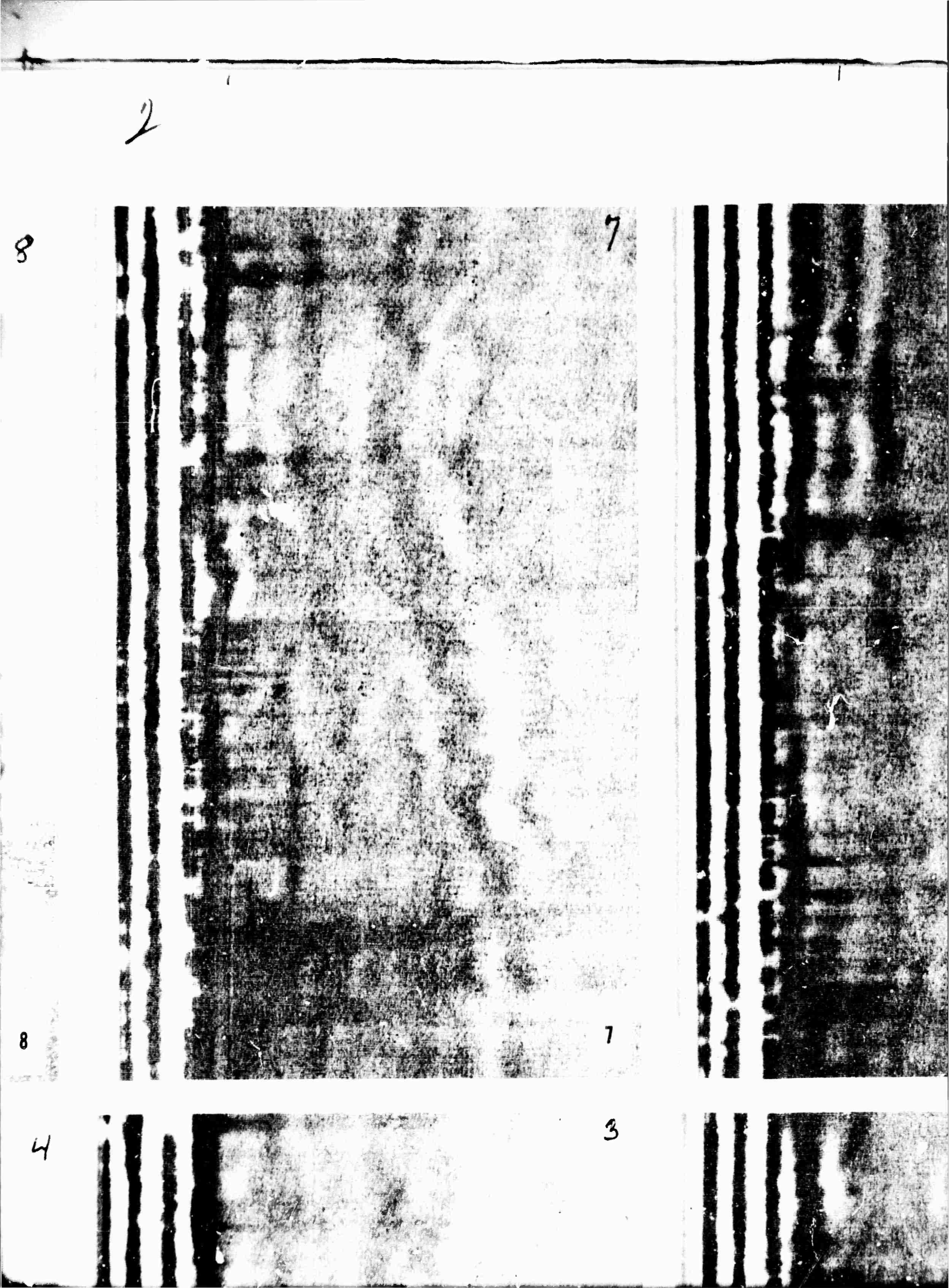
2
8
7
8
7
4
3

Confidential

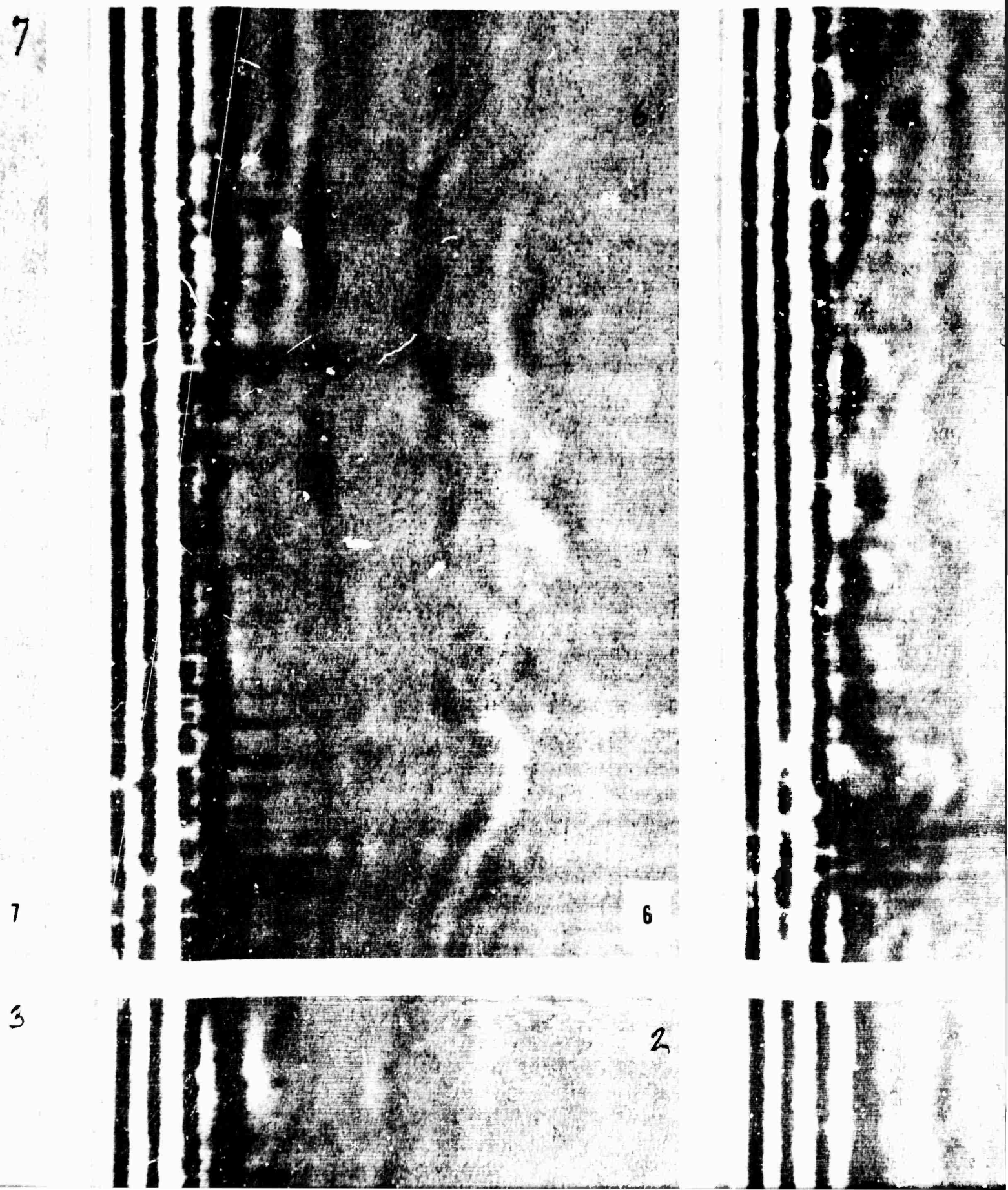

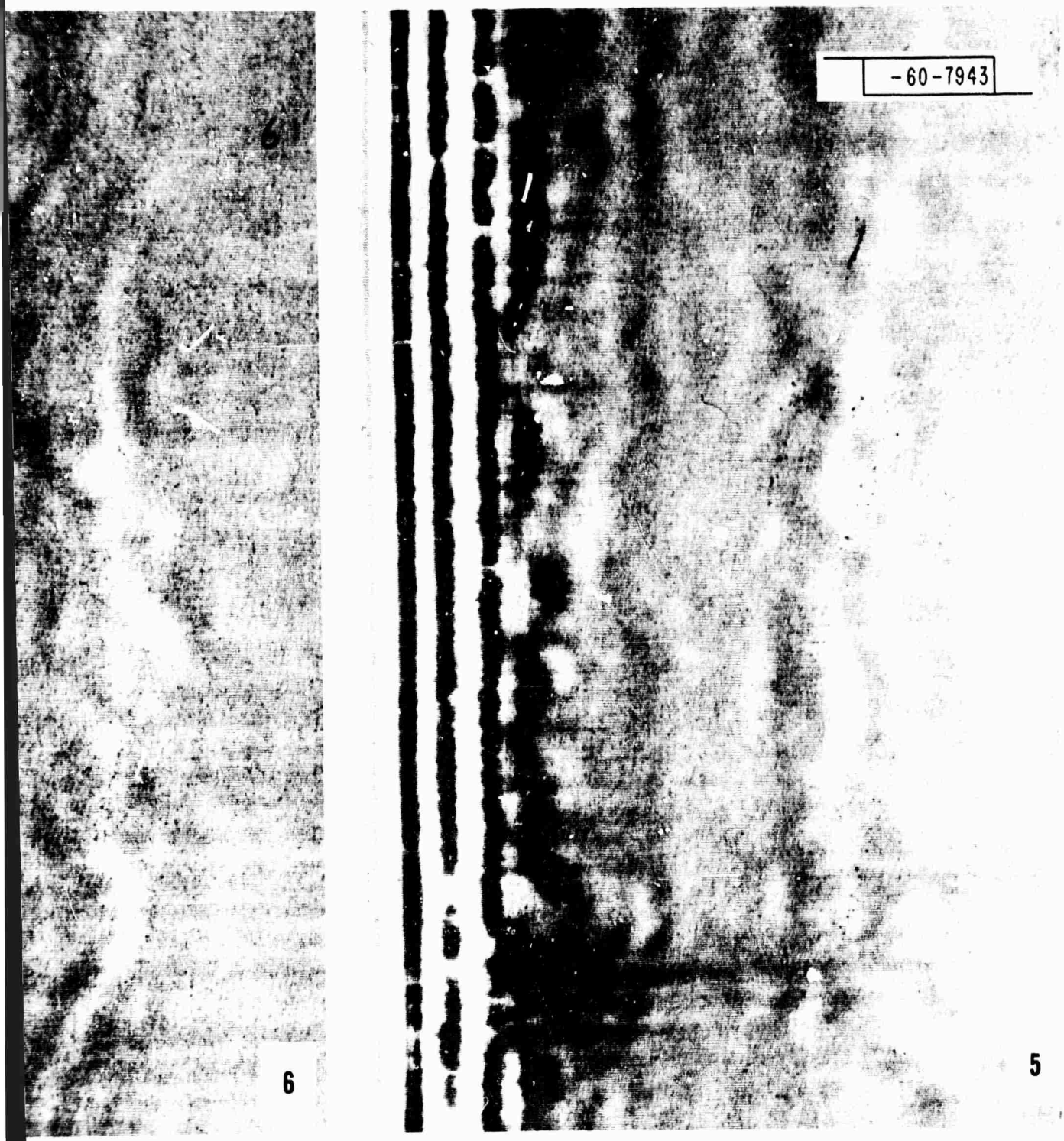
-60-7943
6
5
2
1

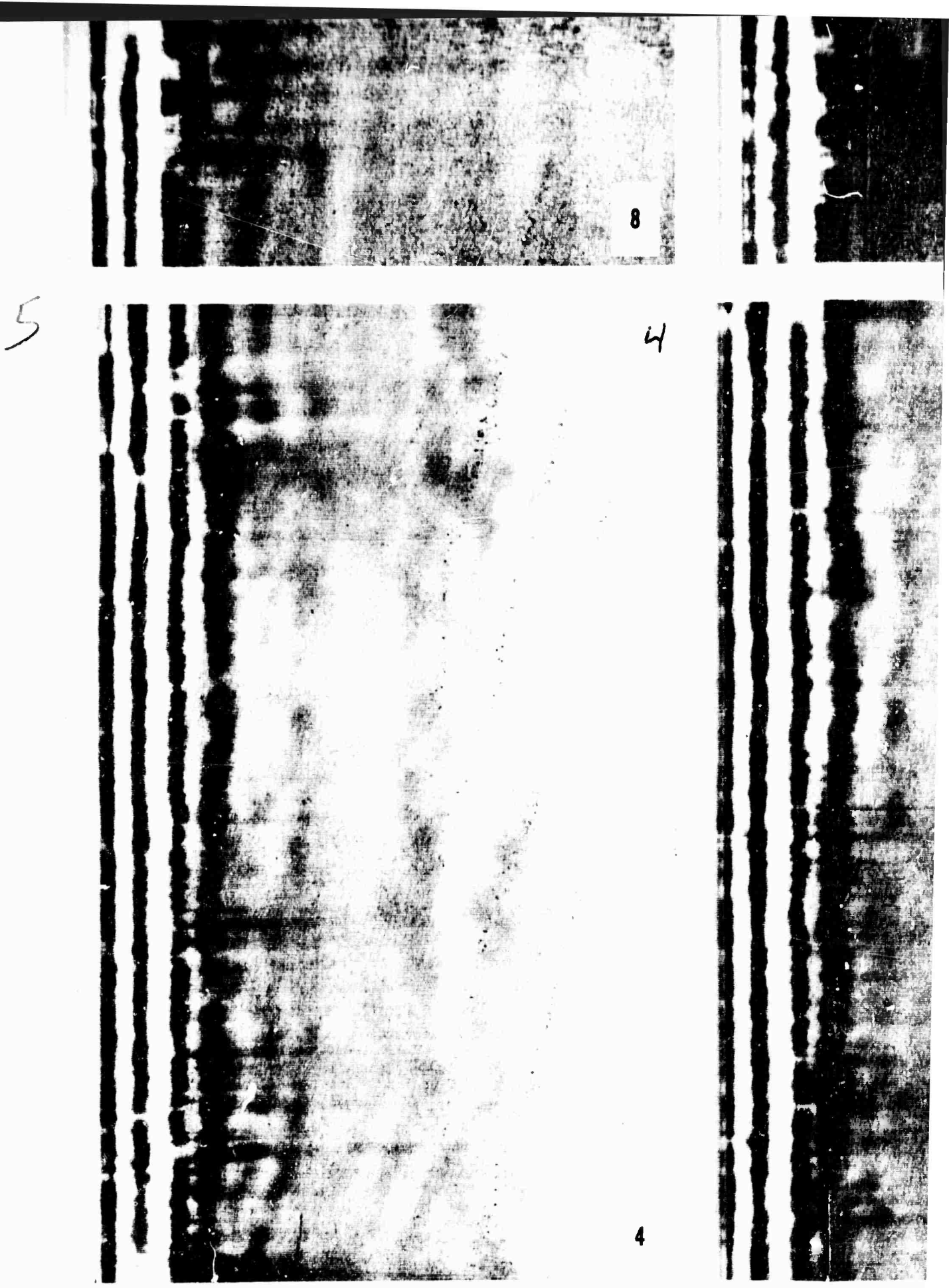

Fig. 8-9.
correspondi

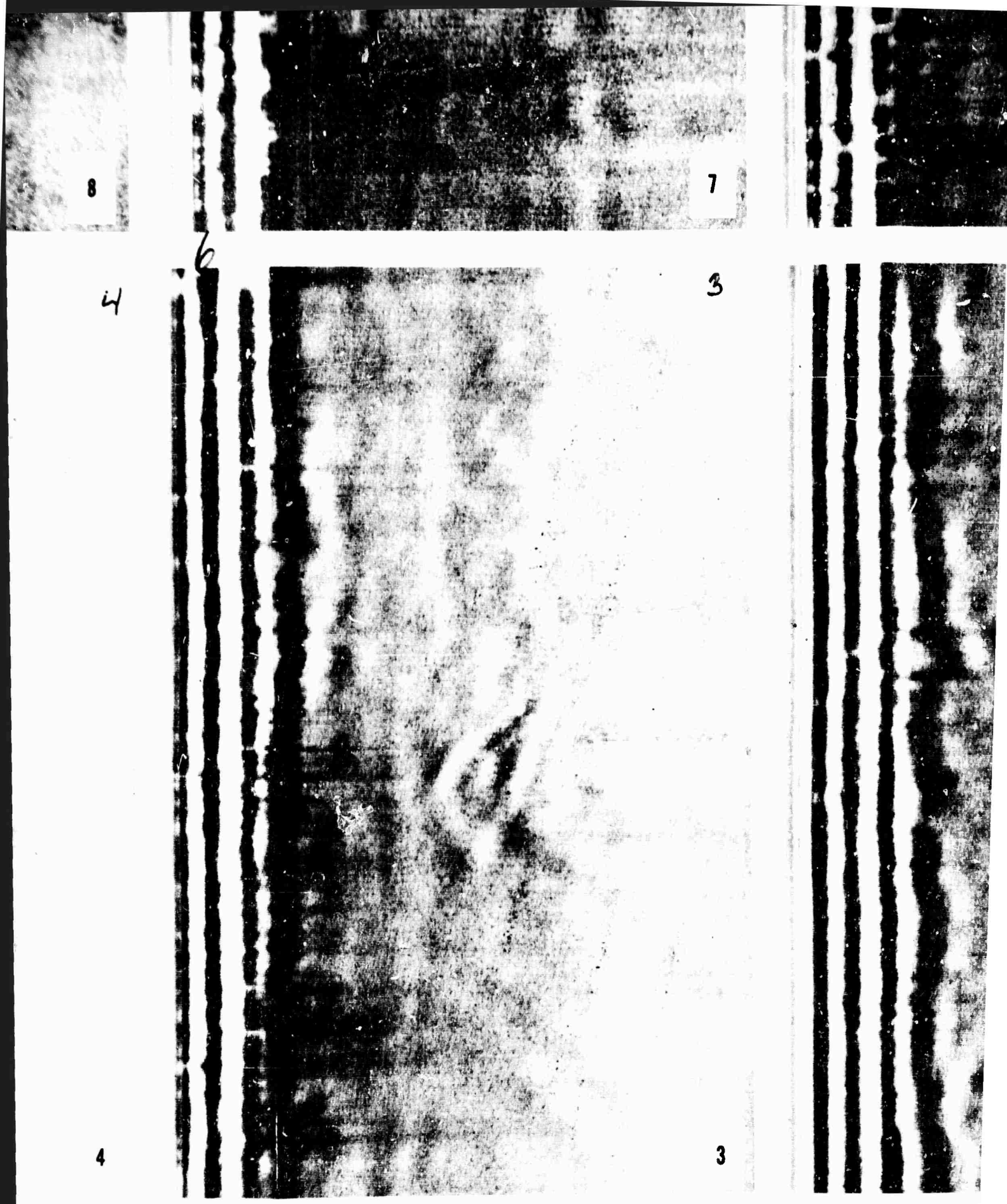

Fig. 8-9. Eight helix recordings (actual size) corresponding to passes shown in Fig. 8-8.

(actual size)

Confidential

dential

Fig. 8-9. Eight helix recordings (actual size) corresponding to passes shown in Fig. 8-8.

9. POWER

Initially, Mark I could be powered by 115 v AC, 12 v DC, or internal batteries (Fig. 9-1). The 12 v DC and internal batteries were primarily for field operation. Because the 115 v AC Honda generator provided trouble-free operation, the DC options were never required. To reduce weight and provide space for fans, the DC-to-AC inverter and batteries were removed.

Eleven power supply modules in the base of the Mark I display cabinet provide DC power for the control circuit, pulser, video amplifiers and sampling unit (Fig. 9-2). The oscilloscope operates directly from 115 v AC. Power consumption is 175 watts.

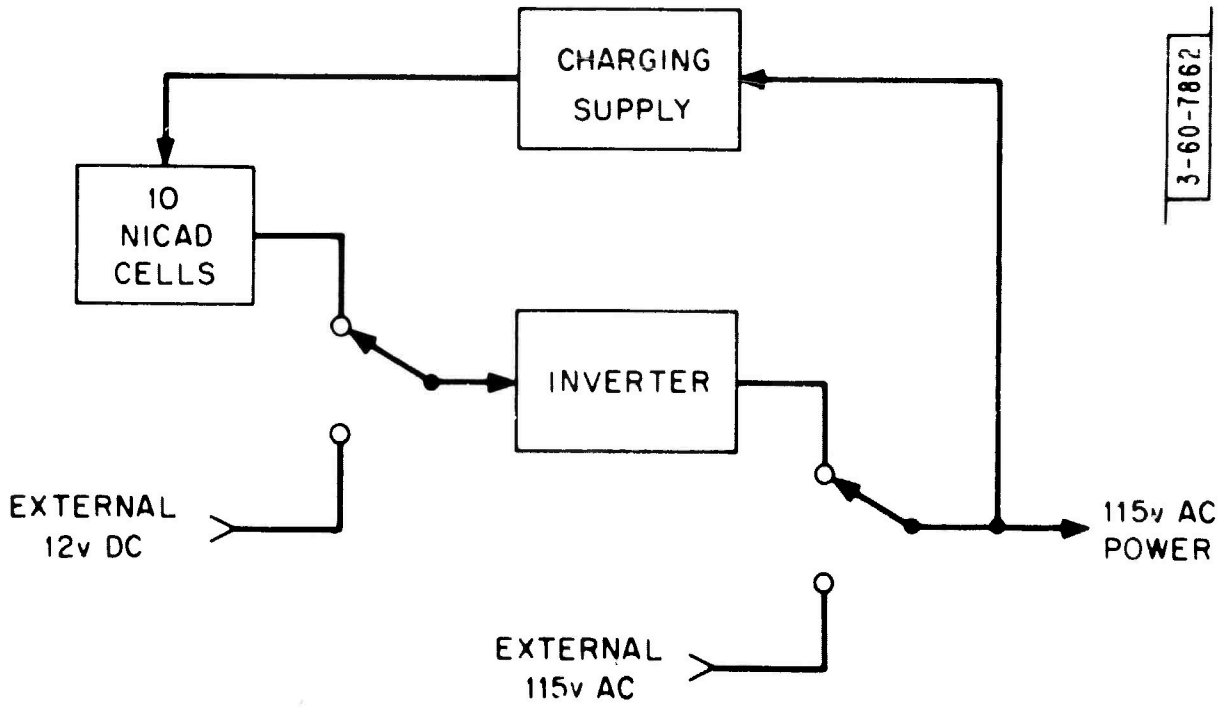

Fig. 9-1. Initial power options for Mark I.

Mark II consumes 135 watts power (Fig. 9-3). An extra power supply module was added to power a back-up Avantek amplifier, but it has not been used.

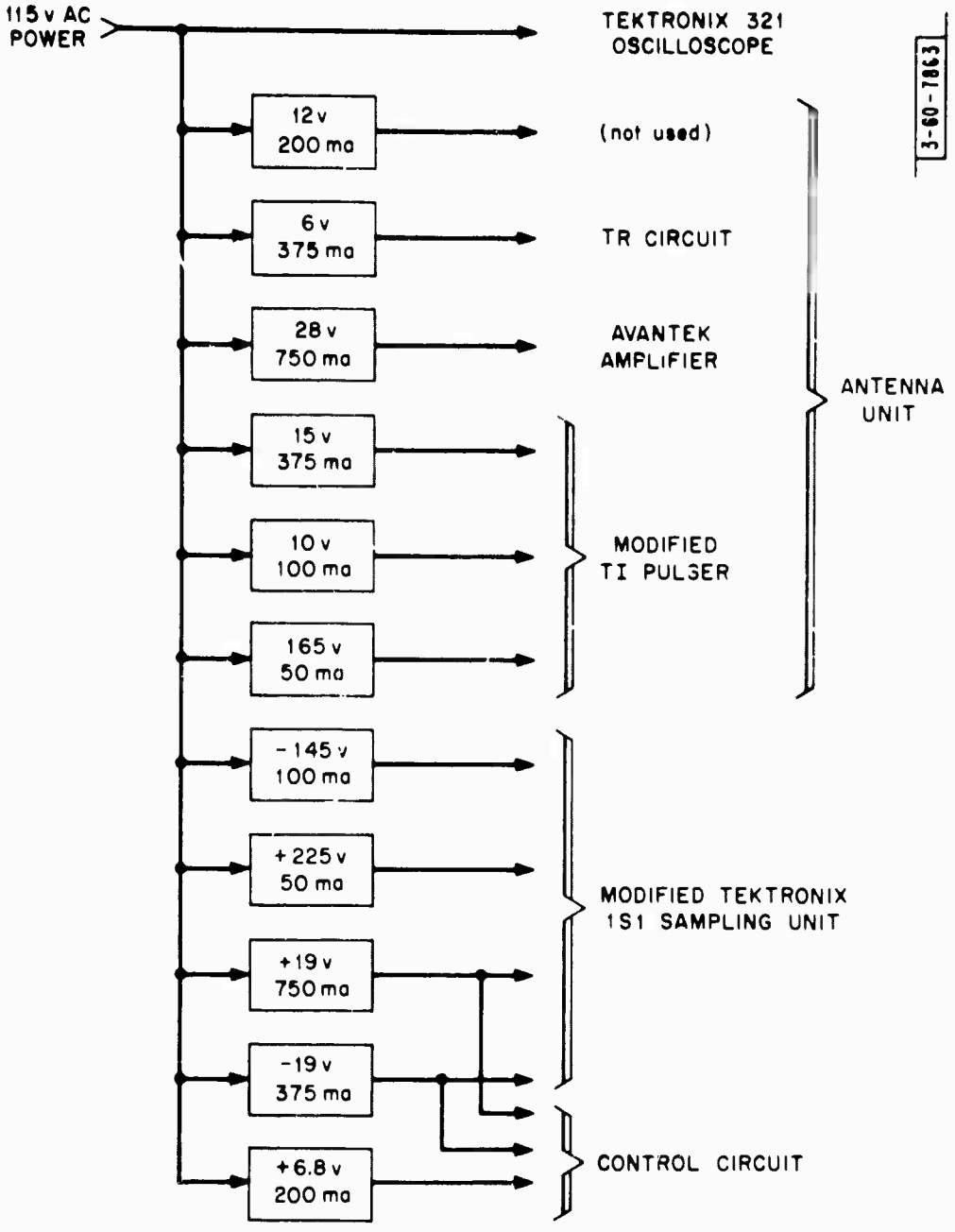

Fig. 9-2. Power distribution, Mark I.

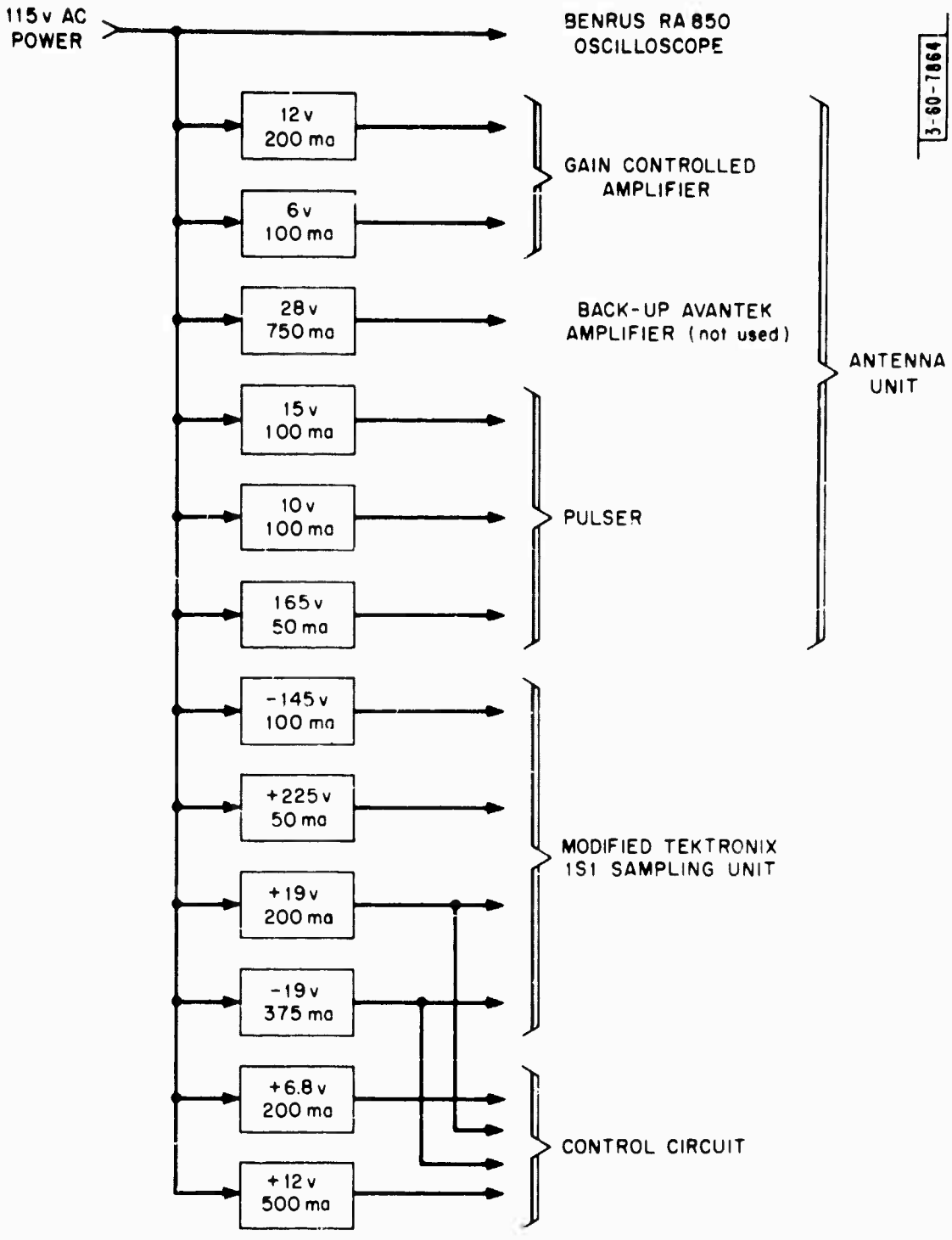

Fig. 9-3. Power distribution, Mark II.

Wiring that interconnects the display, control and power supply modules are shown in diagrams for Mark I (Fig. 9-4) and II (Fig. 9-5).

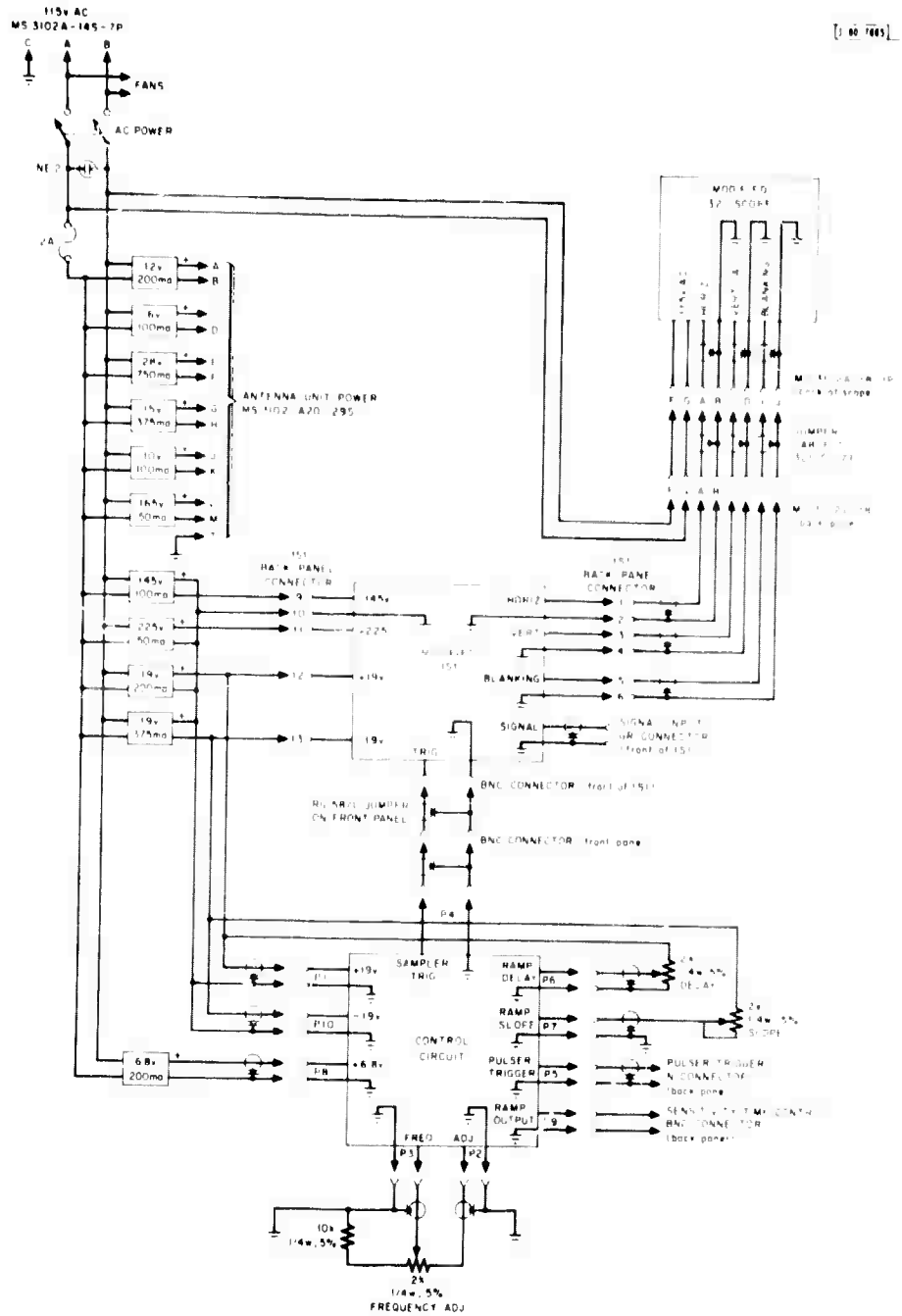

Fig. 9-4. Wiring interconnecting Mark I display, control and power units.

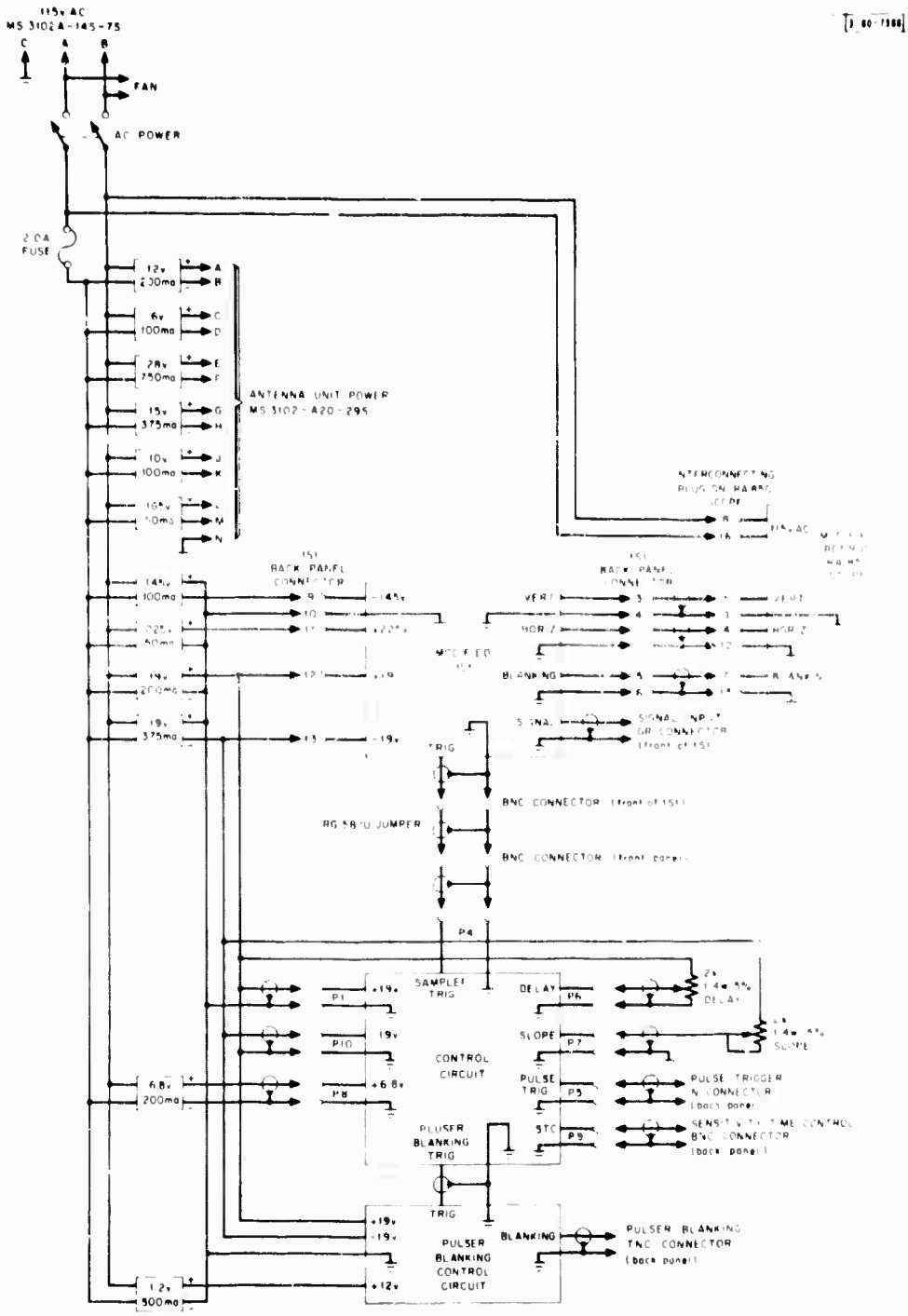

Fig. 9-5. Wiring interconnecting Mark II display, control and power units.

10. PULSE PROPAGATION MEASUREMENTS ON SELECTED SOILS

The simplest solution to Maxwell's equations in an unbounded isotropic medium is the monochromatic plane wave solution, which varies spatially as exp (ikz). Here the wave number k is given in terms of the radian frequency ω, permeability μ, permittivity ϵ and conductivity σ as $k^2 = i\omega\mu\ (-i\omega\epsilon + \sigma)$. Distance z is measured in the direction of propagation. When knowledge of the propagation properties of a medium is needed, therefore, it is natural to use the monochromatic plane wave as the primary example of a propagating wave. (In principle, it is possible to generate an arbitrary electromagnetic field by superposing plane waves of various directions, polarizations and frequencies, whereby the plane-wave properties define completely all wave-propagation properties of the medium.)

However, in the case of wide-band electromagnetic signals propagated through soil, both ϵ and σ are unknown functions of ω. Thus, the plane-wave transient behavior of the electromagnetic field can be obtained only from monochromatic measurements by computing numerically the Fourier transform of the product of the plane wave solution with the spectral representation of the input transient. Even for a particular soil with a particular water content, it is time consuming and tedious to measure the monochromatic properties over the frequency range of interest; and since transient properties are fundamental to the design of a tunnel-detecting radar, it was decided to measure the plane-wave transient properties directly.

Measurements

Pulse propagation measurements were made on various soil compositions with pulse lengths of 2.5, 5 and 10 nsec. The soil tested was packed into a coaxial line. Pulses applied at one end of the line were observed at positions along the line by a voltage probe and sampling oscilloscope.

The coaxial line was an eight-foot-long brass channel, 2 in. wide by 1 in. deep, with a slotted lid. A 1- x 1/8-in. brass strip, center conductor connected the coaxial connectors in the end plates. The channel was packed with soil to slightly less than half its depth. The center conductor was laid on top of the packed soil and soldered to the coaxial connectors. Soil was then packed into the remaining space, and the lid was placed in position.

The transverse dimensions of the channel were chosen small compared with the shortest wavelength likely to be encountered in the test soils, yet large enough to pack granular material without difficulty. The first of these requirements ensured that only the TEM mode would propagate in the line; thereby, simulating plane-wave propagation in an infinite medium.

During the tests, the coaxial connector at the far end of the line was left open-circuited so that perfect reflections of the propagating pulse would take place. Using a voltage probe, a measurement made at the midpoint of the line showed: (1) the pulse having propagated four feet into the medium, and (2) the pulse reflected from the far end having propagated a

total distance of 12 feet. Multiple reflections--back and forth between the open circuit at the end of the line and mismatch at the input to the line--were observed occasionally; but usually, attenuation through the soil was so large the pulse was undetectable, even at the 12-foot effective range.

Oscilloscope displays for 5- and 10-nsec pulses transmitted through illite soil (Figs. 10-1 and 10-2) show the pulse at three probe positions--0, 2 and 4 feet from the input end. The curves show effective ranges of 0, 2, 4, 12, 14 and 16 feet; but pulse height at the 16-foot range is actually the sum of the pulse incident on the mismatch at the line input, together with its reflection at that mismatch.

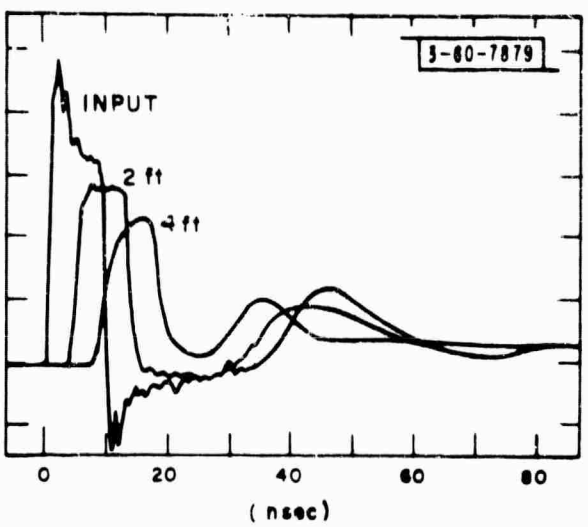

Fig. 10-1. Oscilloscope display of 10-nsec pulse transmitted through illite of 5-percent water content.

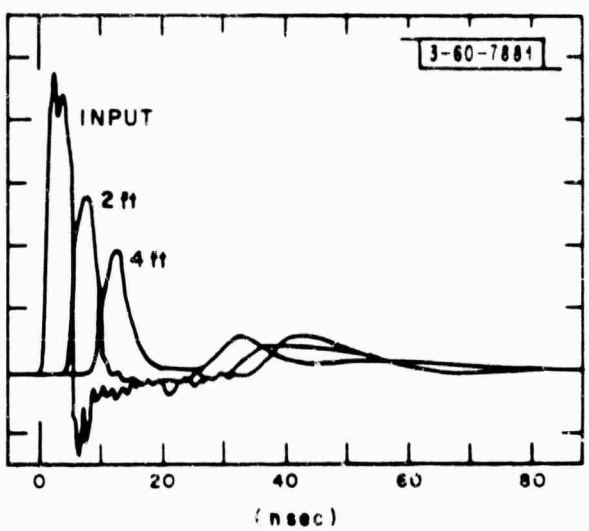

Fig. 10-2. Oscilloscope display of 5-nsec pulse transmitted through illite of 5-percent water content.

The curves also show clearly the attenuation, distortion and spreading experienced by the pulse as it propagates through the medium. The effective speed of propagation is indicated by the time displacement of the various downrange pulses from the leading edge of the input pulse.

Results obtained from tests on nine different soils are summarized in Table 10-1. Water content entries are the weight of water in the soil sample expressed as a percentage of the weight of the dry soil. Liquid limit entries are the maximum water content at which the test soil has mechanical stability. Speed of propagation is recorded as a slowness number, which is equal to the speed of light in free space divided by the speed of pulse propagation. The speed of propagation was calculated by dividing the range by the time displacement between the leading edges of the input pulse and the downrange pulse.

Because it is impossible to define a single number giving the attenuation per meter for pulse propagation in a dispersive medium, attenuation was defined as a direct comparison of the height of the downrange pulse to the height of the input pulse. Accordingly, a ratio of these quantities is entered in the table for each soil specimen, input pulse length, and range.

No measurements were made of pulse distortion, but for most soils the severity of distortion appears to be small for pulses of the widths chosen. However, a calculation could be made to indicate the degree of pulse distortion. If the distortion is small, the height ratio at 12 feet, for example, should be equal to the height ratio at 4 feet raised to the third power.

Comprehensive conclusions about the results are difficult

TABLE 10-1

TEST RESULTS ON NINE DIFFERENT SOILS

Soil	Liquid Limit (%)	Water Content (%)	Slowness	Height Ratio								
				10-nsec pulse			5-nsec pulse			2.5-nsec pulse		
				2 ft.	4 ft.	12 ft.	2 ft.	4 ft.	12 ft.	2 ft.	4 ft.	12 ft.
S. Carolina Clay Loom	42.0	8	2.2	–	1.25	2.25	–	1.5	3.9	–	2.2	7.5
		17	3.0	–	1.55	4.3	–	1.9	9.5	–	3.5	20.0
		20	3.8	–	2.6	10	–	3.1	17.0	–	5.7	?
		26	4.6	–	1.8	10.4	–	2.8	19.4	–	4.8	?
Ottawa Sand	–	0	1.6	–	1	1	–	1	1	–	1	1
		wet	4.8	–	1.4	2.8	–	1.4	2.8	–	1.4	2.8
Peat Loam (Test Site)	38.0	15	2.3	–	1.2	1.7	–	1.3	2.0	–	1.4	2.8
		23	2.9	–	1.4	2.7	–	1.5	3.6	–	1.6	4.7
		34	4.6	–	1.9	7.0	–	2.4	13.0	–	2.8	18.4
Cloy Loam (Test Site)	34.1	14	2.3	–	1.2	1.8	–	1.3	2.2	–	1.35	2.9
		18	2.6	–	1.2	1.6	–	1.3	2.0	–	1.5	2.8
		23	3.3	–	1.3	2.6	–	1.3	3.6	–	1.6	4.8
Bentonite	710	39	2.5	1.2	1.4	3.3	1.2	1.6	5.5	–	–	–
		68	3.2	1.8	4.2	?	2.3	8.0	?	–	–	–
		80	4.0	2.7	15.0	?	5	28	?	–	–	–
		102	5.0	6.5	?	?	–	–	–	–	–	–
		108	5.2	6.5	?	?	–	–	–	–	–	–
		116	6.0	7.0	?	?	16	?	?	22	?	?
Illite	120	5	2.0	1.4	1.6	3.8	1.5	2.2	8.5	–	–	–
		13	2.5	1.8	2.7	?	2.1	4.8	?	–	–	–
		19	3.0	2.5	6.3	?	–	6.6	?	–	–	–
		28	3.8	4.5	?	?	–	–	–	–	–	–
		31	4.0	5.6	?	?	–	–	–	–	–	–
		34	4.0	7	?	?	11	?	?	18	?	?
Kaolinite	53	3	1.8	1.4	2.0	7.0	1.6	2.7	16	–	–	–
		20	2.8	1.6	2.3	8.7	1.8	3.4	19	–	–	–
		31	3.4	–	3.4	?	–	5.4	?	–	–	–
		44	4.0	–	3.5	?	–	–	–	–	–	–
		49	4.2	–	3.7	?	–	–	–	–	–	–
		54	4.6	–	3.6	?	–	5.5	?	–	10	?
Millstane	–	12	3.1	–	1.4	3.2	–	1.5	4.6	–	2.0	9.0
Ft. Belvoir	–	–	2.1	–	1.3	2.2	–	1.6	3.6	–	2.2	8.0

– No measurement made.

? Pulse too small for identification on the oscilloscope.

to make, except that dry sand is essentially a perfect dielectric, and wet, pure clay (e.g., Bentonite) is both very attenuating and very dispersive. Commonly occurring soil mixtures appear to be sufficiently low in attenuation for pulse propagation over ranges of up to perhaps 10 feet.

Since wet sand is essentially nondispersive for the pulse lengths used in these experiments, one concludes that the dispersion observed in the other soils tested is due to the low-energy, ion-exchange bonds known to be present in water-clay mixtures. The characteristic frequencies of these bonds (bonds are of low energy) must be much lower than the characteristic frequency of the higher-energy water molecule bond, and, therefore, lie closer to the spectrum of the pulses used in the soil tests. Thus, it appears that the more clay and water in the soil, the more attenuating and dispersive it will be.

One other factor to be considered is the possibility that water contained in the soil possesses an appreciable conductivity due to the presence of dissolved salts. It is known, for example, that ocean water has an attenuation per meter measured in tens of db in the VHF band. Thus, it is likely that where the salt content of ground water is high and where the water content of the soil is high, the effect of dissolved salts on pulse propagation will be marked. However, no measurements have been made to investigate this effect.

11. BACKSCATTERING FROM CYLINDERS IMMERSED IN AN UNBOUNDED, DISSIPATIVE MEDIUM

A. Backscattering from Hollow, Circular Cylinders

The standard cylindrical-wave series solution for the field scattered by an infinitely long, circular cylinder illuminated by a plane-wave propagating in a direction normal to the cylinder axis was written as a computer program. The medium is which the cylinder is immersed was assumed to be isotropic and dissipative. Because no standard subroutine was available to compute Bessel functions of a complex argument that arose because of the dissipative media, an appropriate subroutine was written.

Accuracy of the Bessel function subroutine was established by comparing its computed values against published values tabulated for various specimen arguments distributed in the complex plane. Accuracy of the complete program was checked against published values for the field scattered by a dielectric cylinder in free space, and against values obtained from another program that uses matrix methods to compute the fields scattered by cylinders of arbitrary geometrical cross section.

The results are presented graphically in Figs. 11-1, 11-2, 11-3, and 11-4. Each curve is the squared magnitude of the backscattered electric field at a range of four cylinder radii plotted as a function of $k_o a = 2\pi a/\lambda_o$, where a is the cylinder radius and λ_o is the free-space wavelength.

The conductivity σ and relative permittivity κ are held constant at the indicated values for each curve. Two sets of

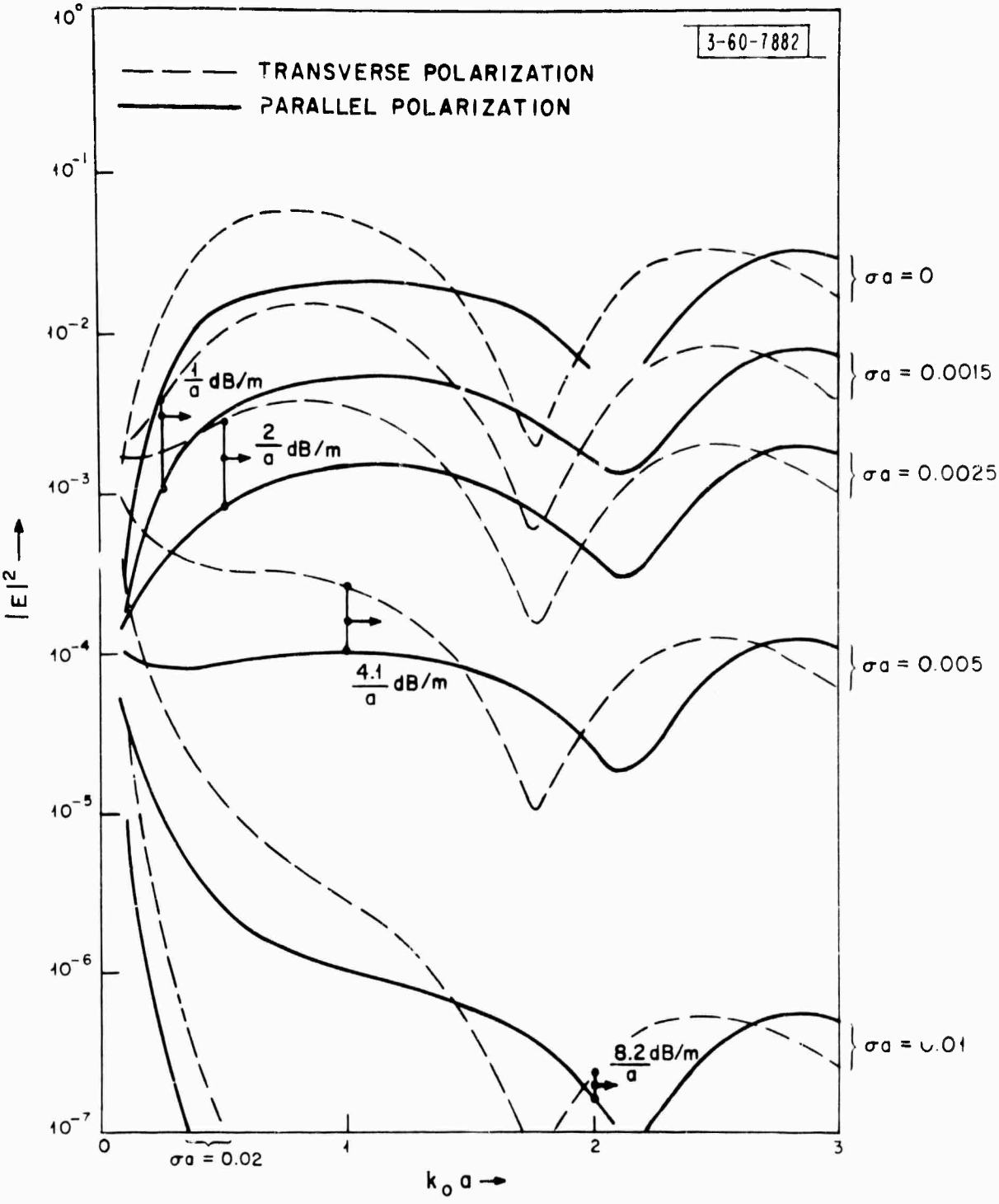

Fig. 11-1. Backscattered field for k = 4.

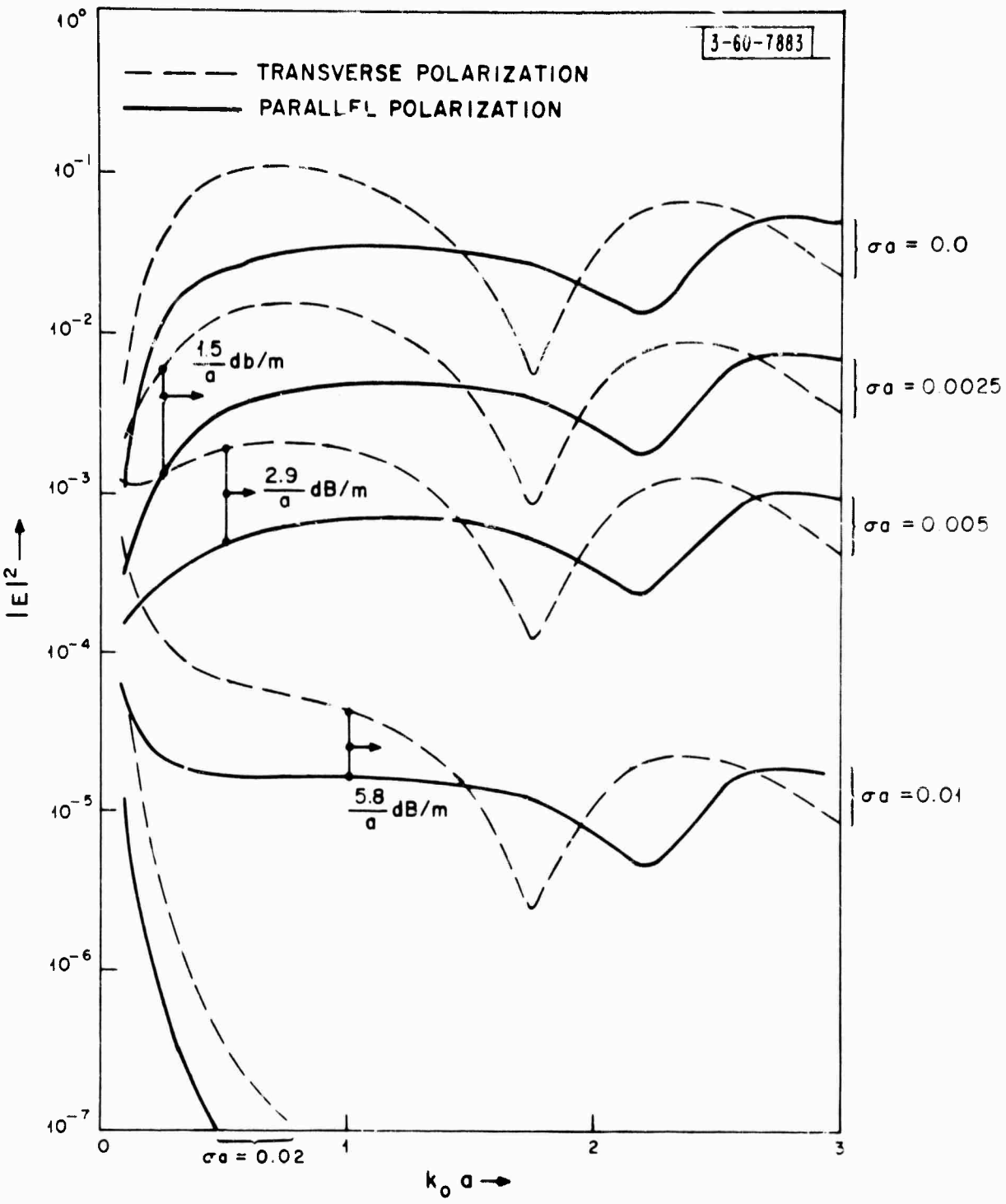

Fig. 11-2. Backscattered field for k = 8.

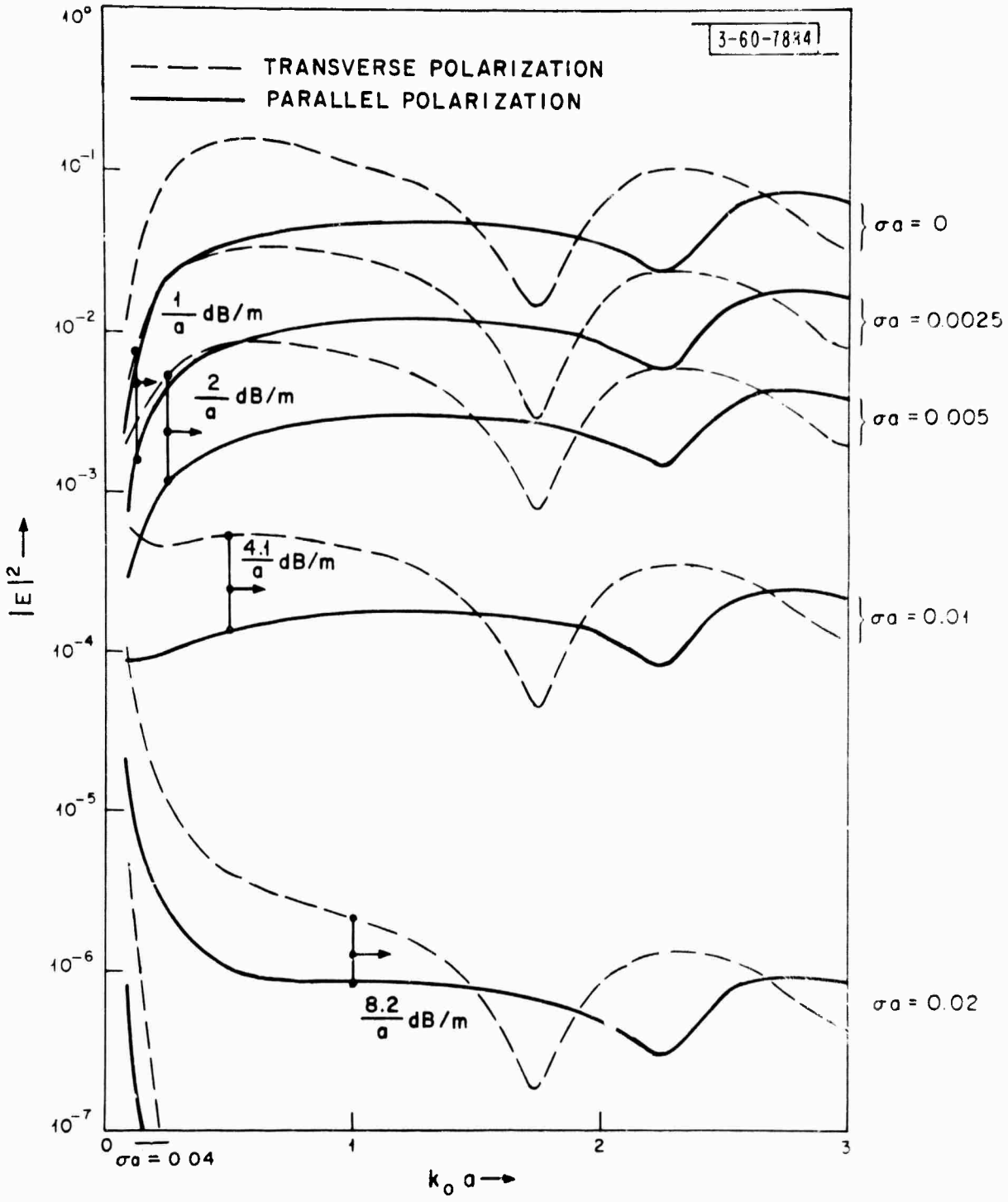

Fig. 11-3. Backscattered field for k = 16.

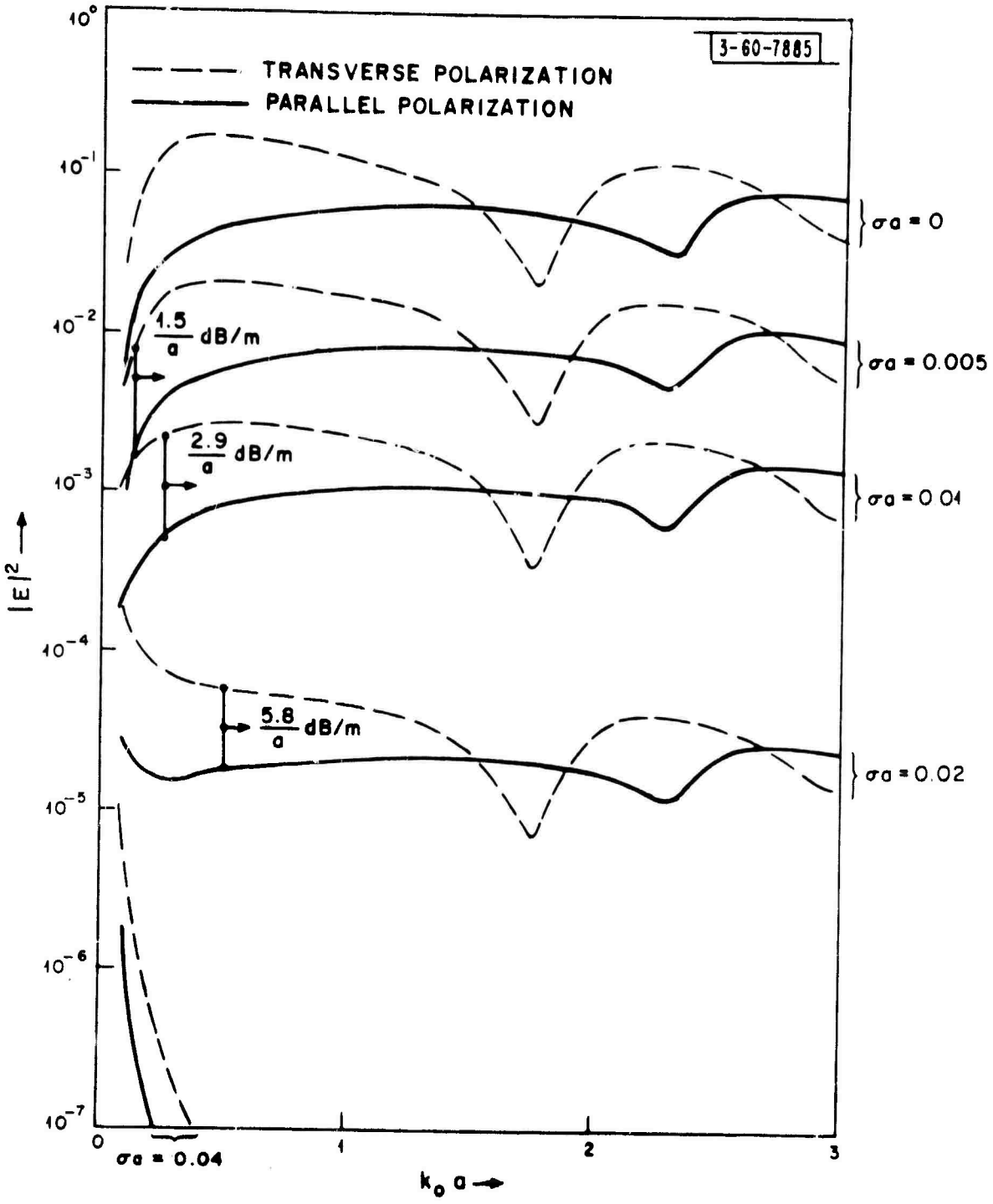

Fig. 11-4. Backscattered field for k = 32.

curves are presented: one for the incident plane wave linearly polarized in the direction of the cylinder axis (parallel polarization) and the other for the incident wave polarized normal to the cylinder axis (transverse polarization). The amplitude of the incident wave was chosen to be unity at a distance 4a from the cylinder axis in the backscattering direction. Thus, the curves include the attenuation experienced by the incident wave before it reaches the cylinder, in addition to the cylinder reflection factor and subsequent attenuation of the scattered field.

The upper limit for $k_o a$ of 3 was chosen because it is equivalent to a cylinder radius of 0.5 meter at a frequency of $9 \times 10^8/\pi$Hz, or about 300 MHz.

For a sufficiently high frequency, the attenuation of a plane wave in db per meter remains essentially constant at

$$0.868\sigma \left[\frac{\mu_o}{\kappa\epsilon_o}\right]^{\frac{1}{2}} ,$$

if the permittivity and conductivity are independent of frequency. Accordingly, appended to each curve is additional information specifying this asymptotic attenuation value and also indicating the lower bounding frequency (i.e., $k_o a$ value) of the region to which it applies. At lower frequencies, the attenuation is less than the specified value.

Significant points of interest are:

(a) The locations of the maxima and minima of the curves appear to be independent of properties of exterior

medium. This independence indicates that standing waves within the cylinder (rather than creeping waves circulating in the exterior medium) are the origin of these resonance phenomena.

(b) A fairly deep "null" exists in reflected power at a $k_o a$ value of about 2 for both polarizations. This null is equivalent to a frequency of about 200 MHz for a cylinder radius of 0.5 meter.

(c) A transverse polarized wave is consistently reflected more strongly than a parallel polarized wave, except in the vicinity of nulls.

(d) At a particular value of permittivity, the effect of increasing the conductivity appears to be mainly a lowering of the curve by an amount equal to the two-way attenuation.

B. Backscattering from Hollow, Noncircular Cylinders

A computer program was written to compute the field scattered by cylinders of more-or-less arbitrary shape immersed in a lossy dielectric medium. Figures 11-5 and 11-6 are representative information provided by the program. The execution time of the program was about 25 minutes.

Figure 11-5 is a contour plot of the backscattered electric field at range 4a for an incident wave electrically polarized in the axial direction when the cylinder has the "quadrant-cornered" square shape (Fig. 11-7). The contours are marked in db with respect to the intensity of the incident wave and give the backscattered field as a function of $k_o a$ (the free-space wave

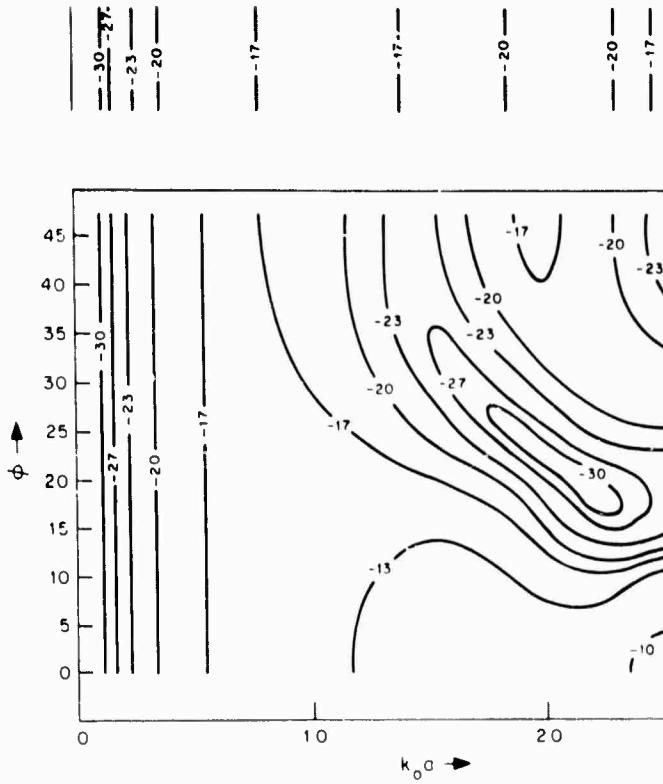

Fig. 11-5. Backscattered $|E_z|^2$ at range 4a--parallel polarization.

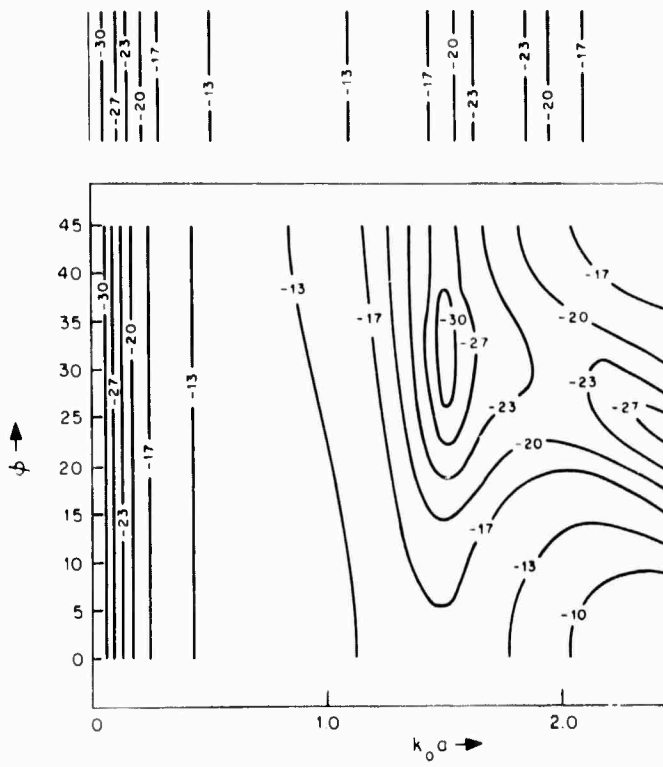

Fig. 11-6. Backscattered $|H_z|^2$ at range 4a--transverse polarization.

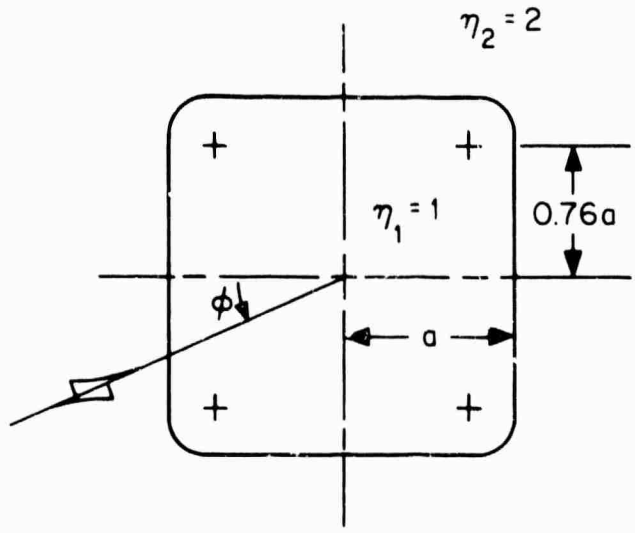

Fig. 11-7. "Quadrant-cornered" square shape.

number times the half-width) and of aspect angle ω. The internal refractive index η_1 is unity (free-space) and the external refractive index η_2 is 2. For comparison, behavior of a circular cylinder of radius a under the same conditions is included.

The corresponding contour plot for the backscattered magnetic field for an incident wave electrically polarized in a direction transverse to the cylinder axis is given in Fig. 11-6.

12. TEST RESULTS

The measurements made on Geodar are mainly predictive of the system performance, because there is not yet a complete body of extensive field experience, with a wide variety of objects, under a wide variety of soil conditions, at a wide variety of depths, with a wide variety of operational and surface conditions.

Geodar, however, has been thoroughly tested with objects buried in a homogeneous pile of New England loam and a field of glacial till. It has been less extensively tested on natural objects, and objects buried in a glacial sand deposit. Geodar has been demonstrated successfully on a hand-dug tunnel in typical subtropical soil in the North Carolina coastal plain. It also has been tested on alternate sand and clay layers from an upraised ocean bottom at Ft. Belvoir, Virginia.

The results of these tests indicate that Geodar will be able to locate hand-dug voids of two- to three-feet in diameter at depths of three- to twenty-feet (beyond 12 feet being an extrapolation) in most alluvial, glacial and loessial soils. It is anticipated that the highly leached and oxidized state of tropical soils are advantageous for Geodar. However, from laboratory data, it appears that soils abnormally high in chemically active clays of the montmorillonite and illite types may be troublesome. In tropical regions, such clays may exist in river deltas.

A. Soil Characteristics

(U) From a purely mechanical point of view, soils are made up of water, clay, sand, gravel, organic matter, and a variety of larger

rubble. From an electrical point of view, water is the most important constituent, and has a dielectric constant of 80 compared with 4 to 6 for the materials found in dry soil. It is possible to deduce from published data about the dielectric properties of soils (principally from Von Hipple's classic compendium) that for the interesting range of wavelengths the ground appears to be a lossy dielectric. The ground no longer behaves like a poor conductor as it does at low frequencies.

Measurements were made on soils mainly to supplement published data and for specific application to Geodar. In addition, an attempt was made to anticipate the electrical properties of soils in areas where Geodar might be needed. The principal "tool" of this investigation was an eight-foot-long coaxial transmission line in which the center conductor was surrounded with about a 1-cm thickness of the soil being tested. A complete report on pulse propagation in a number of soils appears in Chapter 10. Some general results are:

(1) Soils that range in appearance and feel from normal to moist. have seven to ten nsec of delay per foot of radar range as opposed to two nsec per foot of range in air. Course sand seems to be an exception. Sand that looks and feels slightly damp, nevertheless, measures four to five nsec of delay per foot of radar range, even in the field.

(2) The most important factor in determining attenuation seems to be the amount and chemical makeup of the clay component of the soil. Other substances (such as salt) may cause conductivity-induced losses in the soil, but clay is the principal source frequency-dependent attenuation. These losses rise precipitously with increasing

frequency. In the laboratory, an attempt was made to propagate five- and 10-nsec pulses through a transmission line packed with moist montmorillonite (ion exchange capacity of 120 milliequivalents per gram of clay). After a few feet, these pulses had completely lost their shape and were stretched out to the order of a 50-nsec duration. At 50-nsec duration, the corresponding wavelength in the ground would be too long to support effective reflection from an object two or three feet in diameter. Thus, little use for Geodar is expected in a clay bank of such materials. Illite-type clays (30 to 40 percent of the dry weight of a typcial clay-based soil) are more typical of New England soils. Illites have exchange capacity of the order of 50 milliequivalents per gram. The typical clay of well-drained tropical and subtropical soils is mineralogically kaolinite with exchange capacity as low as 10 millieq/gr. Indeed, the low chemical activity of such soils is responsible for the low fertility of tropical soils. After eight feet of propagation in a damp kaolinite-packed transmission line, a 10-nsec pulse was stretched to 20 nsec and attenuated at the rate of two or three db per foot of radar range.

Summarizing the other soil measurements: Above and beyond the free-space path losses and the normal reflection losses, an excess attenuation of the Geodar transient by about five to ten db per meter can be expected in most soils. Some attempt was made to take advantage of the observation that both the delay and the loss of return signals tend to increase with increasing moisture content. Presentation of the results in terms of loss per unit delay reduced the dynamic range of parameters by giving about 0.2 to 0.4 db per nsec of round-trip travel time.

Reflections from rock rubble up to 1 foot in size and/or tree roots do not appear as significant targets when Geodar is operated at its normal settings. A loaf-shaped boulder (18- x 18- x 24-in.) buried at 4-ft. depth in a glacial deposit of coarse sand was just visible when one went looking for it.

(U) Large rubble in the soil is a natural product of glaciation, and the unnatural result of the junkyards of civilization. South of the lines of glacial penetration one does not find boulders away from hillside scree or rushing streams. However, in tropical climates there are waterborne deposits of iron oxide in the soil. These deposits give the soil a typical reddish appearance and tend to produce iron oxide-cemented plinthitic layers. There has been no opportunity to test Geodar through a soil with known plinthitic horizons. It was hoped that such an opportunity would be present in North Carolina, but such did not turn out to be the case. Because these layers are formed in situ in tropical soils it is possible that the difference between the plinthite and the surrounding soil is mainly mechanical.

B. Antenna System Measurements

Extensive tests were made with a number of antenna systems at the two Lincoln Laboratory test sites. At the Lexington Field Station a number of boxes (14 ft. x 27 in. x 21 in.) were buried at depths of 3 1/2, 5 1/2 and 9 1/2 ft. in a homogeneous pile of peaty loam whose work space was 40-ft. in diameter and 12-ft. deep [Fig. 12-1 (a, b)]. At Millstone Hill, round, square, and diamond-shaped cross sections of glazed clay pipe were buried at 5 1/2 and 9 1/2 ft. depths (Fig. 12-2).

A typical series of transient response measurements of the Mark IC antenna [Fig. 12-3 (a, b, c, d)] were made with the

feed points of two IC antennas facing each other. One antenna was moved by increments of 16 in. on the surface of the work pile while the other was fixed against the roof of an access tunnel 5 1/2 ft. below the surface.

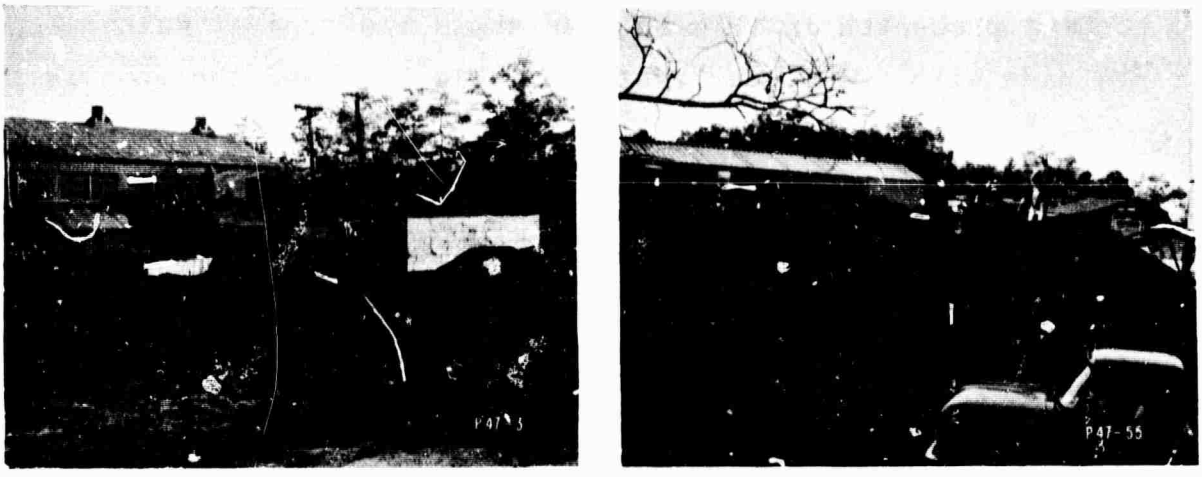

Fig. 12-1. Construction of Lexington Field Station test site.

Roughly speaking, the same kind of two-way transient response should be seen from a box buried 3 1/2 feet below the surface. A corresponding sequence of transients is shown in Fig. 12-4 (a, b, c, d).

Fig. 12-2. Construction of Millstone Hill test site.

In support of comments made in Chapter 2 about low frequency radiation from the antenna at angles away from the vertical, a similar set of measurements to the transient response between two antennas were made in the frequency domain [Fig. 12-5 (a, b, c, d)]. The antenna at the

surface was moved 32 in. between spectra. The peak of the radiation moves down from 100 MHz to 50 MHz as the angle between the test antennas exceeds 45°.

C. System Performance

Data presented in this section shows the type of measurements made with the Geodar systems (Table 1-1) and the results.

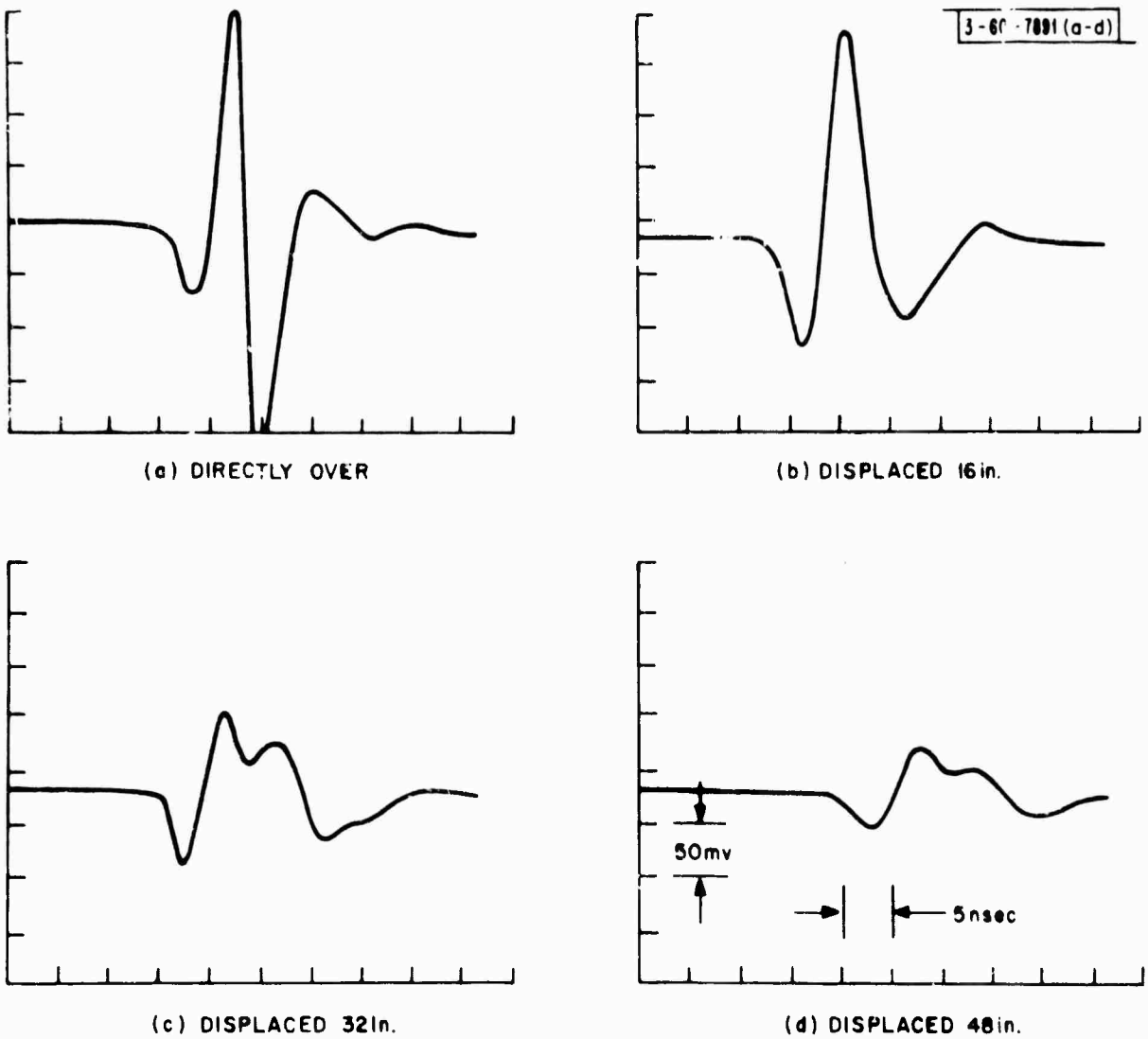

Fig. 12-3. Transient response of Mark IC antenna as transmitting antenna is moved away from receiving antenna fixed to top of tunnel 5 1/2 ft below the ground surface.

The antenna was positioned over the 36 in. square tunnel, 9 1/2 ft. below the surface at the Millstone Hill test site, to obtain a maximum signal return (Fig. 12-6). To compare different signal returns at the test site, the sensitivity time controls were set to their minimum values. Thus, the waveform shown in Fig. 12-6 has exaggerated signal perturbations directly after the transients caused by the transmitted pulse. The signal

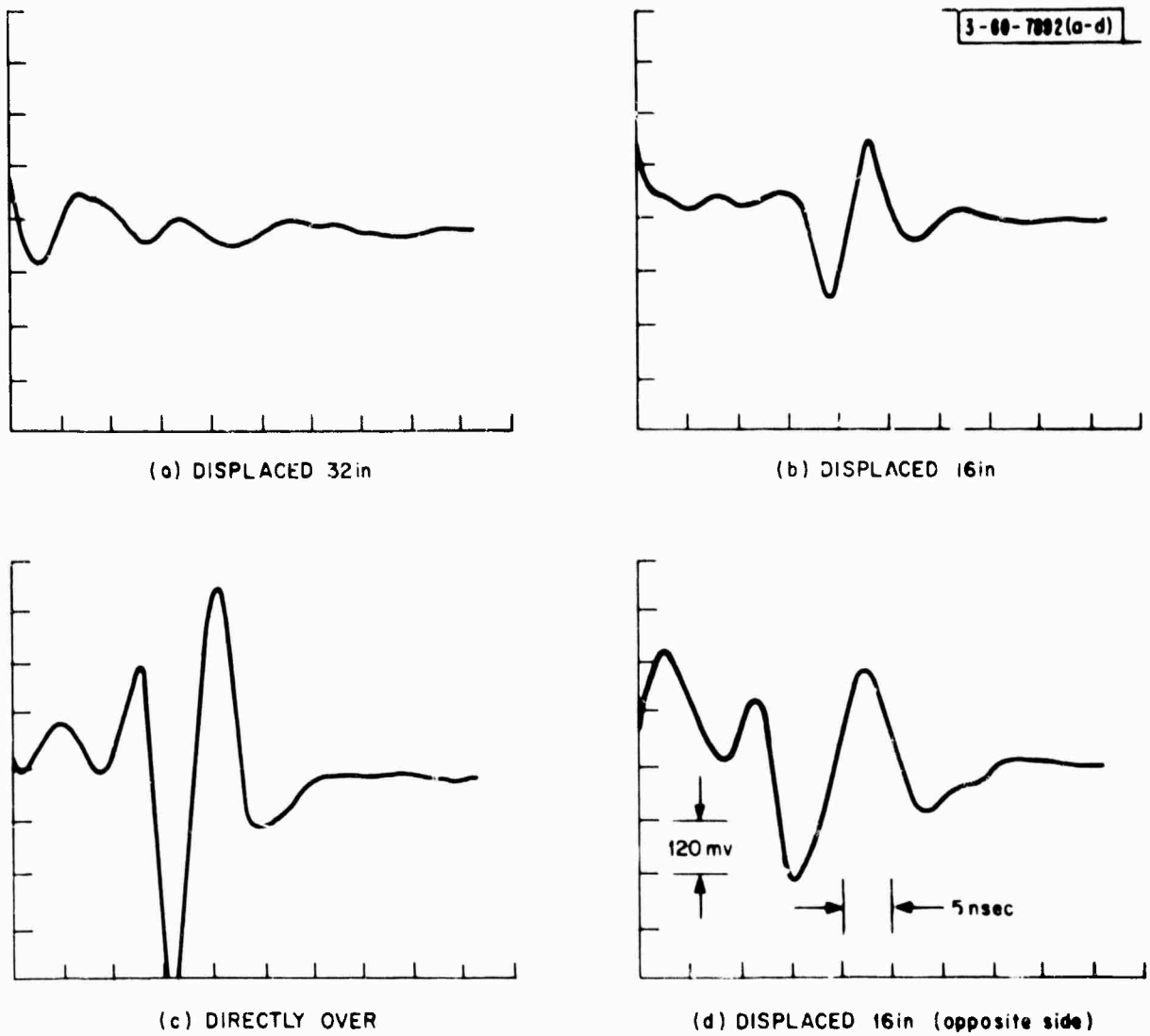

Fig. 12-4. Transient response of Mark IC antenna as it is moved over a tunnel 3 1/2 ft below the ground surface.

return from the 18 in. square tunnel at a 5-1/2 ft. depth (Fig. 12-7) was measured under identical conditions. The additional signal return, 15 nsec after the tunnel signal, is a reflection from the layer of gravel placed below the tunnel for drainage.

The signal return from a hand-dug tunnel, 6 to 9 feet below the surface at the Raleigh, North Carolina, test site was clearly identified on the A-scope display (Fig. 12-8). The sensitivity time controls were set for a 100-nsec ramp, delayed 80-nsec

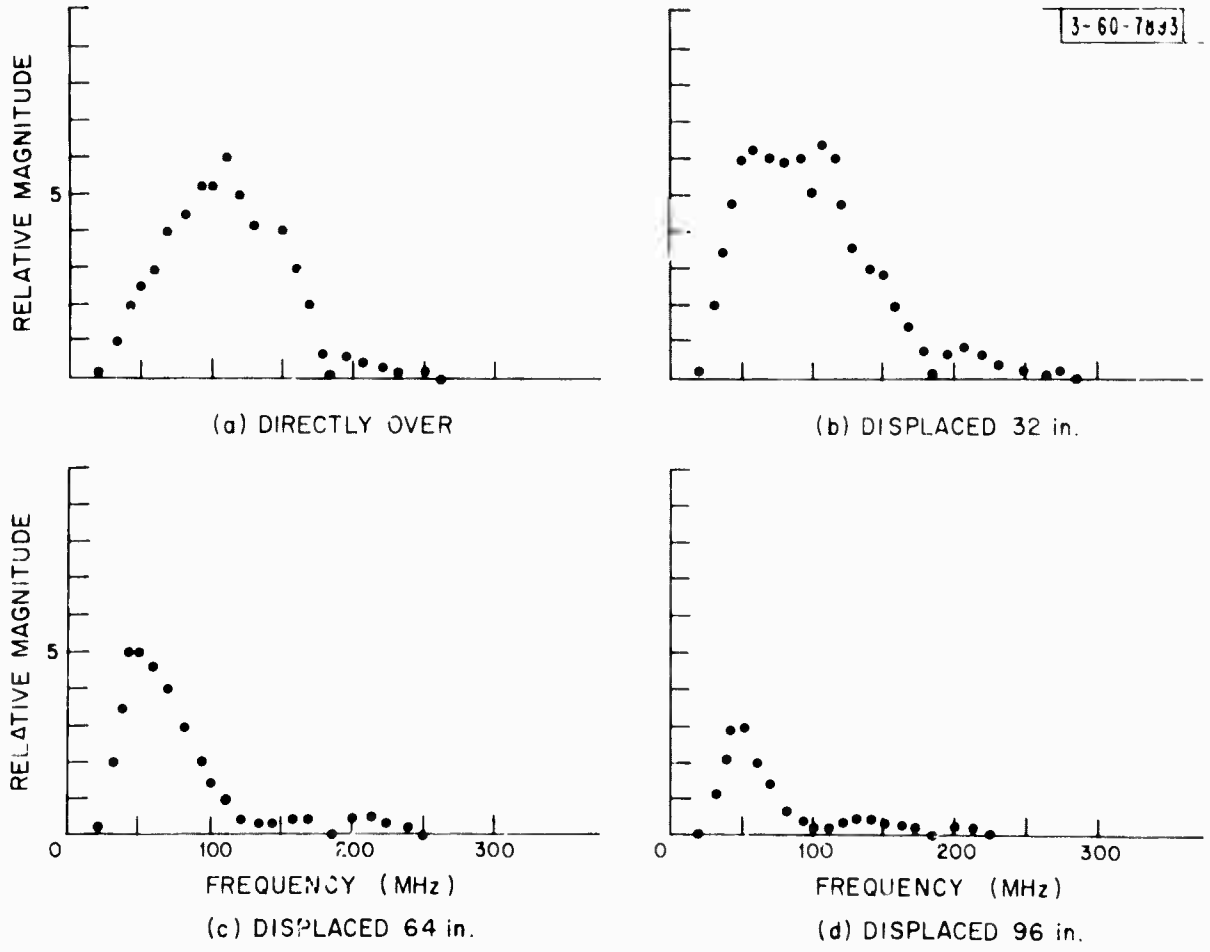

Fig. 12-5. Spectrum of Mark IC antenna as transmitting antenna is moved away from receiving antenna fixed to top of tunnel 5 1/2 ft below the ground surface.

TABLE 12-1

PEAK-TO-PEAK SIGNAL RETURNS

MILLSTONE HILL TEST SITE

Tunnel Shape	$5\frac{1}{2}$-ft. Deep Tunnels		$9\frac{1}{2}$-ft. Deep Tunnels	
	Antenna Axis Perpendicular to Tunnel Axis	Antenna Axis Parallel to Tunnel Axis	Antenna Axis Perpendicular to Tunnel Axis	Antenna Axis Parallel to Tunnel Axis
18-in. square	150 mv	240 mv		
18-in. round	100 mv	220 mv		
24-in. diamond	280 mv	280 mv		
24-in. square	290 mv	310 mv	42 mv	50 mv
24-in. round	160 mv	270 mv	28 mv	42 mv
30-in. square	320 mv	320 mv		
30-in. round	160 mv	280 mv		
36-in. square	380 mv	380 mv	75 mv	105 mv
36-in. round	160 mv	270 mv	30 mv	56 mv

Note: All measurements made with sensitivity time control set at minimum.

from the transmitted pulse. The base line of the receiver output was uncluttered as the antenna was moved away from the tunnel (Fig. 12-9). The lack of signal perturbation about the base line indicates the homogeneity of the soil, and the absence of internal reflections in the antenna and receiver.

Table 12-1 summarizes peak-to-peak signal returns at the receiver output for tunnels of different size, shape, and depth at Millstone Hill. Again, the sensitivity time controls were

set to a minimum so that a direct comparison could be made of the different signal levels. Also included in the table is the effect of the orientation of the antenna with respect to the tunnel. For each measurement the axis of symmetry for the antenna was first placed perpendicular to the tunnel, then parallel to the tunnel. All measurements indicated a maximum signal level was attained when the antenna was directly over the tunnel except for the 24-in. diamond-shaped tunnel where a maximum occurred 2 ft. either side of the tunnel, as expected.

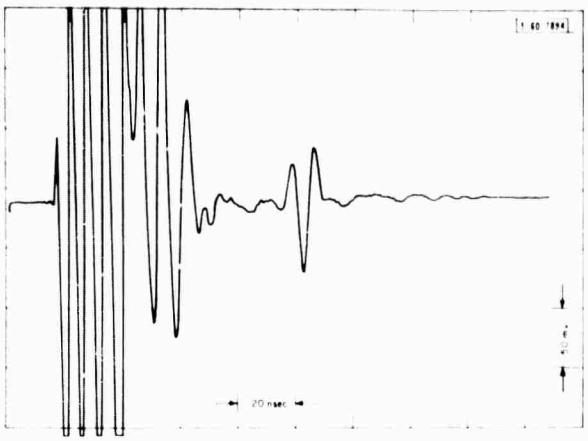

Fig. 12-6. Signal return from 36-in. sq. tunnel 9 1/2 ft below surface at Millstone.

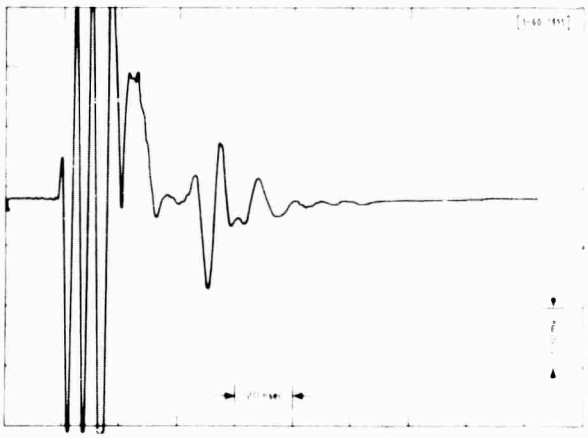

Fig. 12-7. Signal return from 18-in. sq. tunnel 5 1/2 ft below surface at Millstone.

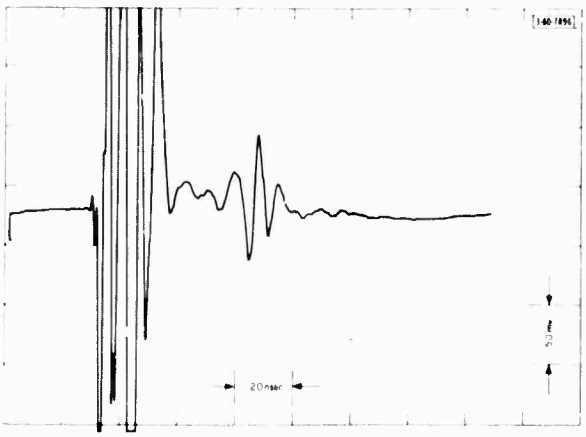

Fig. 12-8. Signal return from hand-dug tunnel at Raleigh, N.C., test site.

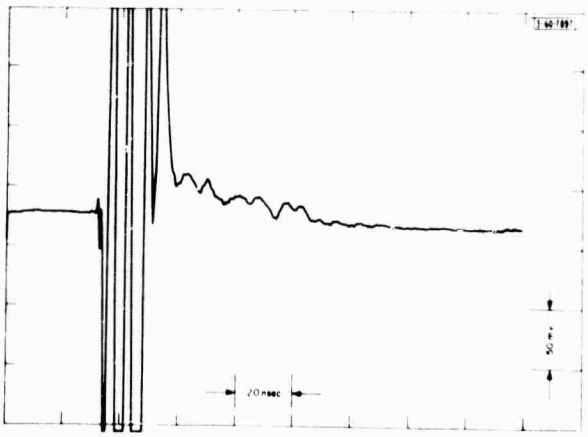

Fig. 12-9. Oscilloscope display for an area away from the tunnel at the Raleigh N.C., test site.

Typical A-scope displays (Figs. 12-10, 12-11, and 12-12) show the signal properties of the reflections from the square and round tunnels. For the 36-in. square tunnel 5 1/2-ft. in depth, no appreciable changes in the signal return were noted when the antenna was rotated through 360° directly above the tunnel (Fig. 12-10). However, there was a distinct change in the signal return when the antenna was rotated above the 36-in. round tunnel 5 1/2-ft. in depth. Maximum signal level occurs when the axis of the antenna is parallel to the axis of the tunnel (Fig. 12-11), and a minimum when it is perpendicular to the axis of the tunnel (Fig. 12-12).

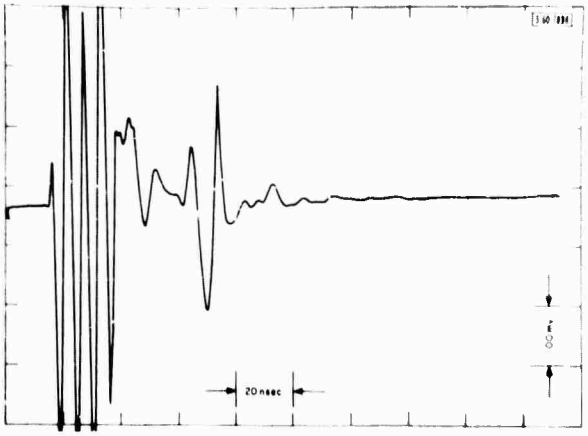

Fig. 12-10. Signal return from 36-in. sq. tunnel 5 1/2 ft below surface at Millstone.

All of the previously discussed measurements were made with the Mark I system. To demonstrate the superior ring down time of the Mark II system, figures 12-13 and 12-14 show signal returns from the tunnel 3 1/2 ft. below the surface at the

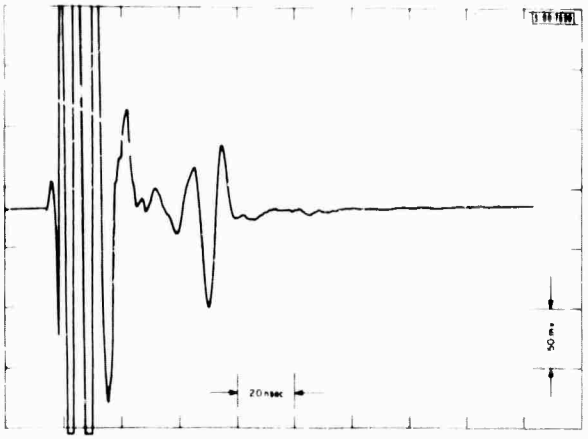

Fig. 12-11. Signal return from 36-in. round tunnel 5 1/2 ft below surface at Millstone.

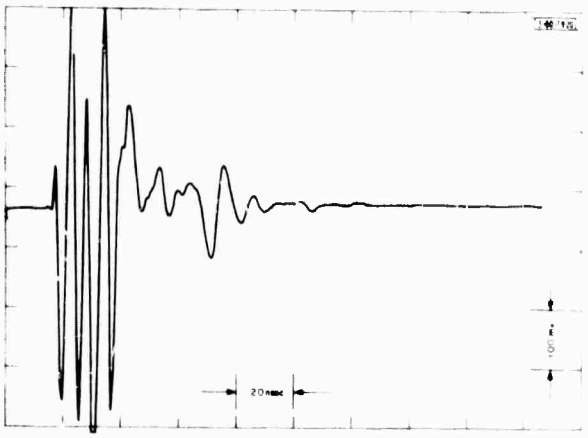

Fig. 12-12. Signal return from 36-in. round tunnel 5 1/2 ft below surface at Millstone.

Lexington Field Station test site. The sensitivity time controls were set for a -10 nsec delay and a 300-nsec slope.

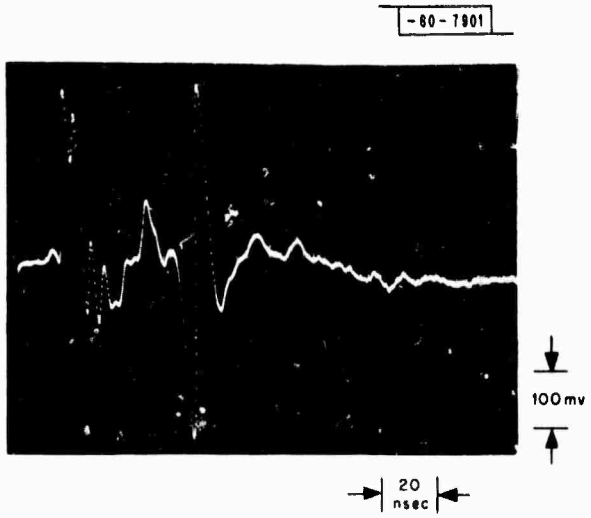

Fig. 12-13. Signal return from tunnel 3 1/2 ft below ground surface at Lexington Field Station test site. Antenna axis parallel to tunnel axis.

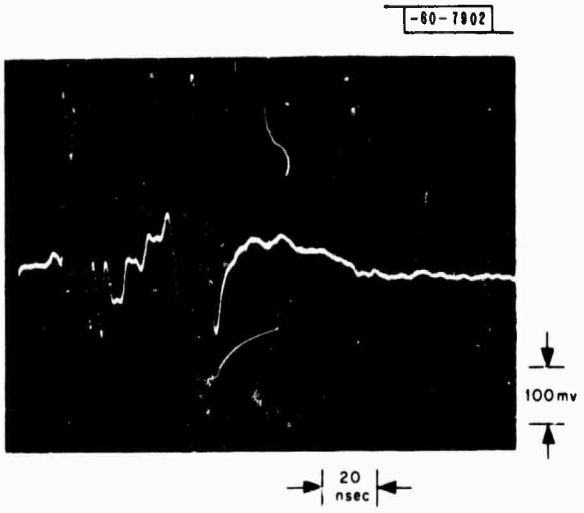

Fig. 12-14. Signal return from tunnel 3 1/2 ft below ground surface at Lexington Field Station test site. Antenna axis perpendicular to the tunnel axis.

TABLE 12-2

MARK II SIGNAL AMPLITUDE

Height of Antenna Above Surface of Ground	Relative Peak-to-Peak Signal Return
2 in.	1.00
8 in.	.77
14 in.	.66
20 in.	.57
26 in.	.50
32 in.	.46

A series of measurements were taken with the Mark II system to demonstrate the change in the signal return amplitude as the antenna is raised above the ground. The antenna was first placed over the 36-in. square tunnel 9 1/2-ft in depth, and then lifted in 6-in. increments (Table 12-2).